The Discrete Two Dimensional Fourier Transform in Polar Coordinates

A thesis submitted to

the Faculty of Engineering

in partial fulfillment of the requirements for the

degree of Master of Applied Science in

Mechanical Engineering

by

Xueyang Yao

Ottawa-Carleton Institute for Mechanical and Aerospace Engineering

University of Ottawa

Ottawa, Ontario, Canada, K1N 6N5

April 2018

Abstract

The discrete Fourier transform in Cartesian coordinates has proved to be invaluable in many disciplines. However, less theory has been developed for functions that are best described in polar coordinates. In this thesis, a new discrete 2D-Fourier transform in polar coordinates is proposed and tested by numerical simulations. Guidelines for choosing sample size are developed. Furthermore, to be as useful as its Cartesian counterpart, improvements are made to reduce the computing time.

Key words: 2D Fourier Transform, discrete, polar coordinates

Acknowledgements

I would like to express my gratitude to my supervisor Dr. Natalie Baddour, who helped me and guided me with my thesis and my life, for her patience, kindness and professional advice. I would also like to appreciate Dr. Liang Ming, who first gave me the opportunity to study at the University of Ottawa. At last, my grateful thanks to my parents and my friend Zuwen who supported and helped me get through it when life gets hard.

Table of Contents

List of Tables

List of Figures

Nomenclature

$f(r,\theta)$ Continuous original function in polar coordinates.

$F(\rho,\psi)$ 2D Fourier transform in polar coordinates.

f_{pk} Sampled original function in polar coordinates.

F_{ql} Discrete 2D Fourier transform in polar coordinates.

$E^{-}\left(ql;pk\right)$ Kernel for forward transform.

$E^{+}\left(ql;pk\right)$ Kernel for inverse transform.

N_1 Sample size in radial direction.

N_2 Sample size in angular direction.

J_n Bessel function with order *n.*

j_{nk} The *kth* zero of Bessel function with order *n*.

r_{pk} Sample point in radial direction in space domain.

θ_p Sample point in angular direction in space domain.

ρ_{ql} Sample point in radial direction in frequency domain.

ψ_q Sample point in angular direction in frequency domain.

R Effective space limit.

W_p Effective band limit.

f_s Sample frequency.

$f_{\max}$ Highest frequency of a function.

P Period of a function.

A_r Grid coverage in space domain.

A_ρ Grid coverage in frequency domain.

$\mathbb{H}_n$ Discrete Hankel transform with order *n*.

$E(v)$ Dynamic error to test the accuracy.

$E_{\max.}$ Maximum of dynamic error.

$E_{avg.}$ Average of dynamic error.

ε Average of absolute error to test precision.

1 Introduction

1.1 Background

The Fourier transform is a powerful analytical tool and has proved to be invaluable in many disciplines such as physics, mathematics and engineering. The development of the Fast Fourier Transform (FFT) algorithm [1], which computes the discrete Fourier transform with a fast algorithm, established the Fourier transform as a practical tool in diverse areas, most notably signal processing and image processing.

In two dimensions, the FFT can still be used to compute the discrete Fourier transform in Cartesian coordinates. However, in many applications such as photoacoustics [2] and tomography ([3], [4], [5]), it is often necessary to compute the Fourier transform in polar coordinates. Moreover, for functions that are naturally described in polar coordinates, a discrete version of the 2D Fourier transform in polar coordinates is needed. There have been some attempts to calculate the Fourier transform in polar coordinates, most notably through the Hankel transform, since the zeroth order Hankel transform is known to be a 2D Fourier transform in polar coordinates for rotationally symmetric functions. However, prior work has focused on numerically approximating the continuous transform. This stands in contrast to the Fourier transform, where the Discrete Fourier Transform (DFT) can stand alone as an orthogonal transform, independent of the existence of its continuous counterpart.

1.2 Objectives of the thesis

The goal of this thesis is to propose an orthogonal discrete 2D Fourier transform in its own right (similar to the DFT) which can also be used to approximate the continuous 2D Fourier transform in polar coordinates. Moreover, since computing speed is one of the most important criteria for a discrete transform, the algorithm must be improved to a useful level.

1.3 Contributions of the thesis

The contributions of the thesis are as follow:

1. An orthogonal discrete 2D Fourier transform in polar coordinates has been proposed.
2. Interpretation of the 2D transform as a 1D DFT, 1D Discrete Hankel Transform (DHT) and 1D inverse DFT (IDFT) in sequence has been presented.

3. Tests of the discrete transform to approximate the continuous 2D Fourier transform in polar coordinates were performed on different functions and accuracy of the approximations were demonstrated.
4. Factors that affect the accuracy of the approximation have been discussed, based on which guidelines for using the proposed discrete transform were presented.
5. Methods of reducing the computing time of the transform were investigated which brought the transform to a computationally useful level.
6. Matlab code to implement the transform has been developed.

2 Literature Review

2.1 Discrete Hankel Transform

Similar to the Fourier transform, the Hankel transform is one of the most commonly used tools and has far reaching applications in science and engineering. In optics, the Hankel transform has seen applications in the study of propagation of optical beams [6], propagation of cylindrical electromagnetic fields [7], and reconstruction of optical fields [8]. Within these applications, a numerical computation of the Hankel transform was needed, and many attempts were made to compute the Hankel transform numerically. However, most of the prior work focused on approximating the continuous Hankel transform, which is contrast to the approach taken with the Fourier transform, where the DFT can stand alone as a mathematical theory and has its own set of transformation rules.

In 1977, Siegman [9] proposed an algorithm to calculate the discrete Hankel transform called the quasi-fast Hankel transform (QFHT), where a nonlinear change of variable was used to convert the one-sided Hankel transform integral into a two-sided cross-correlation integral, which was then evaluated by using an FFT. Agrawal and Lax [10] improved the QFHT algorithm by using end corrections. Agnesi et al. [11] found a new analytical form to calculate the discrete Hankel transform with comparable accuracy with that of Siegman's approach without lower-end corrections.

In 1987, Johnson [12] proposed a new algorithm for computing the discrete Hankel transform which does not rely on the FFT. Compared to the QFHT, this new algorithm showed better simplicity and had the same reciprocity properties of the continuous transform, which provided a large improvement in speed and accuracy of the inverse transform. Yu [13] developed a zero-order Hankel transform termed the "Quasi-discrete Hankel Transform" which shared some similarities with Johnson's definition in that the zeros of Bessel functions were involved. Guizar-Sicairos and Gutiérrez-Vega [6] extended Yu's work to *nth* order. The works of Yu [13], Guizar-Sicairos and Gutiérrez-Vega [6] were the first to demonstrate a discrete version of the Parseval theorem for the discrete Hankel transform.

Baddour and Chouinard [14] proposed a fully discrete algorithm for the Hankel transform with its own rules including shift, modulation, convolution and

multiplication. In this thesis, it is shown that the DHT as developed by Baddour and Chouinard is one of the steps of the discrete 2D Fourier transform in polar coordinates.

2.2 Discrete 2D Fourier Transforms with Polar Coordinates

Similar to the discrete Hankel transform, the study of the discrete 2D Fourier transform in polar coordinates has often focussed on evaluating the continuous transform.

Computing the FFT on polar coordinates can be implemented by using non-equispaced spaced FFTs (NUFFTs). In recent years, many efforts have been made to propose an algorithm to calculate the FFT on a nonequispaced grid including a local Chebyshev approximation [15], a method by Dutt and Rohlin [16] and an algorithm based on local Taylor polynomials [17]. In [18], the relative efficiency of different methods were compared and it was pointed out that local Chebyshev and Taylor polynomial approximations showed better accuracy when the function is smooth and when the sample points are only slightly different from the points on a regular grid. Due to local interpolations, NUFFT can be prohibitively slow for large input sizes and it is not easily inverted.

In 2006, Averbuch et al. [19] proposed a new discrete polar Fourier transform (DPFT) , where the original function was sampled on a near-polar grid called a pseudo-polar grid followed by 1D equispaced FFT and 1D interpolations. Based on Averbuch's work, this new method was more accurate than the NUFFT method.

It should be noted that all the methods discussed above sample the original function in Cartesian coordinates and then aim at evaluating the continuous Fourier transform in polar coordinates. This is in contrast with the definition of the standard DFT from two aspects: 1. both the functions in the space and frequency domain of the DFT are in the same coordinates. 2. The DFT is defined as a transform in its own right, which means the existence of the DFT is valid even if without the existence of the continuous Fourier transform. Therefore, to the best of the author's knowledge, a discrete definition of the 2D Fourier transform in coordinates that parallels the way that the DFT is defined is missing in the literature.

3 The Discrete Transform

3.1 Background theory of 2D Fourier transforms

There is no discrete version of the 2D Fourier transform in polar coordinates. It was shown in [20], [21] that a continuous 2D Fourier transform in polar coordinates is actually a combination of a single dimensional Fourier transform and a Hankel transform.

The 2D Cartesian Fourier transform of a function $f(x,y)$ is defined as [21]:

$$F\left(\vec{\omega}\right)=F(\omega_x,\omega_y)=\int_{-\infty}^{\infty}\int_{-\infty}^{\infty}f(x,y)\,e^{-j\vec{\omega}\cdot\vec{r}}dx\,dy\,. \tag{3.1}$$

The inverse Fourier transform is given by

$$f\left(\vec{r}\right)=f(x,y)=\frac{1}{\left(2\pi\right)^2}\int_{-\infty}^{\infty}\int_{-\infty}^{\infty}F(\omega_x,\omega_y)e^{j\vec{\omega}\cdot\vec{r}}d\omega_x\,d\omega_y\,, \tag{3.2}$$

where the shorthand notation of $\vec{\omega}=\left(\omega_x,\omega_y\right),\vec{r}=\left(x,y\right)$ has been used. Polar coordinates can be introduced as $x=r\cos\theta,\ \ y=r\sin\theta$ and similarly in the spatial frequency domain as $\omega_x=\rho\cos\psi$ and $\omega_y=\rho\sin\psi$, otherwise written as, $r^2=x^2+y^2$, $\theta=\arctan\left(y/x\right)$ and $\rho^2=\omega_x^2+\omega_y^2$, $\psi=\arctan\left(\omega_y/\omega_x\right)$. It then follows that the two-dimensional Fourier transform can be written as

$$F\left(\rho,\psi\right)=\int_{0}^{\infty}\int_{-\pi}^{\pi}f(r,\theta)\,e^{-ir\rho\cos(\psi-\theta)}rdrd\theta\,. \tag{3.3}$$

Thus, in terms of polar coordinates, the Fourier transform operation transforms the spatial position radius and angle $\left(r,\theta\right)$ to the frequency radius and angle $\left(\rho,\psi\right)$. The corresponding 2D inverse Fourier transform is written as

$$f(r,\theta)=\frac{1}{\left(2\pi\right)^2}\int_{0}^{\infty}\int_{-\pi}^{\pi}F(\rho,\psi)e^{jr\rho\cos(\psi-\theta)}d\psi\,\rho d\rho\,. \tag{3.4}$$

3.2 2D Fourier transform in polar coordinates

A function $f(r,\theta)$ expressed in polar coordinates, where r is the radial variable and θ is the angular variable, can be expanded into a Fourier series as

$$f\left(\vec{r}\right) = f(r,\theta) = \sum_{n=-\infty}^{\infty} f_n(r)\, e^{jn\theta} \tag{3.5}$$

where the Fourier coefficients are given by

$$f_n(r) = \frac{1}{2\pi} \int_{-\pi}^{\pi} f(r,\theta)\, e^{-jn\theta} d\theta\,. \tag{3.6}$$

This transform is well suited for functions that are separable in r and θ. Similarly, the 2D Fourier transform $F\left(\rho,\psi\right)$ of $f(r,\theta)$ is a function of radial frequency and angular frequency variables $\left(\rho,\psi\right)$, and can also be expanded into its own Fourier series so that

$$F\left(\vec{\omega}\right) = F\left(\rho,\psi\right) = \sum_{n=-\infty}^{\infty} F_n(\rho)\, e^{jn\psi} \tag{3.7}$$

where

$$F_n(\rho) = \frac{1}{2\pi} \int_{-\pi}^{\pi} F(\rho,\psi) e^{-jn\psi} d\psi\,. \tag{3.8}$$

It is extremely important to note that $F_n(\rho)$ is NOT the Fourier transform of $f_n(r)$. Complete details of the development are given in [20], where it is shown that this relationship is given by

$$\begin{aligned} F_n\left(\rho\right) &= 2\pi\, i^{-n} \int_0^{\infty} f_n(r) J_n(\rho r)\, r dr \\ &= 2\pi\, i^{-n} \mathbb{H}_n\left\{ f_n(r) \right\} \end{aligned} \tag{3.9}$$

where $J_n(\bullet)$ denotes the nth order Bessel function and $\mathbb{H}_n\left\{\bullet\right\}$ denotes an *n*th order Hankel transform [3]. The inverse relationship is

$$\begin{aligned} f_n(r) &= \frac{i^n}{2\pi} \int_0^{\infty} F_n(\rho) J_n(\rho r)\, \rho d\rho \\ &= \frac{i^n}{2\pi} \mathbb{H}_n\left\{ F_n(\rho) \right\}. \end{aligned} \tag{3.10}$$

Thus, it can be observed that the *n*th term in the Fourier series for the original function will Hankel transform into the *n*th term of the Fourier series of the Fourier transform function. However, it is an *n*th order Hankel transform for the *n*th term, so that all the terms are not equivalently transformed.

3.3 Kernel for Discrete 2D Polar Discrete Fourier Transform

To propose and work with a 2D polar DFT, the following kernels are proposed

$$E^{-}(ql;pk)=\frac{2}{N_2}\sum_{n=-M}^{M}\frac{J_n\left(\frac{j_{nk}j_{nl}}{j_{nN_1}}\right)}{j_{nN_1}J_{n+1}^2(j_{nk})}i^{-n}e^{-in\frac{2\pi p}{N_2}}e^{+in\frac{2\pi q}{N_2}}$$
$$E^{+}(ql;pk)=\frac{2}{N_2}\sum_{n=-M}^{M}\frac{J_n\left(\frac{j_{nl}j_{nk}}{j_{nN_1}}\right)}{j_{nN_1}J_{n+1}^2(j_{nl})}i^{n}e^{+i\frac{2\pi np}{N_2}}e^{-i\frac{2\pi nq}{N_2}} \tag{3.11}$$

where p,k,q,l,n , N_1 , and N_2 are integers such that $-M\le n\le M$, where $2M+1=N_2$, $1\le l,k,\le N_1-1$ and $-M\le p,q\le M$. The integers N_1 and N_2 represent the size of the spaces in which we work, with N_2 representing the dimension in the angular direction and N_1 represents the dimension in the radial direction. Since $N_2=2M+1$, N_2 must be an odd integer.

3.4 Definition of the discrete transform

The 2D-Discrete Fourier Transform in polar coordinates is defined as the discrete transform that takes the matrix (or double-subscripted series) f_{pk} to the matrix (double-subscripted series) F_{ql}

$$\begin{aligned}F_{ql}&=\mathbb{F}\left(f_{pk}\right)\\F_{ql}&=\sum_{k=1}^{N_1-1}\sum_{p=-M}^{M}f_{pk}E^{-}(ql;pk)\\&=\sum_{k=1}^{N_1-1}\sum_{p=-M}^{M}f_{pk}\frac{2}{N_2}\sum_{n=-M}^{M}\frac{J_n\left(\frac{j_{nk}j_{nl}}{j_{nN_1}}\right)}{j_{nN_1}J_{n+1}^2(j_{nk})}i^{-n}e^{-in\frac{2\pi p}{N_2}}e^{+in\frac{2\pi q}{N_2}}\end{aligned} \tag{3.12}$$

The notation for $E^{-}\left(ql;pk\right)$ and $E^{+}\left(ql;pk\right)$ are the discrete kernels for the forward and inverse transform, respectively. The subscript (+ or -) indicated the sign on the $i^{\pm}$ and on the exponent containing the *p* variable; the *q* variable exponent then takes the opposite sign. From a matrix point of view, both f_{pk} and F_{ql} are $N_2 \times \left(N_1 - 1\right)$ sized matrices. The inverse transform is then given by

$$\begin{aligned} f_{pk} &= \mathbb{F}^{-1}\left(F_{ql}\right) \\ f_{pk} &= \sum_{l=1}^{N_1-1} \sum_{q=-M}^{M} F_{ql} E^{+}\left(ql;pk\right) \\ &= \sum_{l=1}^{N_1-1} \sum_{q=-M}^{M} F_{ql} \frac{2}{N_2} \sum_{n=-M}^{M} \frac{J_n\left(\frac{j_{nl} j_{nk}}{j_{nN_1}}\right)}{j_{nN_1} J_{n+1}^2\left(j_{nl}\right)} i^n e^{+i\frac{2\pi np}{N_2}} e^{-i\frac{2\pi nq}{N_2}} \end{aligned} \tag{3.13}$$

3.5 Orthogonality

3.5.1 Orthogonality of the Discrete Complex Exponential

The success of the one dimensional Discrete Fourier Transform (DFT) is based on the exploitation of known discrete orthogonality relationships for the complex exponential evaluated at a finite number of certain special points [24]. This relationship is traditionally given by

$$\frac{1}{N} \sum_{p=0}^{N-1} e^{-\frac{ip2\pi n}{N}} e^{+\frac{ip2\pi m}{N}} = \delta_{mn} \tag{3.14}$$

where m, n, p, N are integers. In equation (3.14), δ_{mn} is the Kronecker delta function, defined as

$$\delta_{mn} = \begin{cases} 1 & \text{if } m = n \\ 0 & \text{otherwise} \end{cases} \tag{3.15}$$

Suppose we define shifted values so that $p' = p - M$, where $2M + 1 = N$ so that any range of a variable in $\left[0, N-1\right]$ is equivalent to $\left[-M, M\right]$ in the primed variable. Hence, in terms of new variables equation (3.14) becomes

$$\sum_{p'=-M}^{M} e^{-\frac{i(p'+M)2\pi n}{N}} e^{+\frac{i(p'+M)2\pi m}{N}} = \underbrace{e^{-\frac{iM2\pi n}{N}} e^{+\frac{iM2\pi m}{N}}}_{=e^0=1} \sum_{p'=-M}^{M} e^{-\frac{ip'2\pi n}{N}} e^{+\frac{ip'2\pi m}{N}} = N\delta_{mn}$$

(3.16)

Hence, equation (3.16) states that

$$\sum_{p'=-M}^{M} e^{-\frac{ip'2\pi n}{N}} e^{+\frac{ip'2\pi m}{N}} = N\delta_{mn} \tag{3.17}$$

Equation (3.17) is the version of the discrete orthogonality of the complex exponential that will be required for the definition of the 2D Fourier transform in polar coordinates.

3.5.2 Orthogonality of the Bessel functions

It is shown in [12] that the following discrete orthogonality relationship is true

$$\sum_{k=1}^{N-1} \frac{J_n\left(j_{nm} j_{nk} \middle/ j_{nN}\right) J_n\left(j_{ni} j_{nk} \middle/ j_{nN}\right)}{J_{n+1}^2\left(j_{nk}\right)} = \frac{j_{nN}^2}{4} J_{n+1}^2\left(j_{nm}\right)\delta_{mi} \tag{3.18}$$

where j_{nm} represents the mth zero of $J_n(x)$.

3.5.3 Orthogonality of the 2D kernel

Based on, the orthogonality expressions given in equation (3.17) and (3.18), the following relationships can be shown to be true:

$$\sum_{l=1}^{N_1-1} \sum_{q=-M}^{M} E^-(ql, pk) E^+(ql, p'k') = \delta_{pp'}\delta_{kk'} \tag{3.19}$$

The proof of the preceding equation is as follows:

$$\sum_{l=1}^{N_1-1} \sum_{q=-M}^{M} E^-(ql, pk) E^+(ql, p'k') =$$

$$\sum_{l=1}^{N_1-1} \sum_{q=-M}^{M} \frac{4}{N_2^2} \sum_{n=-M}^{M} \frac{J_n\left(\frac{j_{nk} j_{nl}}{j_{nN_1}}\right)}{j_{nN_1} J_{n+1}^2\left(j_{nk}\right)} i^{-n} e^{-in\frac{2\pi p}{N_2}} e^{+in\frac{2\pi q}{N_2}} \sum_{n'=-M}^{M} \frac{J_{n'}\left(\frac{j_{n'l} j_{n'k'}}{j_{n'N_1}}\right)}{j_{n'N_1} J_{n'+1}^2\left(j_{n'l}\right)} i^{n'} e^{+i\frac{2\pi n' p'}{N_2}} e^{-i\frac{2\pi n' q}{N_2}}$$

(3.20)

Summing over the index q and using equation (3.14) returns a $N_2\delta_{nn'}$ so that $n'=n$ and equation (3.20) becomes

$$\frac{4}{N_2}\sum_{l=1}^{N_1-1}\sum_{n=-M}^{M}\frac{J_n\left(\frac{j_{nk}j_{nl}}{j_{nN_1}}\right)}{j_{nN_1}^2J_{n+1}^2\left(j_{nk}\right)}e^{-in\frac{2\pi p}{N_2}}\frac{J_n\left(\frac{j_{nl}j_{nk'}}{j_{nN_1}}\right)}{J_{n+1}^2\left(j_{nl}\right)}e^{+i\frac{2\pi np'}{N_2}} \tag{3.21}$$

which can be rewritten as

$$\frac{1}{N_2}\sum_{n=-M}^{M}e^{-i\frac{2\pi np}{N_2}}e^{+i\frac{2\pi np'}{N_2}}\underbrace{\sum_{l=1}^{N_1-1}\frac{4J_n\left(\frac{j_{nk}j_{nl}}{j_{nN_1}}\right)J_n\left(\frac{j_{nl}j_{nk'}}{j_{nN_1}}\right)}{j_{nN_1}^2J_{n+1}^2\left(j_{nk}\right)J_{n+1}^2\left(j_{nl}\right)}}_{=\delta_{kk'}} \tag{3.22}$$

Now summing over the index l and using the orthogonality relationship in equation (3.18) gives

$$\frac{1}{N_2}\sum_{n=-M}^{M}e^{-i\frac{2\pi np}{N_2}}e^{+i\frac{2\pi np'}{N_2}}\delta_{kk'}=\delta_{pp'}\delta_{kk'} \tag{3.23}$$

where the orthogonality relationship of equation (3.14) has been used again.

It can be similarly shown that the following orthogonality relationship is also true

$$\sum_{k=1}^{N_1-1}\sum_{p=-M}^{M}E^{-}\left(ql,pk\right)E^{+}\left(q'l',pk\right)=\delta_{qq'}\delta_{ll'} \tag{3.24}$$

Equation (3.24) could be considered to be the discrete version of

$$\int_0^{\infty}\int_{-\pi}^{\pi}e^{-i\vec{\omega}\cdot\vec{r}}e^{i\vec{\omega}'\cdot\vec{r}}d\vec{r}=\delta\left(\vec{\omega}-\vec{\omega}'\right) \tag{3.25}$$

where the integration over the vector $\vec{r}$ has been replaced with a discrete sum over the $\vec{r}$ vector indices $\left(p,k\right)$.

3.5.4 Interpretation of Orthogonality in the Matrix Sense

In matrix sense, $E^{-}\left(ql,pk\right)$ can be defined as a matrix of matrices, which means that each entry of $E^{-}\left(q,l\right)$ is a matrix $E_{q,l}{}^{-}\left(p,k\right)$. The same can be said for

$E^{+}(ql, pk)$; that is, each entry of $E^{+}(q,l)$ is a matrix $E_{q,l}{}^{+}(p,k)$. Therefore equation (3.19) can be written as

$$\sum_{l=1}^{N_1-1}\sum_{q=-M}^{M} E_{q,l}{}^{-}(p,k)E_{q,l}{}^{+}(p',k') = \delta_{pp'}\delta_{kk'} \tag{3.26}$$

where $E_{q,l}{}^{-}(p,k)$ is a $N_2 \times (N_1 - 1)$ matrix. $E_{q,l}{}^{+}(p',k')$ is the (p',k')th entry of matrix $E_{q,l}{}^{+}(p,k)$. The expression $\delta_{pp'}\delta_{kk'}$ represents an $N_2 \times (N_1 - 1)$ matrix where the entry (p',k') equals 1 and other entries are equal to 0.

Similarly, equation (3.24) can also be written in matrix sense form

$$\sum_{k=1}^{N_1-1}\sum_{p=-M}^{M} E_{q,l}{}^{-}(p,k)E_{q',l'}{}^{+}(p,k) = \delta_{qq'}\delta_{ll'} \tag{3.27}$$

By expressing the relationships in this way, the orthogonality can be checked in Matlab and the code is attached in Appendix A.

3.6 Definition for sampled forward and inverse transforms

Consider a function in the space domain $f(r,\theta)$ which is space limited to $r \in [0,R]$. This implies that the function is zero outside of the circle bounded by $r \in [0,R]$.An approximate relationship between sampled values of the continuous function and sampled values of its continuous forward 2D transform $F(\rho,\psi)$ is given below and has been derived in [23]

$$F\left(\frac{j_{ql}}{R},\frac{2\pi q}{N_2}\right) \approx 2\pi R^2 \sum_{k=1}^{N_1-1}\sum_{p=-M}^{M} f\left(\frac{j_{pk}R}{j_{pN_1}},\frac{2\pi p}{N_2}\right)\frac{2}{N_2}\sum_{n=-M}^{M}\frac{i^{-n}J_n\left(\frac{j_{nk}j_{nl}}{j_{nN_1}}\right)}{j_{nN_1}^2 J_{n+1}^2(j_{nk})}e^{-i\frac{2\pi np}{N_2}}e^{+i\frac{2\pi nq}{N_2}} \tag{3.28}$$

Similarly, an approximate relationship between sampled values of the continuous forward transform $F(\rho,\psi)$ and sampled values of the continuous original function $f(r,\theta)$ has been shown in [23] to be given by

$$f\left(\frac{j_{pk}R}{j_{pN_1}},\frac{2\pi p}{N_2}\right)\approx\frac{1}{2\pi R^2}\sum_{l=1}^{N_1-1}\sum_{q=-M}^{M}F\left(\frac{j_{ql}}{R},\frac{2\pi q}{N_2}\right)\frac{2}{N_2}\sum_{n=-M}^{M}\frac{i^n J_n\left(\frac{j_{nl}j_{nk}}{j_{nN_1}}\right)}{J_{n+1}^2\left(j_{nl}\right)}e^{+i\frac{2\pi np}{N_2}}e^{-i\frac{2\pi nq}{N_2}}$$

(3.29)

In equations (3.28) and (3.29), $f(r,\theta)$ is the original function in 2D space and $F(\rho,\psi)$ is the 2D Fourier transform of the function in polar coordinates. The values of the sampled functions given in equations and can be considered to be the discrete quantities denoted by

$$\begin{aligned} f_{pk} &= f\left(\frac{j_{pk}R}{j_{pN1}},\frac{2\pi p}{N_2}\right) \\ F_{ql} &= F\left(\frac{j_{ql}}{R},\frac{2\pi q}{N_2}\right) \end{aligned} \qquad (3.30)$$

Now consider functions in the frequency domain $F(\rho,\psi)$ with an effective band limit $\rho\in\left[0,W_p\right]$, that is the function is zero outside the circle bounded by $\rho\in\left[0,W_p\right]$ in the frequency domain. The relationship approximate between the discrete transform $F(\rho,\psi)$ and the sampled values of the continuous transform $f(r,\theta)$ is shown below

$$F\left(\frac{j_{ql}W_p}{j_{qN_1}},\frac{2\pi q}{N_2}\right)\approx\frac{2\pi}{{W_p}^2N_2}\sum_{k=1}^{N_1-1}\sum_{p=-M}^{M}f\left(\frac{j_{pk}}{W_p},\frac{2\pi p}{N_2}\right)\sum_{n=-M}^{M}\frac{2i^{-n}J_n\left(\frac{j_{nl}j_{nk}}{j_{nN_1}}\right)}{J_{n+1}^2\left(j_{nk}\right)}e^{-i\frac{2\pi np}{N_2}}e^{+i\frac{2\pi nq}{N_2}}$$

(3.31)

The inverse transform is given by

$$f\left(\frac{j_{pk}}{W_p},\frac{2\pi p}{N_2}\right)\approx\frac{{W_p}^2}{2\pi N_2}\sum_{l=1}^{N_1-1}\sum_{q=-M}^{M}F\left(\frac{j_{ql}W_p}{j_{qN_1}},\frac{2\pi q}{N_2}\right)\sum_{n=-M}^{M}\frac{2i^n J_n\left(\frac{j_{nk}j_{nl}}{j_{nN_1}}\right)}{j_{nN_1}^2J_{n+1}^2\left(j_{nl}\right)}e^{-i\frac{2\pi nq}{N_2}}e^{+i\frac{2\pi np}{N_2}}$$

(3.32)

As before, the relationships in equations and give relationships between the sampled values of the original function

$$f_{pk} = f\left(\frac{j_{pk}}{W_p}, \frac{2\pi p}{N_2}\right) \tag{3.33}$$

and sampled values of its continuous 2D transform

$$F_{ql} = F\left(\frac{j_{ql} W_p}{j_{qN_1}}, \frac{2\pi q}{N_2}\right) \tag{3.34}$$

The relationships given by equation , , and , have motivated a definition of a 2D Discrete Fourier transform defined in polar coordinates. This is an attempt to follow the approach taken with the Fourier transform where the Discrete Fourier Transform (DFT) is a transform in its own right, with its own mathematical theory of the manipulated quantities. In the rest of the thesis, the 2D DFT in polar coordinates is presented and its ability to approximate the continuous counterpart is investigated.

3.7 Discretization points

3.7.1 Functions Limits

Let us consider any function in continuous 2D space. A function cannot be limited in both space and spatial frequency (spatial frequency is the frequency domain when the pretransform variables are considered as space variables rather than the usual temporal variables). When implementing a discrete transform for application to a function in continuous 2D space, it is necessary to truncate the function somewhere in both domains so that after the truncation points, the amplitude of the function could be seen as zero or effectively zero. Therefore the concept of effective limit is used here. A function is defined as being 'effectively limited in space by R' means that if $r > R$, then as $r \to \infty$, $f(r) \to 0$ or in other words, the function can be made arbitrarily small or as close to zero as necessary for all $r > R$. The same idea can be applied to the frequency domain.

3.7.2 Space limited function

We assume that the original function that we are interested in is defined over continuous (r, θ) space where $0 \le r \le R$ and $0 \le \theta \le 2\pi$. Based on the definition of equations (3.28) and (3.29), the sampling spaces used for radial and angular sampling points in regular $\vec{r}$ space (r, θ) and $\vec{\omega}$ frequency (ρ, ψ) space are defined as

$$r_{pk} = \frac{j_{pk} R}{j_{pN_1}} \qquad \theta_p = \frac{p2\pi}{N_2} \tag{3.35}$$

and

$$\rho_{ql} = \frac{j_{ql}}{R} \qquad \psi_q = \frac{q2\pi}{N_2} \tag{3.36}$$

where p,k,q,l,n , N_1 , and N_2 are integers such that $-M \le n \le M$, where $2M+1 = N_2$, $1 \le l,k, \le N_1 - 1$ and $-M \le p,q \le M$. Equations (3.35) and (3.36) give the sampling grid in regular (r,θ) and frequency (ρ,ψ) space. Clearly, the density of the sampling points depends on the numbers of points chosen, that is on N_1 and N_2. Also clear is the fact that the grid is not equi-spaced in the radial variable. The sampling grids are plotted below to enable visualization. In the first instance, the polar grids are plotted for the case R =1, $N_1 = 16$ and $N_2 = 15$. These are shown in space (***r*** space) and frequency (***ρ*** space) in Figures 1 and 2 respectively.

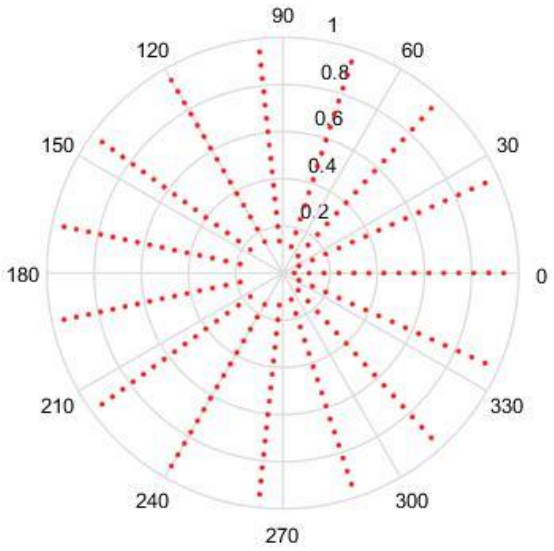

Figure 1 Sampling grid in space domain of a space limited function for R=1, N_1=16 and N_2 = 15

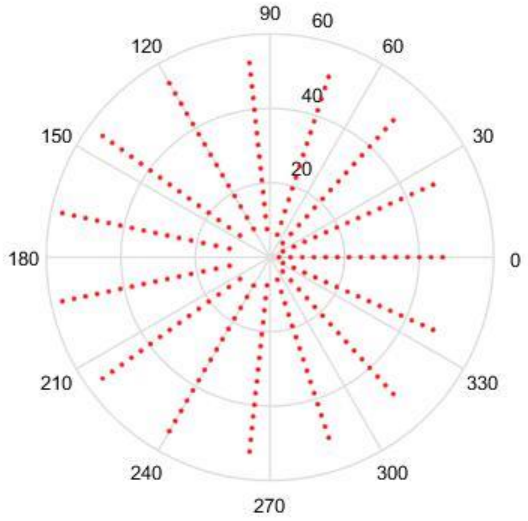

Figure 2 Sampling grid in frequency domain of a space limited function for R=1, N_1=16 and N_2 = 15

Clearly the grids in Figures 1 and 2 are fairly sparse but the low values of N_2 and N_1 have been chosen so that the structure of the sampling points can be easily seen. It can be observed that there is a hole at the center area in both domains which is caused by the special sample points. For higher values of the N_2 and N_1, the grid becomes fairly dense, obtaining good coverage of both spaces, but details are harder to observe. To demonstrate, the polar grids are plotted for the case R =1, $N_1 = 96$ and $N_2 = 95$. These are shown in Figures 3 and 4 respectively.

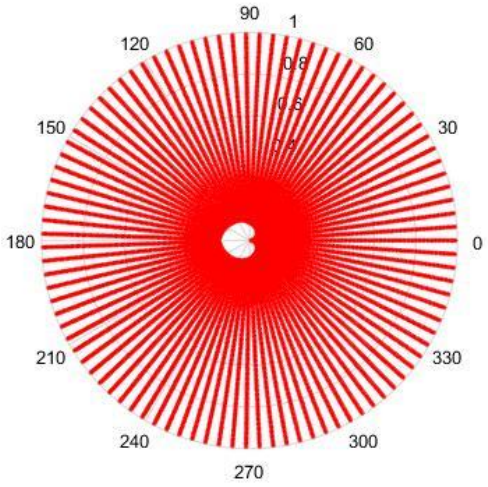

Figure 3 Sampling grid in space domain of a space limited function for R=1, N_1 = 96 and N_2 = 95

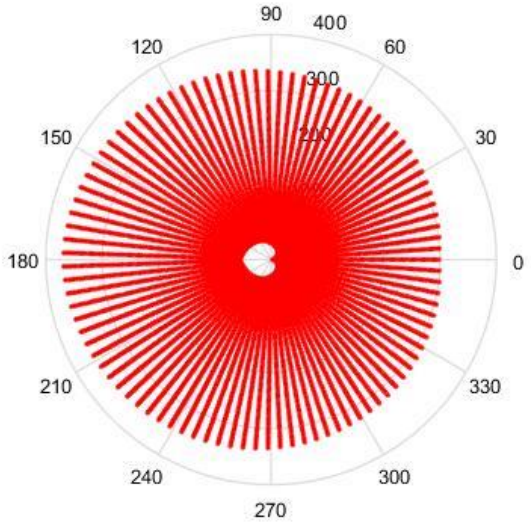

Figure 4 Sampling grid in frequency domain of a space limited function for R=1, N_1 = 96 and N_2 = 95

From Figure 3 and Figure 4, by choosing higher values of N_1 and N_2, the sampling grid becomes denser but there is still a gap in the center area.

3.7.3 Band limited function

Consider the case of a bandlimited functions, such that the function is defined over continuous (ρ,ψ) space where $0 \le \rho \le W_p$ and $0 \le \psi \le 2\pi$ and is effective zero elsewhere (that is the function can be made as close to zero as necessarily, elsewhere in the plane). Based on the motivation provided by equations (3.31) and (3.32), the sampling space used for radial and angular sampling points in regular $\vec{\omega}$ frequency space (ρ,ψ) and $\vec{r}$ space (r,θ) for a bandlimited function are defined as

$$r_{pk} = \frac{j_{pk}}{W_p} \qquad \theta_p = \frac{p2\pi}{N_2} \tag{3.37}$$

and

$$\rho_{ql} = \frac{j_{ql} W_p}{j_{qN_1}} \qquad \psi_q = \frac{q2\pi}{N_2}. \tag{3.38}$$

It can be observed that the sampling points of a frequency limited function are similarly structured to the ones for a space limited function. Hence, the sampling grid should have same shape as before but with the domains reversed (that is, the shape of the spatial grid for the bandlimited function resembles the frequency grid of the

space-limited function and vice versa). The sampling grids are shown below. Similarly to the first instance, the polar grids are plotted for the case $W_p = 1$, $N_1 = 16$ and $N_2 = 15$. In the second case, the polar grids are plotted for the case $W_p = 1$, $N_1 = 96$ and $N_2 = 95$ The grids are shown in Figure 5 to Figure 8.

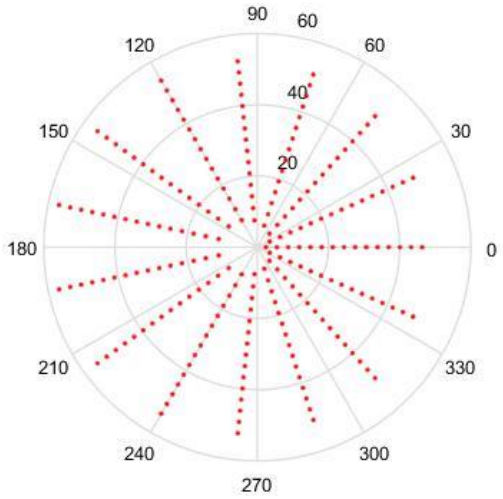

Figure 5 Sampling grid in space domain of a band limited function for W_p=1, N_1=16 and N_2 = 15

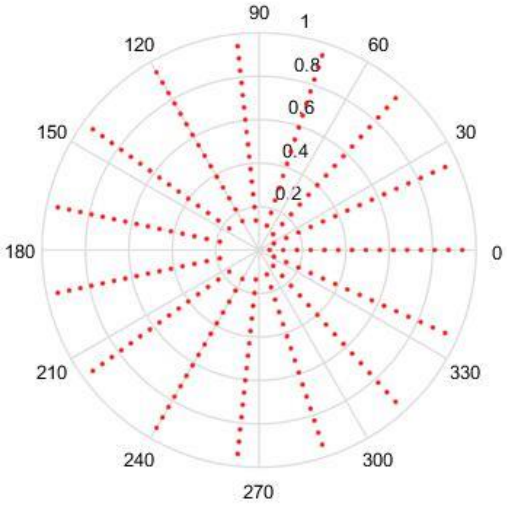

Figure 6 Sampling grid in frequency domain of a band limited function for W_p=1, N_1=16 and N_2 = 15

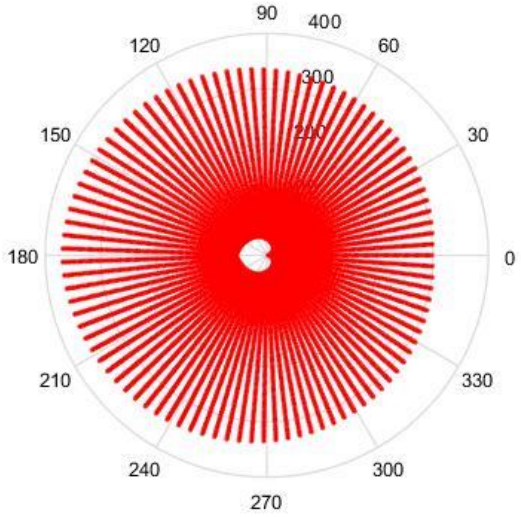

Figure 7 Sampling grid in space domain of a band limited function for W_p=1, N_1=96 and N_2 = 95

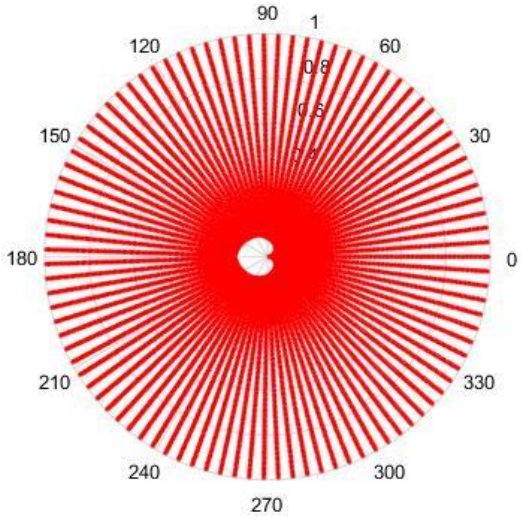

Figure 8 Sampling grid in frequency domain of a band limited function for W_p=1, N_1=96 and N_2 = 95

It can be observed that the sample grid for a band limited function has the same shape as with space limited function but the domains are switched. Moreover, the sample grid for a band limited function also suffers from the problem in that there is a heart-shaped area in the centre could not be covered by the sample grid.

3.8 Approximations to the Bessel function zeros

It is pointed out in [24] that the zeros of $J_n(z)$ are *almost* evenly spaced at intervals of π and that the spacing becomes exactly π in the limit as $z \to \infty$. In fact, it is shown in [24] that a simple asymptotic form for the Bessel function is given by

$$J_n(z) \approx \sqrt{\frac{2}{\pi z}} \cos\left[z - \left(n + \frac{1}{2} \right) \frac{\pi}{2} \right] \tag{3.39}$$

Equation (B.1) becomes a better approximation to $J_n(z)$ as $z \to \infty$. The zeros of the cosine function are at odd multiples of $\pi/2$. Therefore, an approximation to the Bessel zero, j_{pk} is given by

$$j_{pk} - \left(p + \frac{1}{2} \right) \frac{\pi}{2} \approx (2k - 1) \frac{\pi}{2} \tag{3.40}$$

or equivalently

$$j_{pk} \approx \left(2k + p - \frac{1}{2} \right) \frac{\pi}{2}. \tag{3.41}$$

The approximation in equation (B.3) gets better as k gets larger and is also better for smaller p. Numerical simulations with equation (B.3) show that this approximation is an overestimate of the true value.

Using equations (3.35) and (3.36), along with the approximation in equation (B.3), approximate values for the spatial and frequency-spatial grids can be generated. Additionally, these values can be used to generate approximate values of $E^{-}(ql; pk)$ and $E^{+}(ql; pk)$. The details of this analysis are shown in Appendix B. Although the sample grids are well approximated, it was found that the orthogonality properties of $E^{-}(ql; pk)$ and $E^{+}(ql; pk)$ are lost and therefore this was not pursued further. The details are in Appendix B.

3.9 Conclusion

In this Chapter, the discrete 2D Fourier transform with kernel was defined, based on which, the orthogonality of the transform was checked. It was shown that using approximations to the Bessel function zeros will cause the transform to lose

orthogonality. The approach to using the discrete transform to approximate the continuous 2D Fourier transform was also presented. Future numerical tests will be based on this definition.

4 Interpretation of the transform

4.1 Interpretation of the 2D forward DFT in polar coordinates

Let us reconsider equation (3.12) and rewrite it as

$$F_{ql} = \frac{1}{N_2} \sum_{n=-M}^{M} e^{+in\frac{2\pi q}{N_2}} i^{-n} \sum_{k=1}^{N_1-1} \frac{2J_n\left(\frac{j_{nk} j_{nl}}{j_{nN_1}}\right)}{j_{nN_1} J_{n+1}^2(j_{nk})} \left\{ \sum_{p=-M}^{M} f_{pk} e^{-in\frac{2\pi p}{N_2}} \right\} \qquad (4.1)$$

We can think of these as a series of 1D discrete Fourier transforms along with a discrete Hankel transform in the following way. The first step is a forward 1D DFT transforming $f_{pk} \to \overline{f}_{nk}$ where the p subscript is transformed to the n subscript:

$$\overline{f}_{nk} = \sum_{p=-M}^{M} f_{pk} e^{-in\frac{2\pi p}{N_2}} \qquad \text{for } n = -M..M,\ k = 1..N_1 - 1 \qquad (4.2)$$

The overbar is used to indicate a standard 1D DFT. In matrix operations, this is equivalent to stating that each *column* of f_{pk} is DFT'ed to yield $\overline{f}_{nk}$. The second step of equation (4.1) is a discrete Hankel transform of order n, transforming $\overline{f}_{nk} \to \hat{\overline{f}}_{nl}$ so that the k subscript is Hankel transformed to the l subscript:

$$\hat{\overline{f}}_{nl} = \sum_{k=1}^{N_1-1} \frac{2J_n\left(\frac{j_{nk} j_{nl}}{j_{nN_1}}\right)}{j_{nN_1} J_{n+1}^2(j_{nk})} \overline{f}_{nk} \qquad \text{for } n = -M..M,\ l = 1..N_1 - 1 \qquad (4.3)$$

The overhat is used to indicate a Discrete Hankel Transform (DHT), with the DHT as defined in[14]. Using the same transformation matrix notation defined in [14], we define the transformation matrix

$$Y_{l,k}^{nN_1} = \frac{2}{j_{nN_1} J_{n+1}^2(j_{nk})} J_n\left(\frac{j_{nl} j_{nk}}{j_{nN_1}}\right) \qquad 1 \le l, k \le N_1 - 1 \qquad (4.4)$$

Hence equation (4.3) can be written as

$$\hat{\overline{f}}_{nl} = \sum_{k=1}^{N_1-1} Y_{l,k}^{nN_1} \overline{f}_{nk} \qquad \text{for } n = -M..M,\ l = 1..N_1 - 1 \qquad (4.5)$$

In matrix operations, this states that each *row* of $\bar{f}_{nk}$ is DHT'ed to yield $\hat{\bar{f}}_{nl}$. These are now scaled to give the Fourier coefficients of the 2D DFT $\hat{\bar{f}}_{nl} \to \bar{F}_{nl}$ such that

$$\bar{F}_{nl} = i^{-n}\hat{\bar{f}}_{nl} = i^{-n}\sum_{k=1}^{N_1-1} Y_{l,k}^{nN_1}\,\bar{f}_{nk} \qquad \text{for } n=-M..M,\ l=1..N_1-1 \tag{4.6}$$

It is noted that the step in equation (4.6) exactly parallels the continuous form equivalent step where $F_n(\rho) = 2\pi\, i^{-n}\mathbb{H}_n\{f_n(r)\}$, see [20].

The final step of the forward 2D DFT in polar coordinates is then a standard *inverse* 1D DFT, which transforms each *column* of $\bar{F}_{nl} \to F_{ql}$ so that the n subscript is (inverse) transformed to the q subscript via

$$F_{ql} = \frac{1}{N_2}\sum_{n=-M}^{M} \bar{F}_{nl}e^{+in\frac{2\pi q}{N_2}} \qquad \text{for } q=0..N_2-1,\ l=1..N_1-1 \tag{4.7}$$

This last step is a 1D Inverse Discrete Fourier Transform (IDFT) for each *column* of $\bar{F}_{nl}$ to get F_{ql}. This is pointed out since it was shown in [20],[21] that a continuous 2D Fourier transform in polar coordinates is precisely a combination of a Fourier series transform (seen as a transform, transforming the continuous function to its discrete set of Fourier coefficients), a Hankel transform for each Fourier coefficient and then an inverse Fourier series transform (transforming a set of Fourier coefficients back to a continuous function by via the infinite Fourier series summation). Hence, it has been shown here that the proposed 2D-DFT in polar coordinates is also composed of the same group of transformations: a forward DFT, a forward DHT and then an inverse DFT.

4.2 Interpretation of the 2D inverse DFT in polar coordinates

Similarly, the inverse 2D DFT in polar coordinates can be similarly decomposed from equation (3.13) written as

$$f_{pk} = \frac{1}{N_2}\sum_{n=-M}^{M} i^n e^{+i\frac{2\pi np}{N_2}} \sum_{l=1}^{N_1-1} \frac{2J_n\left(\frac{j_{nl}\,j_{nk}}{j_{nN_1}}\right)}{j_{nN_1}J_{n+1}^2(j_{nl})} \left\{ \sum_{q=-M}^{M} F_{ql}e^{-i\frac{2\pi nq}{N_2}} \right\} \tag{4.8}$$

The steps of the inverse 2D DFT are the reverse steps outlined above for the forward 2D DFT. First $F_{ql} \to \bar{F}_{nl}$ via a forward 1D DFT:

$$\bar{F}_{nl} = \sum_{q=M}^{M} F_{ql} e^{-i\frac{2\pi nq}{N_2}} \qquad n = -M..M,\ l = 1..N_1 - 1 \tag{4.9}$$

Then a discrete Hankel transform to obtain $\bar{F}_{nl} \to \hat{\bar{F}}_{nk}$

$$\hat{\bar{F}}_{nk} = \sum_{l=1}^{N_1-1} \frac{2J_n\left(\frac{j_{nl}\, j_{nk}}{j_{nN_1}}\right)}{j_{nN_1} J_{n+1}^2\left(j_{nl}\right)} \bar{F}_{nl} \qquad \text{for } n = -M..M,\ k = 1..N_1 - 1 \tag{4.10}$$

Equation (4.10) can be written as

$$\hat{\bar{F}}_{nk} = \sum_{l=1}^{N_1-1} Y_{k,l}^{nN_1} \bar{F}_{nl} \qquad \text{for } n = -M..M,\ k = 1..N_1 - 1 \tag{4.11}$$

Followed by a scaling operation to obtain $\hat{\bar{F}}_{nk} \to \bar{f}_{nk}$

$$\bar{f}_{nk} = i^{+n} \hat{\bar{F}}_{nk} \qquad \text{for } n = -M..M,\ k = 1..N_1 - 1 \tag{4.12}$$

Again, the step in equation (4.12) parallels the continuous form equivalent which is given by $f_n(r) = \frac{i^n}{2\pi} \mathbb{H}_n\left\{F_n(\rho)\right\}$, see[20].

Then finally an inverse 1D IDFT to obtain $\bar{f}_{nk} \to f_{pk}$

$$f_{pk} = \frac{1}{N_2} \sum_{n=-M}^{M} \bar{f}_{nk} e^{+i\frac{2\pi np}{N_2}} \qquad \text{for } p = -M..M,\ k = 1..N_1 - 1 \tag{4.13}$$

As previously mentioned, this parallels the steps taken for the continuous case, with each continuous operation (Fourier series, Hankel transform) replaced by its discrete counterpart (DFT, DHT).

For both forward and inverse 2D-DFT, the sequence of operations is a DFT of each column of the starting matrix, followed by a DHT of each row, a term-by-term scaling, followed by an IDFT of each column.

4.3 Interpretation of the sampled forward transform in Matlab terms

To use the built-in Matlab function fft, a few operations are required. First Define matlab-friendly indices $p' = p + (M+1)$ and $n' = n + (M+1)$ so that $n = -M..M$ becomes $n' = 1..2M+1 = 1..N_2$ (since $2M+1 = N_2$). Hence, if the matrix **f** with entries $f_{p'k}$ is defined, where $p' = 1..N_2$, $k = 1..N_1 - 1$, then equation (4.2) can be written as the matlab-defined DFT as

$$\overline{f}_{n'k} = \sum_{p'=1}^{N_2} f_{pk} e^{\frac{-2\pi i(p'-1-M)(n'-1-M)}{N_2}} \tag{4.14}$$

The definition of DFT in Matlab can be written as

$$\overline{f}_{n'k} = \sum_{p'=1}^{N_2} f_{p'k} e^{\frac{-2\pi i(p'-1)(n'-1)}{N_2}} \tag{4.15}$$

Since the relationship $\sum_{p'=1}^{N_2} f_{p'k} e^{\frac{-2\pi i(p'-1)(n'-1-M)}{N2}} = \sum_{p'=1}^{N_2} f_{pk} e^{\frac{-2\pi i(p'-1-M)(n'-1-M)}{N2}}$ is valid, we can sample the original function f_{pk} and put it in the matrix $f_{p'k}$ then shift the matrix $f_{p'k}$ by $M+1$ along the column direction. In Matlab, the function $circshift(A, K, dim)$ can be used, which circularly shifts the values in array A by K positions along dimension dim. Inputs K and dim must be scalars. Specifically, $\dim = 1$ indicates the columns of matrix A and $\dim = 2$ indicates the rows of matrix A. Hence, equation (4.14) can be written as

$$\overline{f}_{n'k} = fft\left(circshift\left(f_{p'k}, M+1, 1\right), N_2, 1\right) \tag{4.16}$$

In matrix operations, this is equivalent to stating that each *column* of $f_{p'k}$ is DFT'ed to yield $\overline{f}_{n'k}$.

The second step of equation (4.1) is a discrete Hankel transform of order n, transforming $\overline{f}_{n'k} \rightarrow \hat{\overline{f}}_{n'l}$ so that the k subscript is Hankel transformed to the l subscript. In order to relate the order n to the index n', we need to shift $\overline{f}_{n'k}$ by $-(M+1)$ along column direction so that the order ranges from $-M$ to M.

$$\hat{\bar{f}}_{n'l} = \sum_{k=1}^{N_1-1} \frac{2J_n\left(\frac{j_{nk}j_{nl}}{j_{nN_1}}\right)}{j_{nN_1}J_{n+1}^2(j_{nk})} circshift\left(\bar{f}_{n'k}, -(M+1), 1\right) \quad \begin{cases} \text{for } n' = 1..N_2, \ l = 1..N_1 - 1 \\ \text{where } n = n' - (M+1) \end{cases}$$

(4.17)

By using the Hankel transform matrix defined in [14], equation(4.17) can be rewritten as

$$\hat{\bar{f}}_{n'l} = circshift\left(\bar{f}_{n'k}, -(M+1), 1\right)\left(Y_{l,k}^{nN_1}\right)^T \quad \begin{cases} \text{for } n' = 1..N_2, \ l = 1..N_1 - 1 \\ \text{where } n = n' - M - 1 \end{cases}$$

(4.18)

In matrix operations, this states that each *row* of $\bar{f}_{n'k}$ is DHT'ed to yield $\hat{\bar{f}}_{n'l}$. These are now scaled to give the Fourier coefficients of the 2D DFT $\hat{\bar{f}}_{n'l} \to \bar{F}_{n'l}$. In order to proceed to an inverse DFT in the next step, it is necessary to shift the matrix by $M+1$ along the column direction after scaling:

$$\bar{F}_{n'l} = circshift\left(\frac{j_{nN_1}}{2\pi R^2} i^{-n} \hat{\bar{f}}_{n'l}, M+1, 1\right) \quad \begin{cases} \text{for } n' = 1..N_2, \ l = 1..N_1 - 1 \\ \text{where } n = n' - (M+1) \end{cases}$$

(4.19)

This last step is a 1D IDFT for each *column* of $\bar{F}_{n'l}$ to obtain F_{ql}. Using $2M+1 = N_2$, and $q' = q+1+M$, equation (4.7) can be written as

$$\begin{aligned} F_{q'l} &= \frac{1}{N_2}\sum_{n'=1}^{N_2} \bar{F}_{nl} e^{+i(n'-M-1)\frac{2\pi(q'-1-M)}{N_2}} \qquad \text{for } q' = 1..N_2, \ l = 1..N_1 - 1 \\ &= \frac{1}{N_2}\sum_{n'=1}^{N_2} \bar{F}_{n'l} e^{+i(n'-1)\frac{2\pi(q'-1-M)}{N_2}} \\ &= circshift\left(ifft\left(\bar{F}_{n'l}, N_2, 1\right), -(M+1), 1\right) \end{aligned} \qquad (4.20)$$

4.4 Interpretation of the sampled inverse transform in Matlab terms

Similarly, matlab-friendly indices $q' = q + (M+1)$ and $n' = n + (M+1)$ are also defined. Hence, if the matrix F with entries $F_{q'l}$ is defined, where

$q' = 1..N_{2,}\ l = 1..N_1 - 1$, it then follows that equation (4.9) can be written as the matlab-defined DFT as

$$\begin{aligned} \bar{F}_{n'l} &= \sum_{q'=1}^{N_2} F_{ql} e^{-i(n'-M-1)\frac{2\pi(q'-1-M)}{N_2}} \qquad for\ n' = 1..N_2,\ l = 1..N_1 - 1 \\ &= \sum_{q'=1}^{N_2} F_{q'l} e^{-i(n'-M-1)\frac{2\pi(q'-1)}{N_2}} \end{aligned} \tag{4.21}$$

If the original function can be sampled as F_{ql} and then put into matrix $F_{q'l}$, then we need an *circshift* operation. So equation (4.21) can be written as

$$\bar{F}_{n'l} = fft\left(circshift(F_{q'l}, M+1,1), N_2, 1\right) \tag{4.22}$$

Subsequently, a discrete Hankel transform of order n is required, transforming $\bar{F}_{n'l} \to \hat{\bar{F}}_{n'l}$ so that the l subscript is Hankel transformed to the k subscript. To achieve this, *circshift* is also needed here.

$$\hat{\bar{F}}_{n'k} = circshift\left(\bar{F}_{n'l}, -(M+1), 1\right)\left(Y_{k,l}^{nN_1}\right)^T \qquad \begin{cases} \text{for } n' = 1..N_2,\ l = 1..N_1 - 1 \\ \text{where } n = n' - M - 1 \end{cases}$$

(4.23)

This is followed by a scaling operation to obtain $\hat{\bar{F}}_{n'k} \to \bar{f}_{n'k}$ and then a *circshift* by $(M+1)$ so that

$$\bar{f}_{n'k} = circshift\left(\frac{j_{nN_1}}{2\pi R^2} i^{+n} \hat{\bar{F}}_{n'k}, (M+1), 1\right) \qquad \begin{cases} \text{for } n' = 1..N_2,\ k = 1..N_1 - 1 \\ \text{where } n = n' - \left(M+1\right) \end{cases}$$

(4.24)

This last step is a 1D IDFT for each *column* of $\bar{f}_{n'k}$ to get $f_{p'k}$. Using $2M+1 = N_2$, and $p' = p+1$, equation (4.13) can be written as

$$
\begin{aligned}
f_{p'k} &= \frac{1}{N_2}\sum_{n'=1}^{N_2} \bar{f}_{nk} e^{+i(n'-M-1)\frac{2\pi(p'-1-M)}{N_2}} \qquad \text{for } p' = 1..N_2,\ \ k = 1..N_1 - 1 \\
&= \frac{1}{N_2}\sum_{n'=1}^{N_2} \bar{f}_{n'k} e^{+i\frac{2\pi(n'-1)(p'-1-M)}{N_2}} \\
&= circshift\left(ifft\left(\bar{f}_{n'k}, N_2, 1\right), -(M+1), 1\right)
\end{aligned}
\tag{4.25}
$$

4.5 Conclusion

In this chapter, the interpretation of the discrete 2D Fourier transform in polar coordinates as three operations in sequence was proposed. Based on this interpretation as a sequence of Discrete Fourier Transform, Discrete Hankel Transform and Inverse Discrete Fourier Transform, a Matlab-friendly definition of the transform was shown.

5 Sample Grid Analysis

From Chapter 4, it can be seen that the 2D-Fourier Transform can be interpreted as a Discrete Fourier Transform in the angular direction, a Discrete Hankel Transform in the radial direction and then an inverse Discrete Fourier Transform in the angular direction. So the sample size in the angular direction could have been decided by the Nyquist sampling theorem [25], which states that

$$f_s > 2 f_{\max} \tag{5.1}$$

where f_s is the sample frequency and $f_{\max}$ is the highest frequency or band limit.

For instance, if the function in angular direction is defined as

$$f = \sin(\omega\theta) \tag{5.2}$$

where ω (rad/s) is the angular frequency. $f_{\max}$ can be derived by

$$f_{\max} = \frac{\omega}{2\pi} \tag{5.3}$$

The sample frequency in this case must be

$$f_s > \frac{\omega}{\pi} \tag{5.4}$$

If we define the period as P, it then follows that

$$N_2 = f_s P \tag{5.5}$$

Since the period of a sine function is 2π, equation (5.5) can be rewritten as

$$N_2 > 2\omega \tag{5.6}$$

Therefore, we need at least $N_2 = 2\omega$ points to sample a sine signal of frequency ω.

In the radial direction, the necessary relationship for Discrete Hankel Transform is given by [14]

$$W_p = \frac{j_{nN}}{R} \tag{5.7}$$

where W_p is the effective band-limit, R is the effective space limit and j_{nN} is the N^{th} zero of $J_n(r)$. In 2D Fourier Transform, since $0 \le p \le N_2 - 1$, the order of the Bessel zero ranges from 0 to $N_2 - 1$, the relationship needed becomes

$$min(j_{pN_1}) \ge W_p R \tag{5.8}$$

The relationships $j_{nN} = j_{-nN}$ and $j_{0N_1} < j_{\pm 1N_1} < j_{\pm 2N_1} < ... < j_{\pm MN_1}$ are valid [26], hence equation (5.8) can be written as

$$j_{0N_1} \ge W_p R \tag{5.9}$$

Intuitively, more sample points lead to more information captured, which gives an expectation that increasing N_1 or N_2 individually will give a better sample grid coverage. However, it can be seen from Figure 1-4 that there is a gap in the center of the sample grid. From equation (3.35) , the area of the gap in the center is related to the ranges of p and k, that is N_2 and N_1 . In the sections below, it is assumed that the sampling theorem is already satisfied (that is, an appropriate space and band limit is selected) and the relationship between N_2 , N_1 and the area of the gap will be discussed.

5.1 Space limited function

In this section, it is assumed that the function is a space limited function, defined in $r \in [0, R]$. The sample points are defined as equation (3.35) in the space domain and (3.36) in the frequency domain. In the following a relationship between N_2 , N_1 and the area of the gap in both domains is discussed.

5.1.1 Sample grid in the space domain

In space domain, the effective limit in space domain R is fixed. To analyze how the values of N_2 and N_1 affect the coverage of the grid in space domain, consider

$$A_r = \frac{\pi R^2 - \pi \bar{r}^2}{\pi R^2} \cdot 100\% \tag{5.10}$$

where $\bar{r}$ denotes the average radius of the gap. A_r as defined in equation (5.10) is a measure of the 'grid coverage'. For example, if the average radius of the center gap is

zero, then A_r would be 100%, that is, complete coverage. Based on the observation of Figure 1 and Figure 3, the relationship $r_{01} < r_{\pm 11} < r_{\pm 21} < r_{\pm M1}$ is valid. Therefore, from equation (3.35), the average area of the gap is given by

$$\begin{aligned} \bar{r} &= \frac{(r_{01} + r_{M1})}{2} \\ &= \frac{\left(\frac{j_{01}}{j_{0N_1}} R + \frac{j_{M1}}{j_{MN_1}} R \right)}{2} \end{aligned} \tag{5.11}$$

Hence, equation (5.10) can be written as

$$A_r = \left[1 - \frac{\left(\frac{j_{01}}{j_{0N_1}} + \frac{j_{M1}}{j_{MN_1}} \right)^2}{4} \right] \cdot 100\% \tag{5.12}$$

Table 1 shows the different values of A_r as the values of N_1 and N_2 are changed.

Table 1 A_r with respect to different values of N_1 and N_2 (R is fixed)

N1 / N2	15	75	150	300
15	$A_r = 98.48\%$	$A_r = 99.92\%$	$A_r = 99.98\%$	$A_r = 99.99\%$
75	$A_r = 93.78\%$	$A_r = 99.36\%$	$A_r = 99.81\%$	$A_r = 99.95\%$
151	$A_r = 90.14\%$	$A_r = 98.42\%$	$A_r = 99.46\%$	$A_r = 99.84\%$
301	$A_r = 86.17\%$	$A_r = 96.58\%$	$A_r = 98.59\%$	$A_r = 99.51\%$

From Table 1, it can be seen that increasing N_1 (sample size in the radial direction) tends to increase the coverage. Since effective space limit R is fixed, from equation (5.9), it follows that increasing N_1 is actually increasing the effective band limit. However, increasing N_2 (sample size in angular direction) will result in a bigger gap in the center of the grid, which then decreases the coverage.

5.1.2 Sample grid in the frequency domain

Similarly, coverage of the grid in the frequency domain is defined as

$$A_\rho = \frac{\pi W_p^{\,2} - \pi \bar{\rho}^2}{\pi W_p^{\,2}} \cdot 100\% \tag{5.13}$$

where $\bar{\rho}$ denotes the average radius of the gap. Since

$$\begin{aligned} \bar{\rho} &= \frac{(\rho_{01} + \rho_{M1})}{2} \\ &= \frac{(j_{01} + j_{M1})}{2R} \end{aligned} \tag{5.14}$$

Then, it follows that equation (5.13) can be written as

$$\begin{aligned} A_\rho &= \left[1 - \frac{\left(\frac{j_{01} + j_{M1}}{2R} \right)^2}{W_p^{\,2}} \right] \cdot 100\% \\ &= \left[1 - \frac{(j_{01} + j_{M1})^2}{4R^2 W_p^{\,2}} \right] \cdot 100\% \end{aligned} \tag{5.15}$$

From equation (5.15), it can be observed that the sample grid coverage in the frequency domain is affected by R , W_p and M but is unaffected by N_1 . In order to get a better grid coverage with fixed W_p , R and M can be adjusted. Table 2 shows the grid coverage A_ρ for different values of R and N_2.

Table 2 A_ρ with respect to different values of R and N_2 (W_p=10 is fixed)

R / N_2	15	75	150	300
15	$A_\rho = 99.80\%$	$A_\rho = 99.99\%$	$A_\rho = 100.00\%$	$A_\rho = 100.00\%$
75	$A_\rho = 97.66\%$	$A_\rho = 99.91\%$	$A_\rho = 99.98\%$	$A_\rho = 99.99\%$
151	$A_\rho = 91.88\%$	$A_\rho = 99.68\%$	$A_\rho = 99.92\%$	$A_\rho = 99.98\%$
301	$A_\rho = 70.67\%$	$A_\rho = 98.83\%$	$A_\rho = 99.71\%$	$A_\rho = 99.93\%$

From Table 2, the conclusion in the frequency domain is: when the effective band limit is fixed, increasing R (effective space limit) tends to increase the coverage in the frequency domain, while increasing N_2 (sample size in the angular direction) decreases the coverage. However, from equation (5.9) it should be noted that to satisfy the sampling theorem, increasing R with fixed W_p requires an increase in N_1 at the same time.

5.2 Band limited function

In this section, we suppose the function we have is an effectively band limited function defined in $\rho \in [0, W_p]$. The sample points are defined as equation (3.37) in space domain and (3.38) in frequency domain. Discuss about relationship between N_2 , N_1 and the area of the gap in both domain.

5.2.1 Sample Grid in the space domain

The same definition of coverage of the grid in space domain will be used as given in equation (5.10). Since the sample points of a band limited function are defined by equation (3.37), the average radius of the gap can be defined as

$$\begin{aligned} \bar{r} &= \frac{(r_{01} + r_{M1})}{2} \\ &= \frac{\left(\frac{j_{01}}{W_p} + \frac{j_{M1}}{W_p} \right)}{2} \end{aligned} \tag{5.16}$$

Therefore, the coverage of the grid in space domain can be written as

$$\begin{aligned} A_r &= \left[1 - \frac{\left(\frac{j_{01} + j_{M1}}{2W_p} \right)^2}{R^2} \right] \cdot 100\% \\ &= \left[1 - \frac{(j_{01} + j_{M1})^2}{4{W_p}^2 R^2} \right] \cdot 100\% \end{aligned} \tag{5.17}$$

It can be observed that the grid coverage in the space domain of a band limited function is the same as the grid coverage in the frequency domain of space limited function.

5.2.2 Sample Grid in frequency domain

The coverage of the grid in the frequency domain of a band limited function is defined by equation (5.13). With sample points defined in Equation (3.38), the average radius of the gap can be defined as

$$\begin{aligned}\bar{\rho} &= \frac{(\rho_{01} + \rho_{M1})}{2} \\ &= \frac{\left(\frac{j_{01}}{j_{0N_1}} W_p + \frac{j_{M1}}{j_{MN_1}} W_p \right)}{2}\end{aligned} \tag{5.18}$$

The coverage of the grid in frequency domain can be written as

$$A_\rho = \left[1 - \frac{\left(\frac{j_{01}}{j_{0N_1}} + \frac{j_{M1}}{j_{MN_1}} \right)^2}{4} \right] \cdot 100\% \tag{5.19}$$

It can be observed the grid coverage in the frequency domain of band limited function is the same as the grid coverage in the space domain of space limited function.

5.3 Conclusion

Based on the discussion above, the following conclusions can be made:

1. Increasing N_2 tends to decrease sampling grid coverage in both domains. Increasing N_1 tends to increase sampling coverage in the space domain for a space limited function and in the frequency domain for a frequency limited function. So if a signal changes sharply in the angular direction such that large values of N_2 are needed, a large value of N_1 is also needed to compensate for the effect of increasing N_2 on the grid coverage.
2. For a space-limited function, if it has a lot of energy at the origin in the space domain, a large value of N_1 will be required to ensure that the sample grid gets as close to the origin as possible in the space domain. If the function has a

lot of energy at the origin in the frequency domain, a large value of both N_1 and R will be required to ensure adequate grid coverage.

3. For a bandlimited function, if it has a lot of energy at the origin in the frequency domain, a large value of N_1 will be needed to ensure the sample grid gets as close to the origin as possible in the frequency domain. If the function has a lot of energy at the origin in the space domain, large values of both N_1 and W_p are required.

6 Discrete 2D Fourier Transform test and results

6.1 Method for testing the Algorithm

In this section, the 2D discrete Fourier transform is evaluated for its ability to estimate the continuous Fourier transform at the selected special sampling points in the spatial and frequency domains.

6.1.1 Accuracy

In order to test accuracy of the 2D-DFT and 2D-IDFT to calculate approximate the continuous counterpart, the dynamic error has been used. It is defined as [6]

$$E(\mathrm{v}) = 20\log_{10}\left[\frac{|C(\mathrm{v}) - D(\mathrm{v})|}{\max|D(\mathrm{v})|}\right] \tag{6.1}$$

where $C(\mathrm{v})$ is the continuous forward or inverse 2D-Fourier transform and $D(\mathrm{v})$ is the values obtained from the discrete counterpart. The dynamic error is defined as the ratio of the absolute error to the maximum amplitude of the function, which is calculated on a log scale. Therefore, a large negative value represents an accurate discrete transform. The dynamic error is used instead of the percentage error in order to avoid division by zero.

6.1.2 Precision

The precision of the algorithm is an important evaluation criterion, which is tested by sequentially performing a pair of forward and inverse transforms and comparing the result to the original function. High precision indicates that the transform does not add much error by the calculations. An average of absolute error of each sample points between the original function and the calculated counterpart was used to measure the precision. It is given by

$$\varepsilon = \frac{1}{(N_1 - 1)\cdot N_2} \sum_{n=1}^{(N_1-1)\cdot N_2} \left| f - f^* \right| \tag{6.2}$$

where f is the original function and f^* is the calculated counterpart. An ideal precision would result in the absolute error being zero.

6.2 Test Functions

To test the transform for both accuracy and precision, functions with different properties are chosen. Functions in both domains are plotted and if they are space limited or band limited is decided by observation.

6.2.1 Gaussian

The first function chosen for evaluation is a circular symmetric function which is Gaussian in the radial direction. The function in the space domain is defined as

$$f(r,\theta) = e^{-a^2 r^2} \tag{6.3}$$

where a is some real constant. Since the function is circularly symmetric, the 2D-DFT is a zeroth-order Hankel Transform [27] and can be written as

$$F(\rho,\psi) = \frac{\pi}{a^2} e^{\frac{-\rho^2}{4a^2}} \tag{6.4}$$

The graphs for the original function and its continuous 2D-DFT (which is also a Gaussian) are plotted with $a = 1$ and shown in Figure 9.

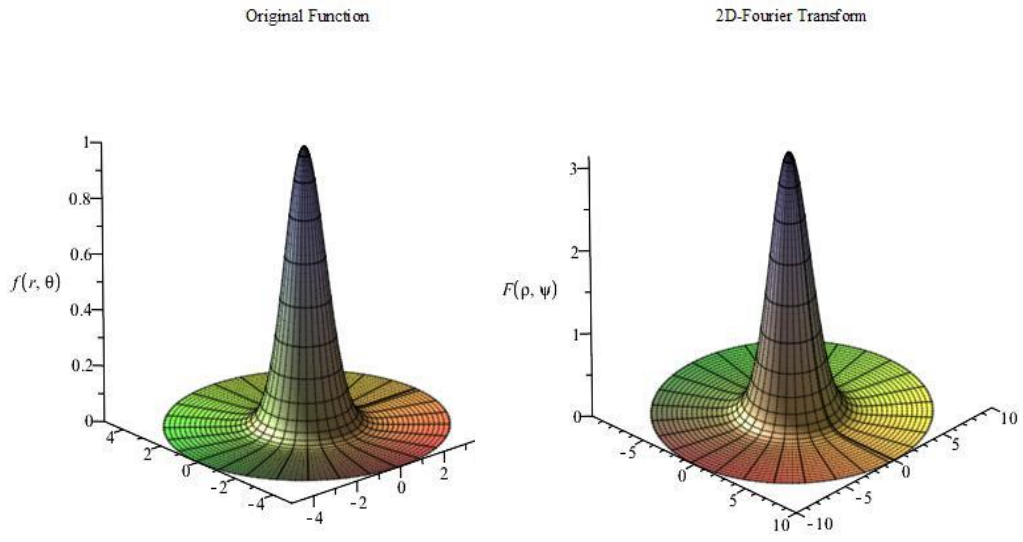

Figure 9 the original Gaussian function and its 2D-Fourier Transform

From Figure 9, the function is circular symmetric in the angular direction and fairly smooth in the radial direction. Moreover, the function can be considered as an effectively space limited function or an effectively band limited function. For the

purposes of testing it, it shall be considered as a space limited function and equations (3.28) and (3.29) will be used to proceed with the forward and inverse transform in sequence.

To perform the transform following variables need to be chosen: N_2, R and N_1.

In the angular direction, since the function in the spatial domain is circularly symmetric, N_2 can be chosen to be small. Thus, $N_2 = 15$ is chosen.

In the radial direction, from plotting the function, it can be seen that the effective space limit can be taken to be $R = 5$ and the effective band limit can be taken to be $W_p = 10$. From equation (5.9), $j_{0N_1} \geq R \cdot W_p = 50$. Therefore, $N_1 = 17$ is chosen. However, most of the energy of the function in in both the space and frequency domains is located in the center near the origin. Based on the discussion in Chapter 5, relatively large values of R and W_p are needed. The effective space limit $R = 40$ and effective band-limit $W_p = 30$ are thus chosen, which gives $j_{0N_1} \geq R \cdot W_p = 1200$. Therefore $N_1 = 383$ is chosen to satisfy this constraint. Both cases ($N_1 = 17$ and $N_1 = 383$) are tested in following.

6.2.1.1 Forward Transform

Test results with $R = 5$, $N_1 = 17$ are shown in Figure 10 and Figure 11.

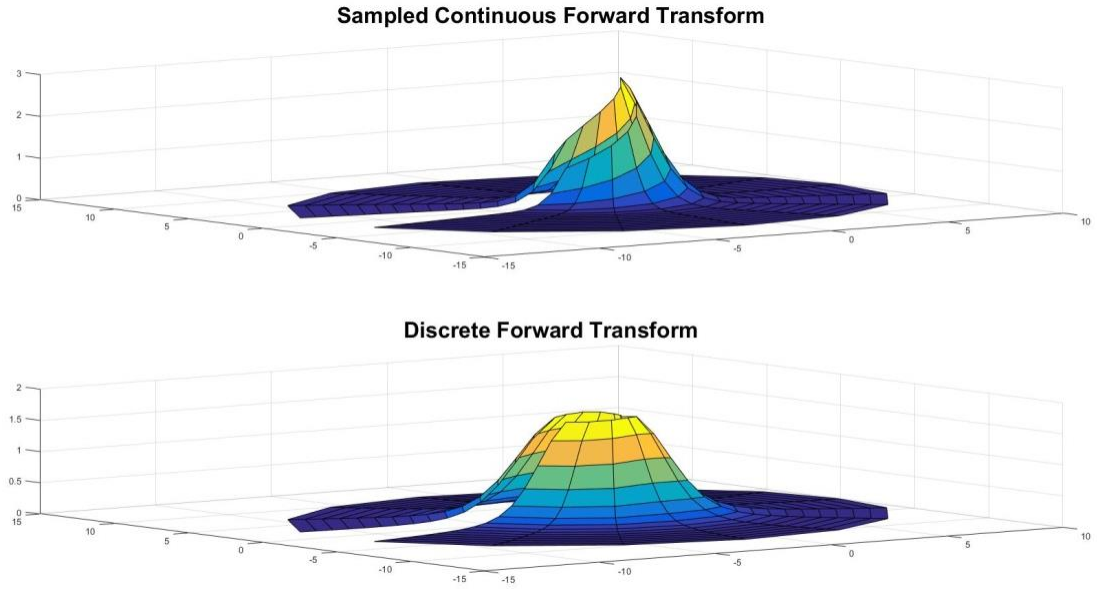

Figure 10 Sampled continuous forward transform and discrete forward transform of the Gaussian function

with R=5, N_2=15, N_1=17

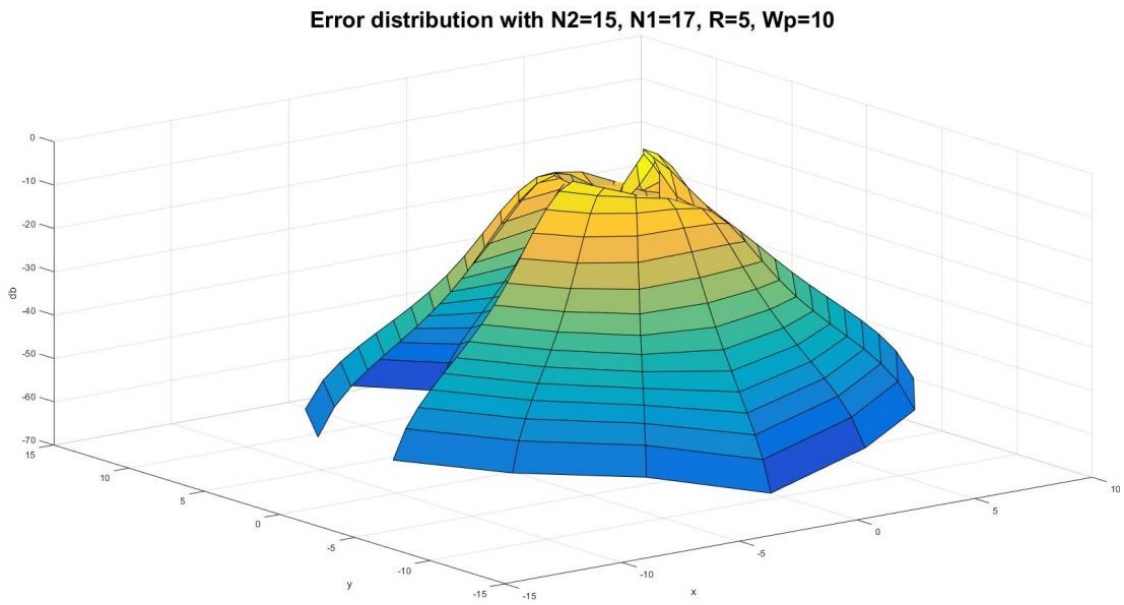

Figure 11 The error distribution of the forward transform of Gaussian Function with R=5, N_2=15, N_1=17

From Figure 11, it can be observed that the error gets bigger at the center, which is as expected because the sampling grid shows that the sampling points can never get to the origin. The maximum value of the error is $E_{\max} = -0.9115 dB$ and this occurs at the center. The average error is $E_{avg.} = -30.4446 dB$.

Test results with $R = 40$, $N_1 = 383$ are shown in Figure 12 and Figure 13 . Similar to the previous case, the error gets bigger at the center as expected. However, the maximum value of the error is $E_{\max} = -8.3842 dB$ and this occurs at the center. The average value of the error is $E_{avg.} = -63.8031 dB$. Clearly, the test with $R = 40$, $N_1 = 383$ gives a better approximation which verifies the discussion in Chapter 5.

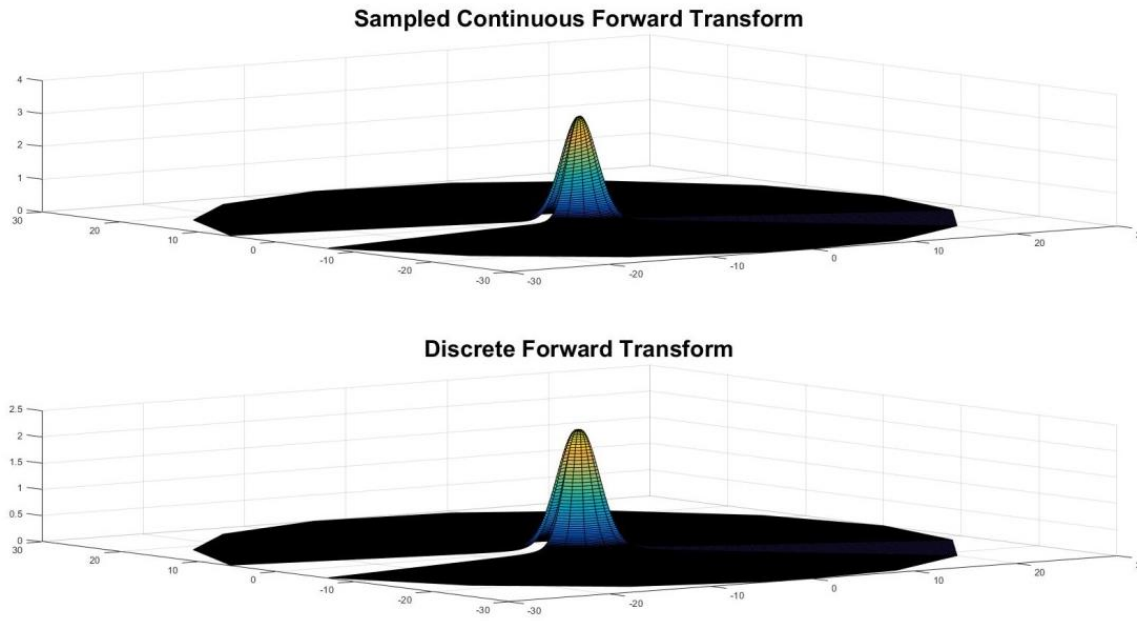

Figure 12 Sampled Continuous forward transform &. Discrete forward transform of Gaussian Function with R=40, N_2=15, N_1=383

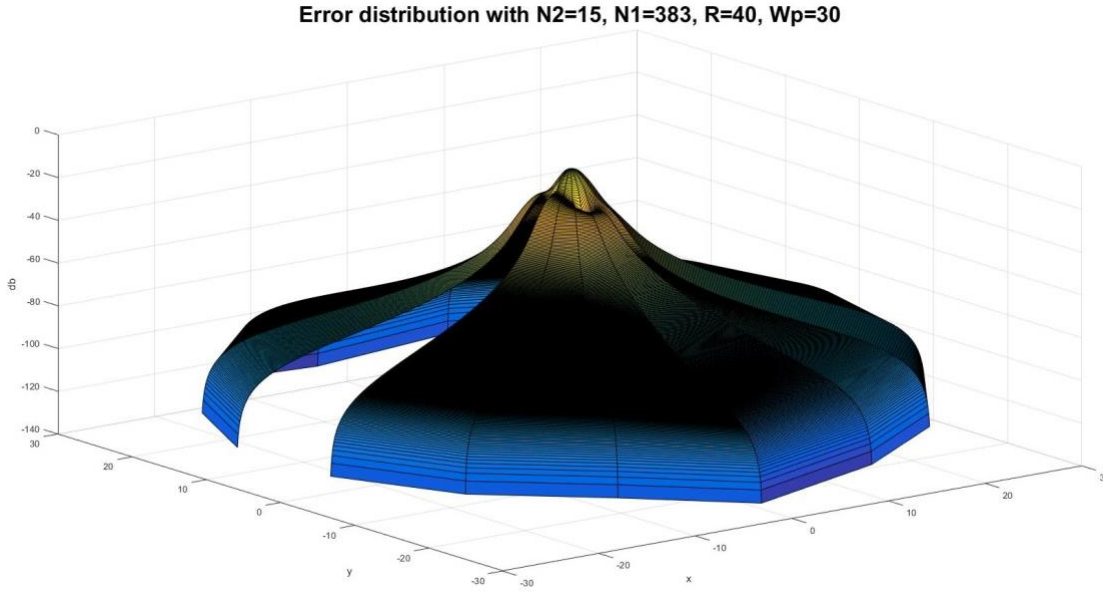

Figure 13 The error distribution of the forward transform of Gaussian Function with R=40, N_2=15, N_1=383

With $R = 40$, Table 3 shows the errors with respect to different value of N_1 and N_2, from which Figure 14 and Figure 15 show the trend.

Table 3 Error (dB) of forward transform of Gaussian Function with R=40, different value of N_1 and N_2

N2 \ N1	283	333	383	433	483
3	$E_{\max.} = -21.6$ $E_{avg.} = -71.3$	$E_{\max.} = -23.0$ $E_{avg.} = -76.9$	$E_{\max.} = -24.3$ $E_{avg.} = -81.8$	$E_{\max.} = -25.4$ $E_{avg.} = -86.0$	$E_{\max.} = -26.3$ $E_{avg.} = -89.8$
7	$E_{\max.} = -12.9$ $E_{avg.} = -62.6$	$E_{\max.} = -14.4$ $E_{avg.} = -68.3$	$E_{\max.} = -15.7$ $E_{avg.} = -73.2$	$E_{\max.} = -16.9$ $E_{avg.} = -77.5$	$E_{\max.} = -17.8$ $E_{avg.} = -81.4$
15	$E_{\max.} = -5.4$ $E_{avg.} = -53.1$	$E_{\max.} = -7.0$ $E_{avg.} = -58.9$	$E_{\max.} = -8.4$ $E_{avg.} = -63.8$	$E_{\max.} = -9.6$ $E_{avg.} = -68.1$	$E_{\max.} = -10.6$ $E_{avg.} = -72.0$
31	$E_{\max.} = 2.3$ $E_{avg.} = -42.0$	$E_{\max.} = 0.5$ $E_{avg.} = -47.6$	$E_{\max.} = -1.0$ $E_{avg.} = -52.5$	$E_{\max.} = -2.3$ $E_{avg.} = -56.9$	$E_{\max.} = -3.4$ $E_{avg.} = -60.7$
61	$E_{\max.} = 9.7$ $E_{avg.} = -32.5$	$E_{\max.} = 7.9$ $E_{avg.} = -37.5$	$E_{\max.} = 6.4$ $E_{avg.} = -42.0$	$E_{\max.} = 5.0$ $E_{avg.} = -46.1$	$E_{\max.} = 3.8$ $E_{avg.} = -49.8$

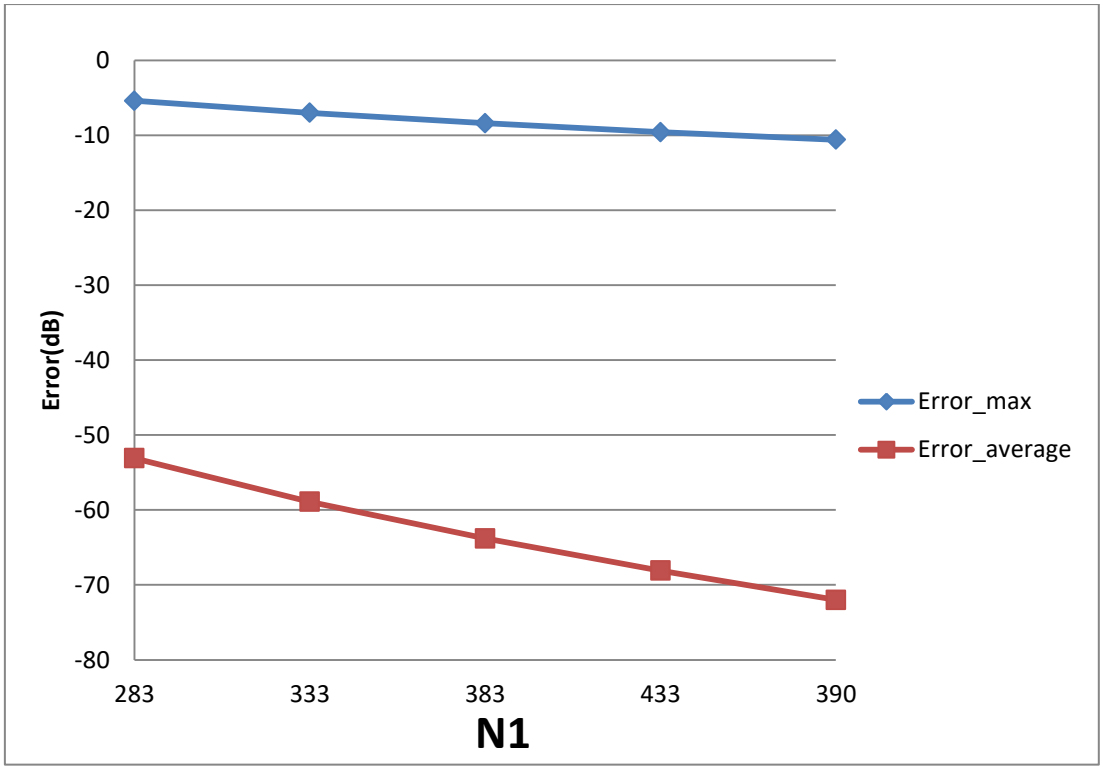

Figure 14 Error of forward transform of Gaussian Function with fixed N_2 (15) and varying N_1

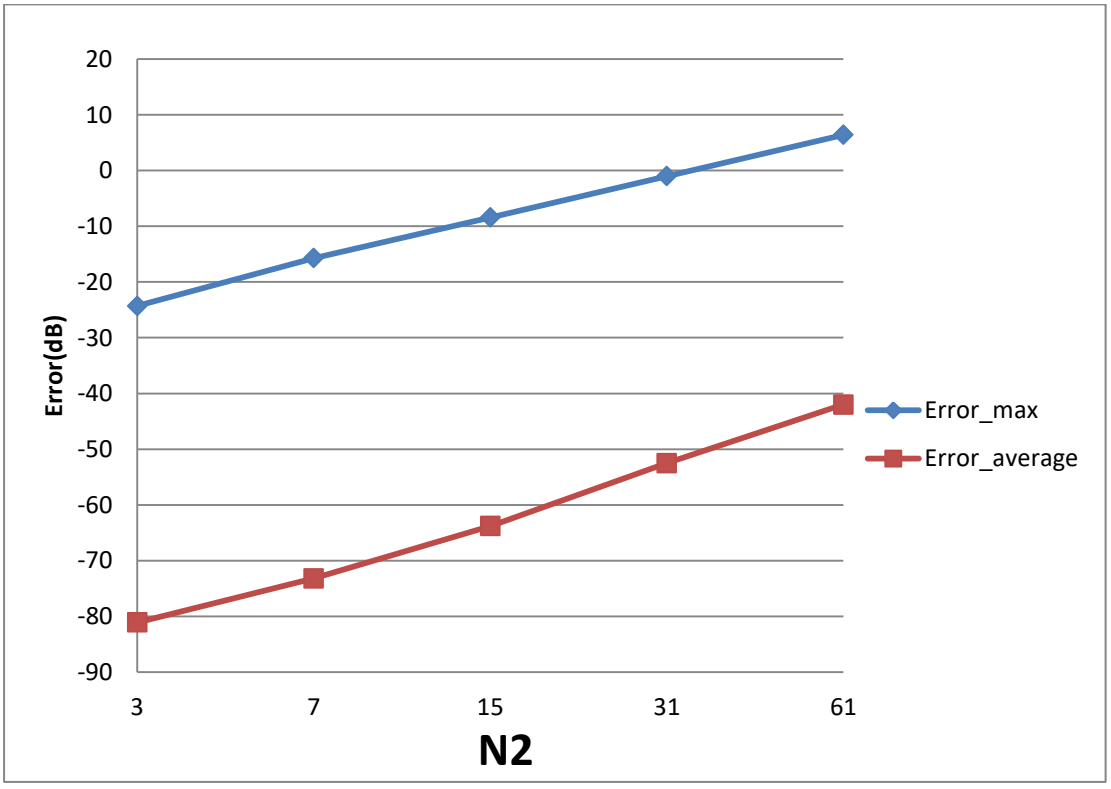

Figure 15 Error of forward transform of Gaussian Function with fixed N_1 (383) and varying N_2

From Figure 14, it can be seen that when N_1 individually is less than the minimum of 383 obtained from the sampling theorem, increasing N_1 will lead to less error, as expected. When N_1 is bigger than 383, increasing N_1 still decreases the error which verifies the discussion about sample grid coverage in Chapter 5. Increasing N_1 tends to increase the sample grid coverage and capture more information at the center area and leads to less error.

From Figure 15, increasing N_2 alone (that means, without a corresponding increase in N_1) leads to larger $Error_{\max}$ and $Error_{average}$. Although at first counterintuitive, this result is actually reasonable because the function is radially symmetric which implies that $N_2 = 1$ should be sufficient based on sampling theorem for the angular direction. Therefore, increasing N_2 will not lead to a better approximation. Moreover, from the discussion of the sample grid coverage in Chapter 5, the sampling grid coverage in both domains gets worse when N_2 gets bigger because more information from the center is lost. This problem can be solved by increasing N_1 at the same time, but it could be computationally time consuming. Therefore, choosing N_2 properly is very important from the standpoint of accuracy and computational efficiency.

6.2.1.2 Inverse Transform

Test results for the inverse transform with $R = 5$, $N_1 = 17$ are shown in Figure 16 and Figure 17.

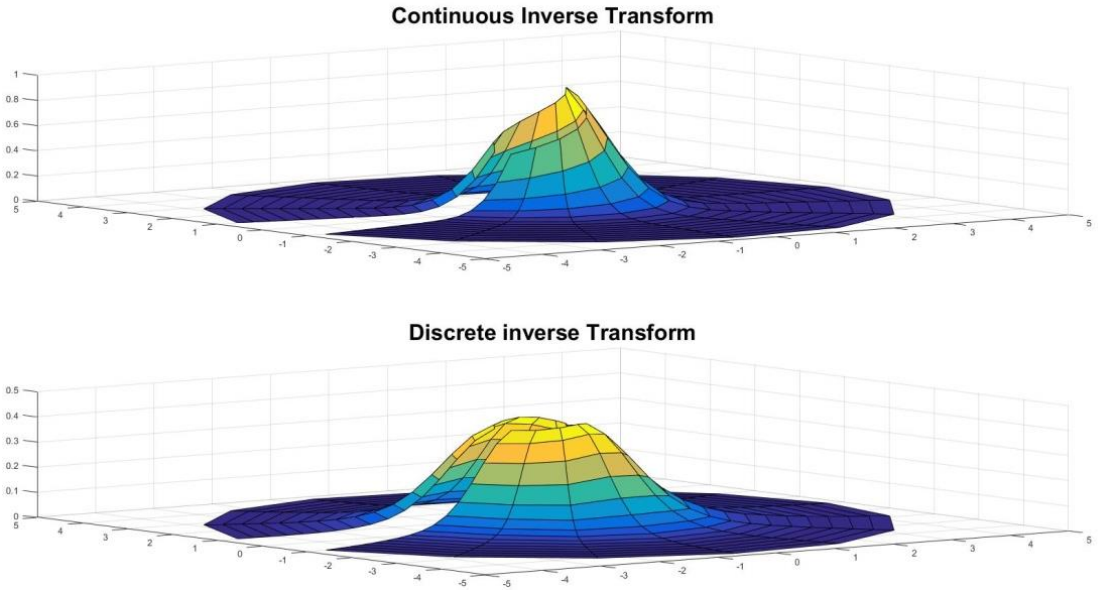

Figure 16 Sampled continuous inverse transform and discrete inverse transform of the Gaussian function with R=5, N_2=15, N_1=17

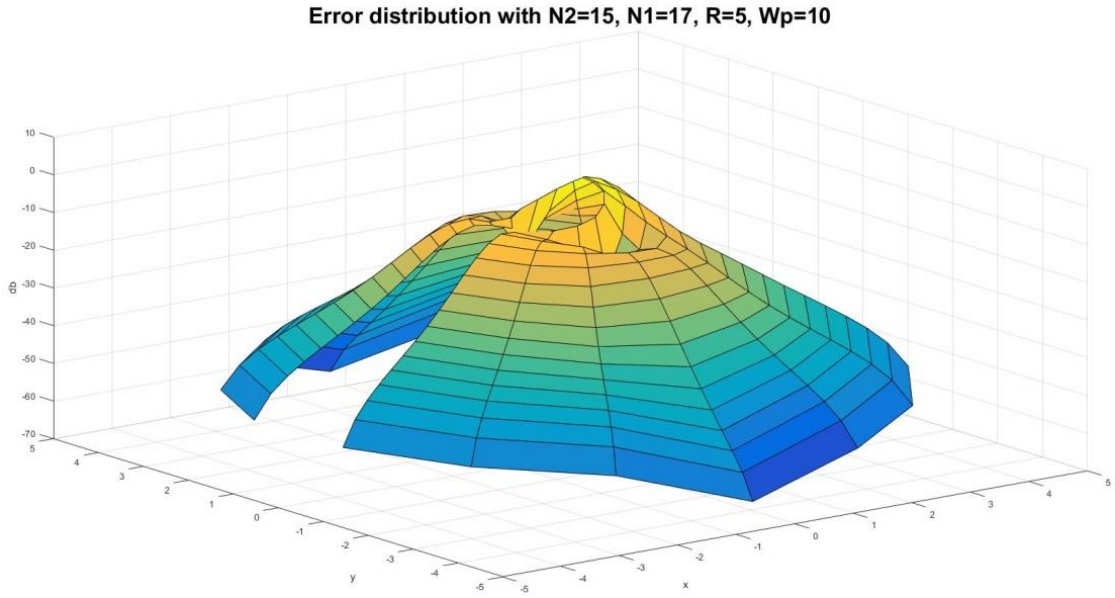

Figure 17 The error distribution of the inverse transform of Gaussian Function with R=5, N_2=15, N_1=17

Similar to the case for the forward transform, the error gets bigger at the center, which is as expected because the sampling grid shows that the sampling points can never get to the center. The maximum value of the error is $E_{\max} = 3.1954 dB$ and this occurs at the center. The average of the error is $E_{avg.} = -25.7799 dB$.

Figure 18 and Figure 19 shows the test result with $R = 40$, $N_1 = 383$.

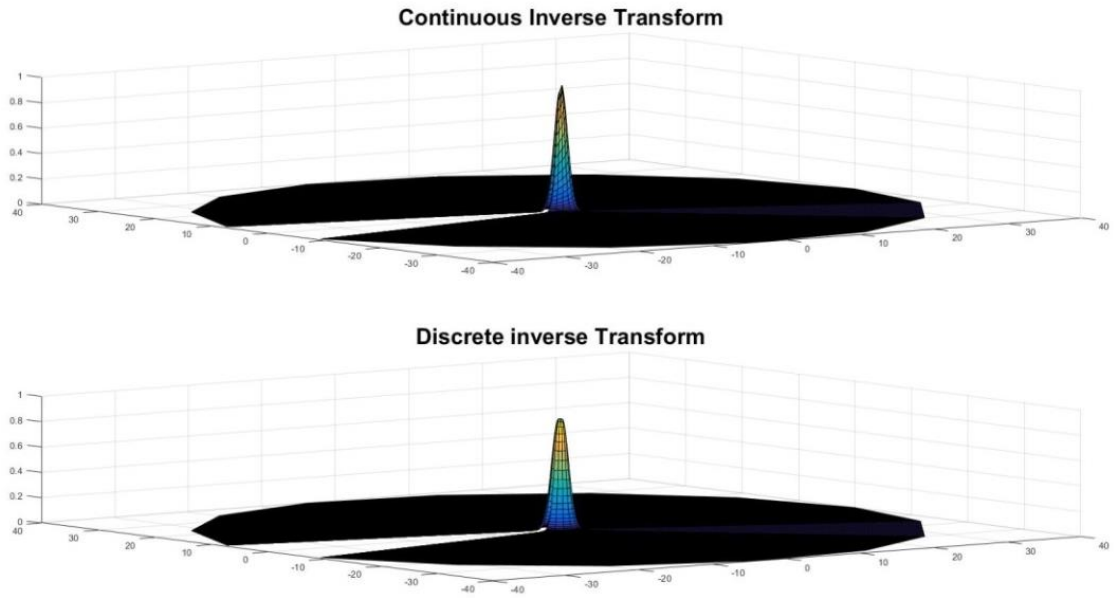

Figure 18 Sampled continuous inverse transform and discrete inverse transform of the Gaussian function with R=40, N_2=15, N_1=383

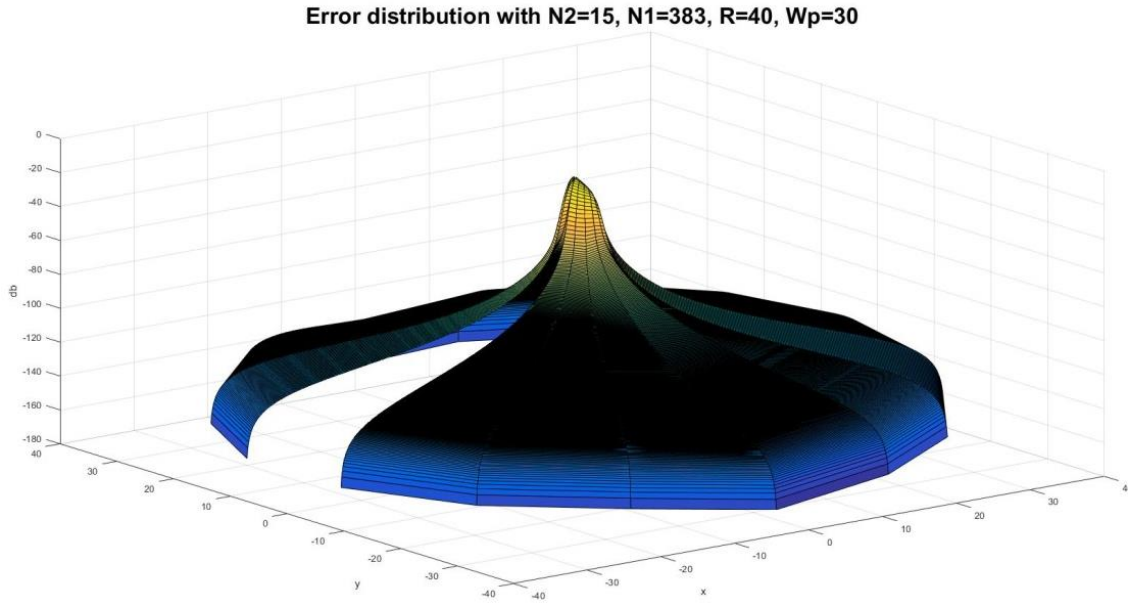

Figure 19 The error distribution of the inverse transform of Gaussian Function with R=40, N_2=15, N_1=383

The maximum value of the error is $E_{\max} = -12.2602\,dB$ and this occurs at the center. The average of the error is $E_{avg.} = -98.0316 dB$. Clearly, testing with $R = 40$, $N_1 = 383$ gives a better approximation which verifies the discussion in Chapter 5. With $R = 40$, Table 4 shows the errors with respect to different value of N_1 and N_2, from which Figure 20 and Figure 21 demonstrate the trend.

Table 4 Error (dB) of inverse transform of Gaussian Function with R=40, different value of N_1 and N_2

N2 \ N1	283	333	383	433	483
3	$E_{\max.} = -25.9$ $E_{avg.} = -115.3$	$E_{\max.} = -27.5$ $E_{avg.} = -115.4$	$E_{\max.} = -28.9$ $E_{avg.} = -115.4$	$E_{\max.} = -30.2$ $E_{avg.} = -115.5$	$E_{\max.} = -31.3$ $E_{avg.} = -115.5$
7	$E_{\max.} = -16.5$ $E_{avg.} = -107.0$	$E_{\max.} = -18.1$ $E_{avg.} = -107.1$	$E_{\max.} = -19.4$ $E_{avg.} = -107.2$	$E_{\max.} = -20.5$ $E_{avg.} = -107.2$	$E_{\max.} = -21.6$ $E_{avg.} = -107.2$
15	$E_{\max.} = -9.7$ $E_{avg.} = -97.9$	$E_{\max.} = -11.0$ $E_{avg.} = -98.0$	$E_{\max.} = -12.3$ $E_{avg.} = -98.0$	$E_{\max.} = -13.4$ $E_{avg.} = -98.1$	$E_{\max.} = -14.4$ $E_{avg.} = -98.1$
34	$E_{\max.} = -4.4$ $E_{avg.} = -86.9$	$E_{\max.} = -5.5$ $E_{avg.} = -86.9$	$E_{\max.} = -6.5$ $E_{avg.} = -87.0$	$E_{\max.} = -7.5$ $E_{avg.} = -87.0$	$E_{\max.} = -8.3$ $E_{avg.} = -87.0$
61	$E_{\max.} = -1.1$ $E_{avg.} = -75.6$	$E_{\max.} = -1.7$ $E_{avg.} = -75.6$	$E_{\max.} = -2.4$ $E_{avg.} = -75.6$	$E_{\max.} = -3.0$ $E_{avg.} = -75.6$	$E_{\max.} = -3.7$ $E_{avg.} = -75.7$

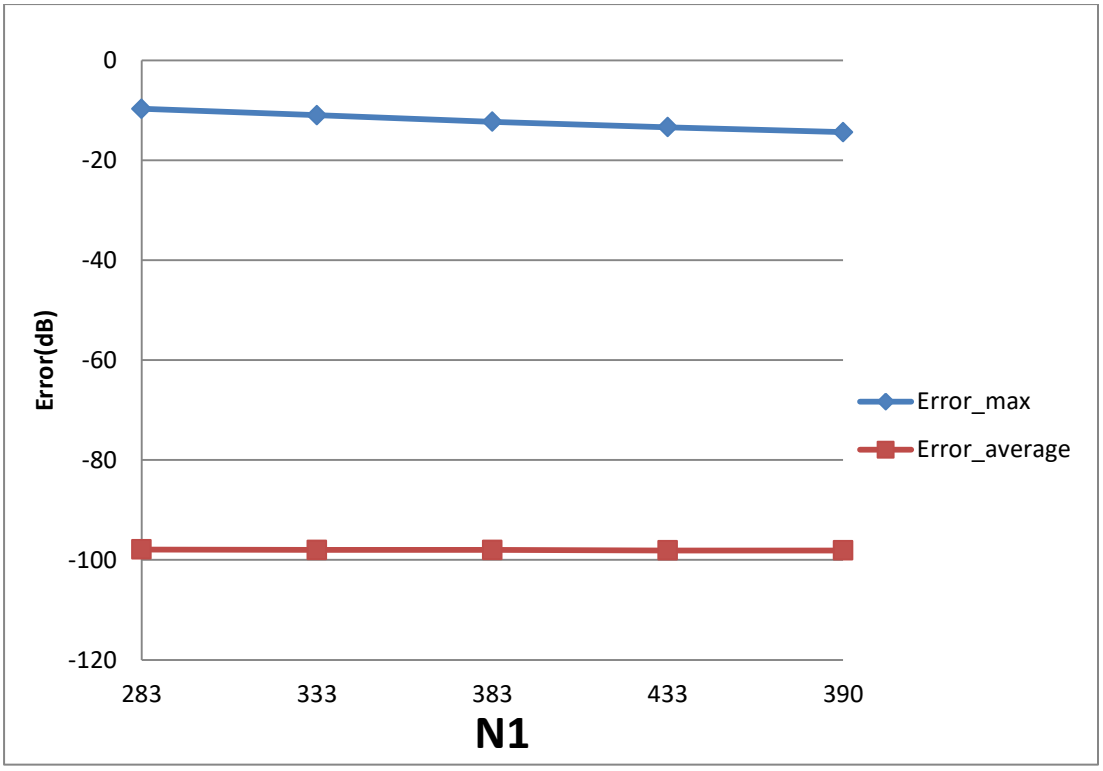

Figure 20 Error of inverse transform of Gaussian Function with fixed N_2 (15) and varying N_1

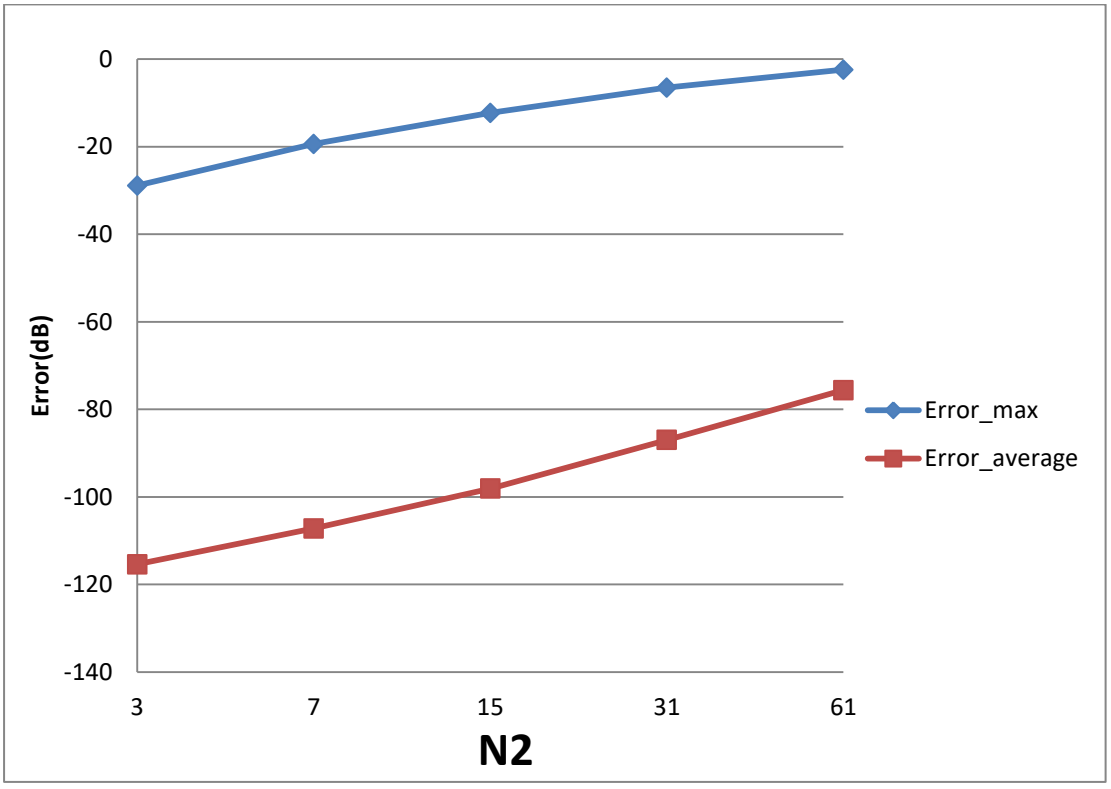

Figure 21 Error of inverse transform of Gaussian Function with fixed N_1 (383) and varying N_2

From Figure 20 it can be observed that increasing N_1 tends to improve the result but not too much. This could be explained by the discussion in Chapter 5 that with fixed

R and W_p, increasing N_1 will not get the sample grid in the frequency domain closer to the origin to capture more information. From Figure 21, increasing N_2 leads to a worse approximation which verifies the discussion in Chapter 5.

Performing sequential 2D-DFT and 2D-IDFT results in $\varepsilon = 4.1656 \times e^{-17}$ where ε is calculated with equation (6.2) . Therefore, performing forward and inverse transform does not add much error.

6.2.2 Square Donut

The second chosen function is a circularly symmetric function which is a square wave in the radial direction. The function is given by

$$f(r,\theta) = \begin{cases} 0, & r < 5 \text{ and } r > 10 \\ 1, & 5 \le r \le 10 \end{cases} \tag{6.5}$$

The continuous 2D-FT can be written as [27]:

$$F(\rho,\psi) = \frac{2\pi}{\rho}[10J_1(10\rho) - 5J_1(5\rho)] \tag{6.6}$$

where $J_n(x)$ is Bessel function of order n .

The graphs for the original function and its continuous 2D-FT are shown in Figure 22.

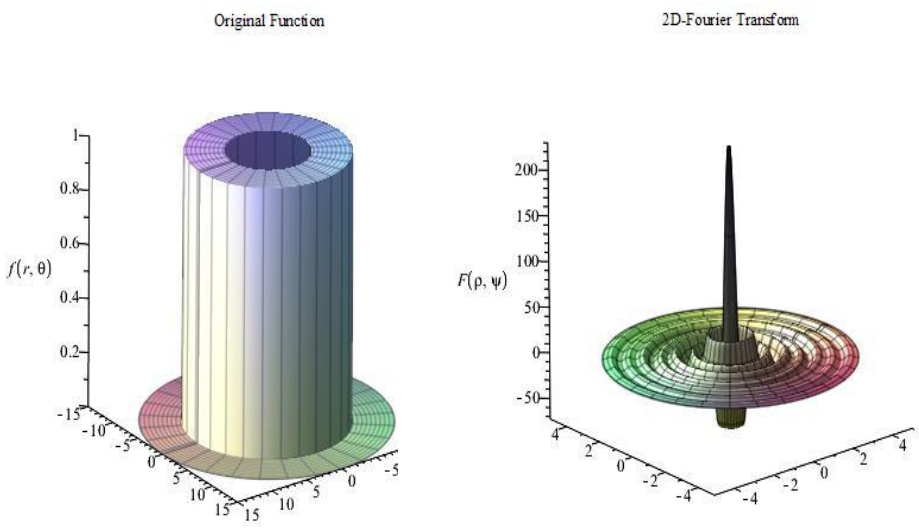

Figure 22 The original function and its 2D-Fourier transform of the 'Square Donut' function.

From Figure 22, different from previous case, this function is sharp in the radial direction and thus contains high frequencies in the frequency domain. Moreover, the function is a space limited function. Therefore equation (3.28) and (3.29) can be used to proceed with the forward and inverse transform in sequence.

In the angular direction, since the function in the space domain is circularly symmetric, N_2 can be chosen to be small. Thus $N_2 = 15$ is chosen. In the radial direction, the function is effectively space limited with $R = 15$ and effectively band limited with $W_p = 6$. From equation(5.9), then $j_{0N_1} \approx 90$, hence, $N_1 = 29$ is chosen. However, most of the energy of the function in frequency domain is located at the center. Hence, based on the discussion in Chapter 5, relatively large values of R are needed. $R = 150$ is chosen here. With the band-limit of $W_p = 6$, $j_{0N_1} \approx 900$ is calculated from equation (5.9). Therefore $N_1 = 290$ is chosen.

6.2.2.1 Forward Transform

The results with $R = 15, N_1 = 29$ are shown in Figure 23and Figure 24.

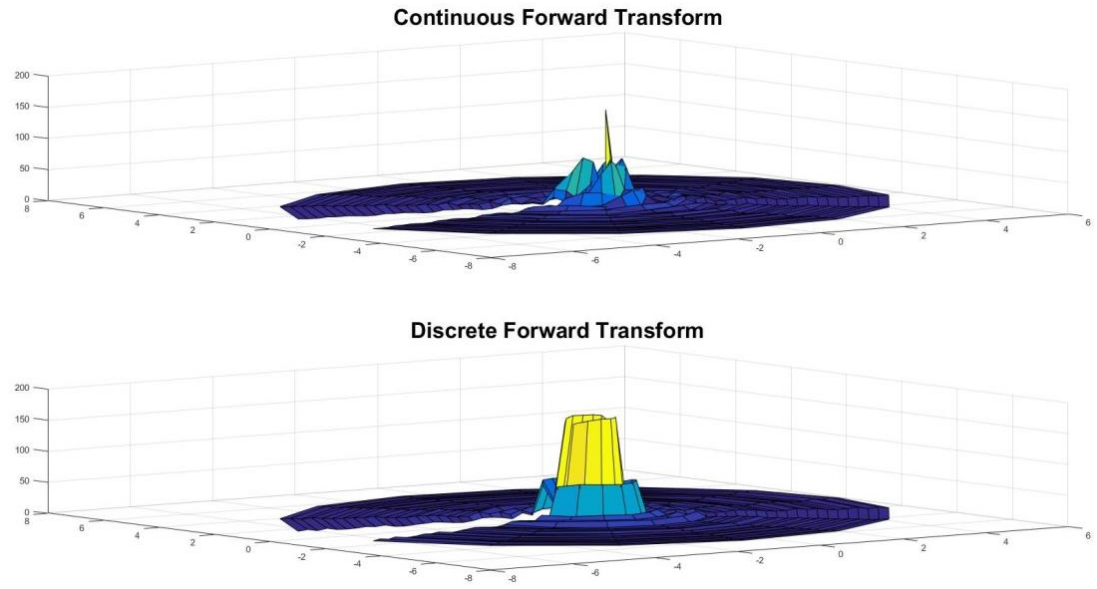

Figure 23 Sampled continuous forward transform and discrete forward transform of the 'Square Donut' function with R=15, N_2=15, N_1=29

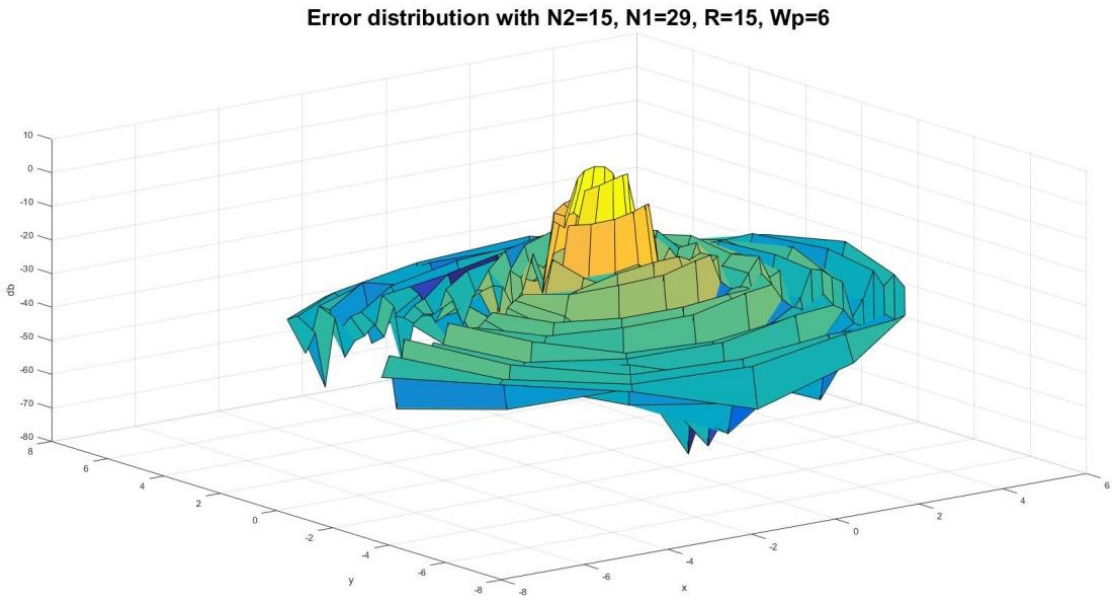

Figure 24 The error distribution of the sampled forward transform of the 'Square Donut' function with R=15, N_2=15, N_1=29

The maximum value of the error is $E_{\max.} = 3.1730\,dB$ and occurs at the center. The average of the error is $E_{avg.} = -32.3276 dB$.

The results for the forward 2D-DFT of Square Donut function with $R = 150$, $N_1 = 290$ are shown in Figure 25 and Figure 26.

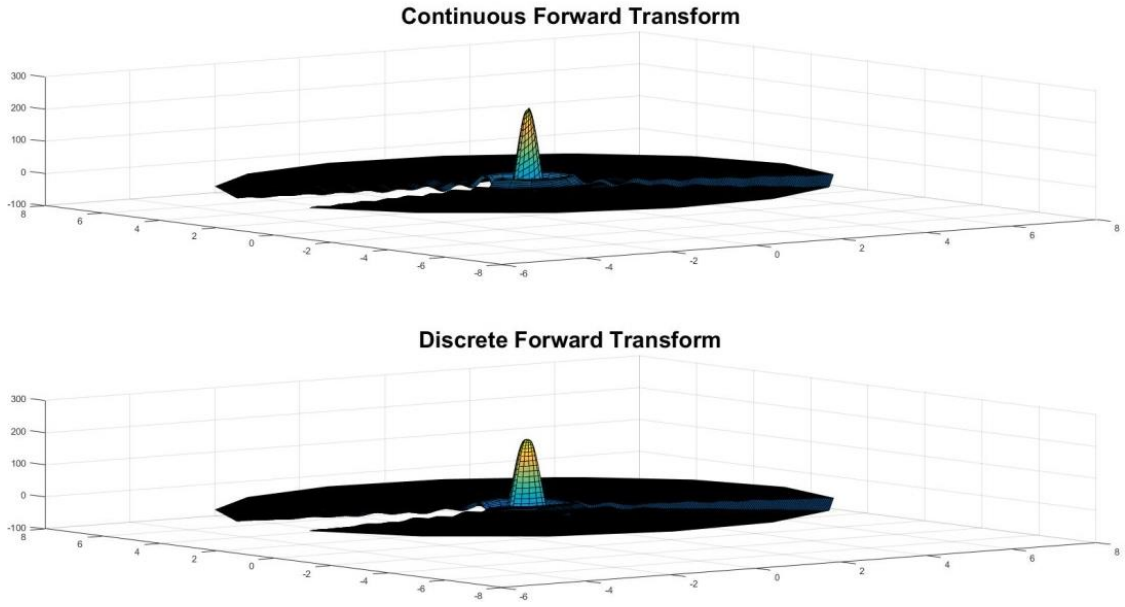

Figure 25 Sampled continuous forward transform and discrete forward transform of 'Square Donut' function with R=150, N_2=15, N_1=290

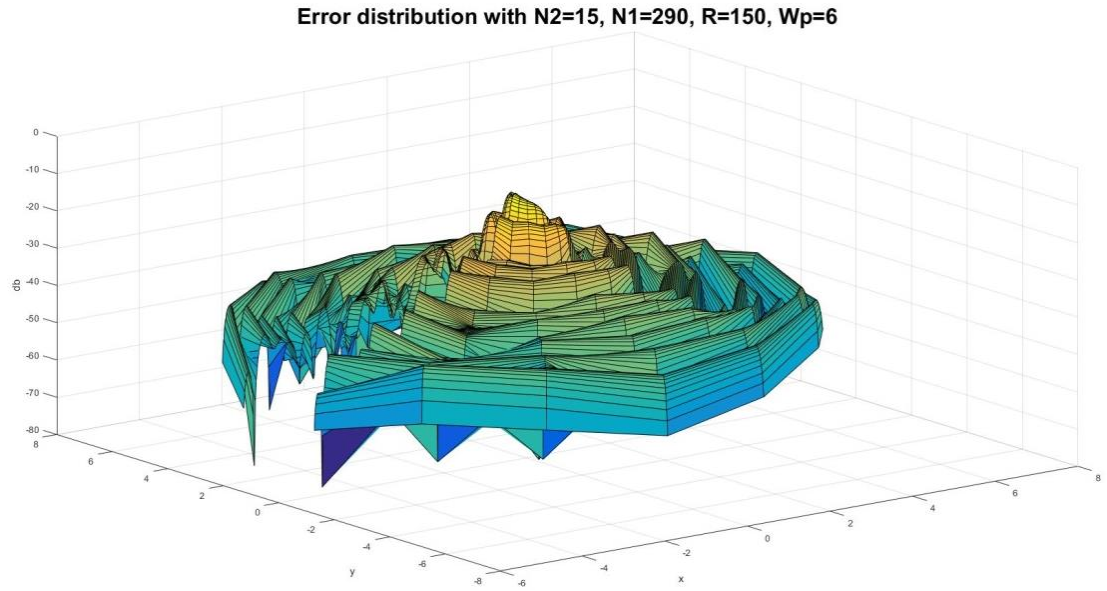

Figure 26 The error distribution of the forward transform of 'Square Donut' function with R=150, N_2=15, N_1=290

From Figure 26, it can be observed that the error gets bigger at the center, which is as expected because the sampling grid shows that the sampling points can never get to the center. The maximum value of the error is $E_{\max} = -8.1664 dB$ and occurs at the center area. The average of the error is $E_{avg.} = -34.5471 dB$.

From Figure 23-Figure 26, it can be observed that even though $R = 15$ is large enough from Figure 22, $R = 150$ results in a better approximation because it captures more information at the center area in the frequency domain. This verifies the

discussion in Chapter 5. With $R=150$, Table 5 shows the errors with respect to different value of N_1 and N_2, from which Figure 27 and Figure 28 show the trend.

Table 5 Error (dB) of forward transform of 'Square Donut' function with R=150, different value of N_1 and N_2

N2 \ N1	190	240	290	340	390
7	$E_{\max.}=-13.6$ $E_{avg.}=-30.8$	$E_{\max.}=-14.0$ $E_{avg.}=-35.2$	$E_{\max.}=-15.2$ $E_{avg.}=-38.3$	$E_{\max.}=-15.6$ $E_{avg.}=-38.4$	$E_{\max.}=-15.4$ $E_{avg.}=-41.6$
15	$E_{\max.}=-6.3$ $E_{avg.}=-28.4$	$E_{\max.}=-7.7$ $E_{avg.}=-32.3$	$E_{\max.}=-8.2$ $E_{avg.}=-34.5$	$E_{\max.}=-8.2$ $E_{avg.}=-36.4$	$E_{\max.}=-8.8$ $E_{avg.}=-38.9$
31	$E_{\max.}=-1.0$ $E_{avg.}=-26.4$	$E_{\max.}=-1.7$ $E_{avg.}=-30.3$	$E_{\max.}=-2.3$ $E_{avg.}=-33.2$	$E_{\max.}=-2.6$ $E_{avg.}=-35.4$	$E_{\max.}=-2.8$ $E_{avg.}=-37.8$
61	$E_{\max.}=3.5$ $E_{avg.}=-22.3$	$E_{\max.}=2.7$ $E_{avg.}=-26.7$	$E_{\max.}=2.2$ $E_{avg.}=-30.0$	$E_{\max.}=1.9$ $E_{avg.}=-32.6$	$E_{\max.}=1.6$ $E_{avg.}=-35.2$
121	$E_{\max.}=11.4$ $E_{avg.}=-17.8$	$E_{\max.}=9.1$ $E_{avg.}=-22.1$	$E_{\max.}=6.8$ $E_{avg.}=-25.6$	$E_{\max.}=5.3$ $E_{avg.}=-28.7$	$E_{\max.}=4.8$ $E_{avg.}=-31.6$

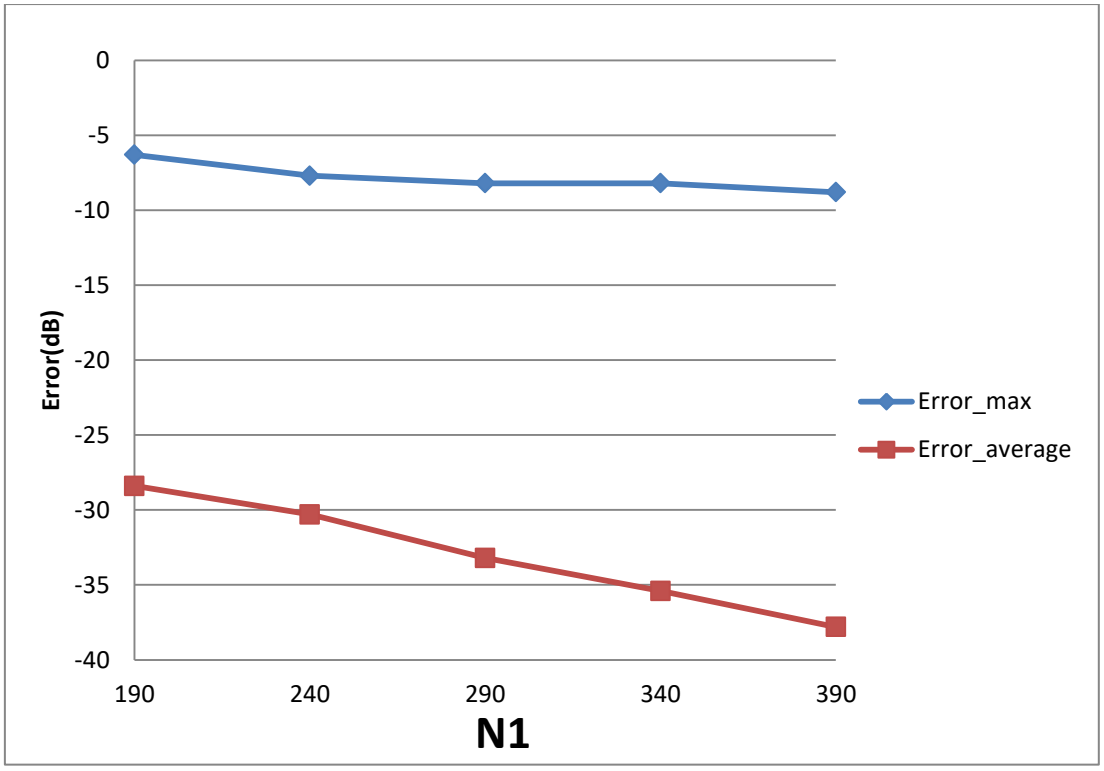

Figure 27 Error of forward transform of 'Square Donut' function with fixed N_2 (15) and variant N_1

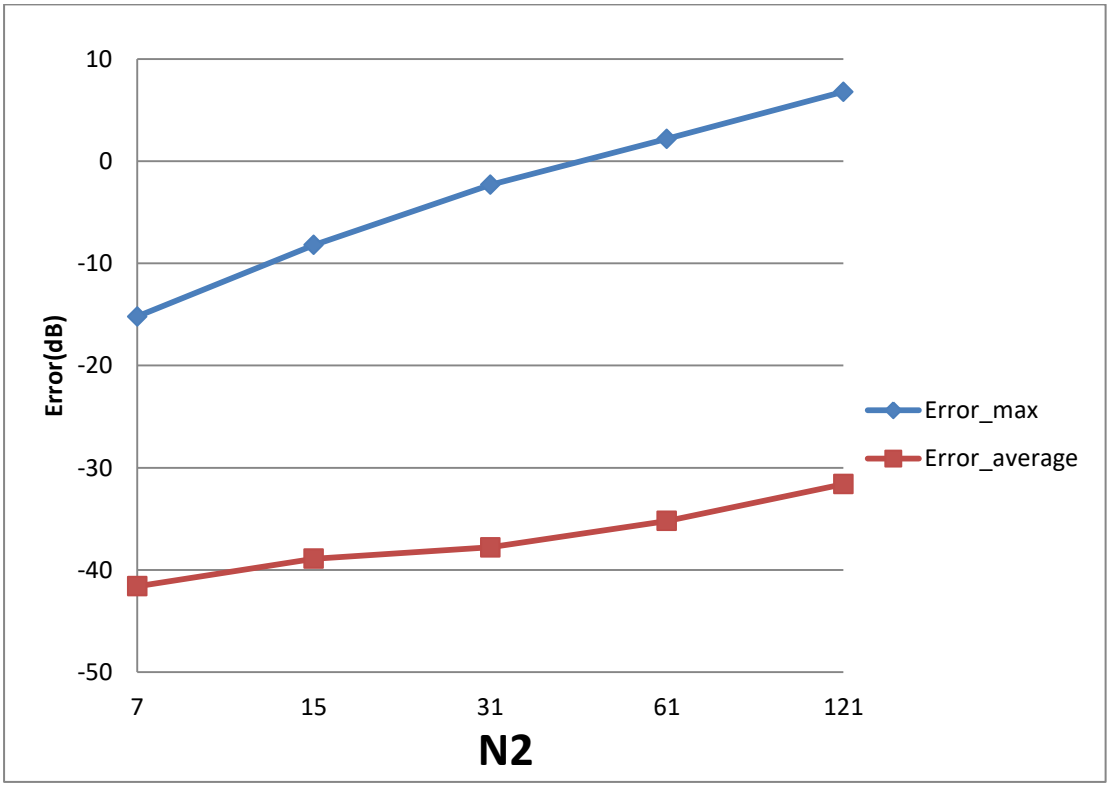

Figure 28 Error of forward transform of 'Square Donut' function with fixed N_1 (512) and varying N_2

From Figure 27, similar to the previous case, increasing N_1 will lead to less error as expected. From the sample points defined in equation (3.36), increasing N_1 will lead to a larger effective band limit. From Figure 22, the function in the frequency domain does not die out. Therefore, increasing N_1 will capture more information at higher frequencies which explains why increasing N_1 still leads to less error even after N_1 is larger than 290 in Figure 27.

From Figure 28, increasing N_2 leads to larger $Error_{\max}$ and $Error_{average}$. This is reasonable from the discussion of sample grid coverage from Chapter 5: the sampling grid coverage in both domains gets worse when N_2 gets larger because more information from the center is lost.

6.2.2.2 Inverse Transform

The results for the inverse transform with $R=15, N_1=29$ are shown in Figure 29 and Figure 30

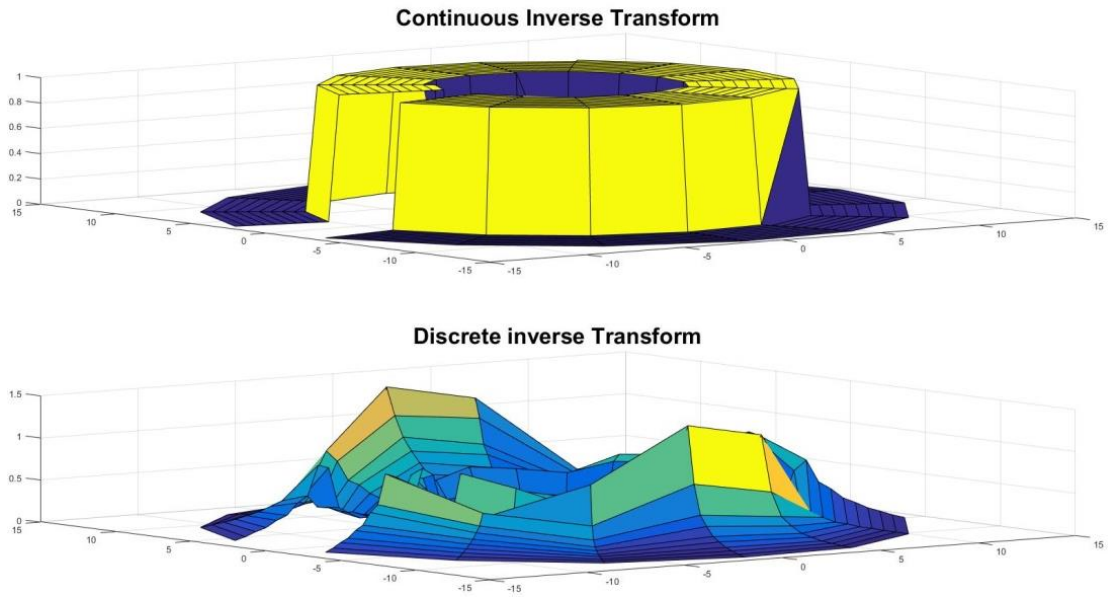

Figure 29 Sampled continuous inverse transform and discrete inverse transform of 'Square Donut' function with R=15, N_2=15, N_1=29

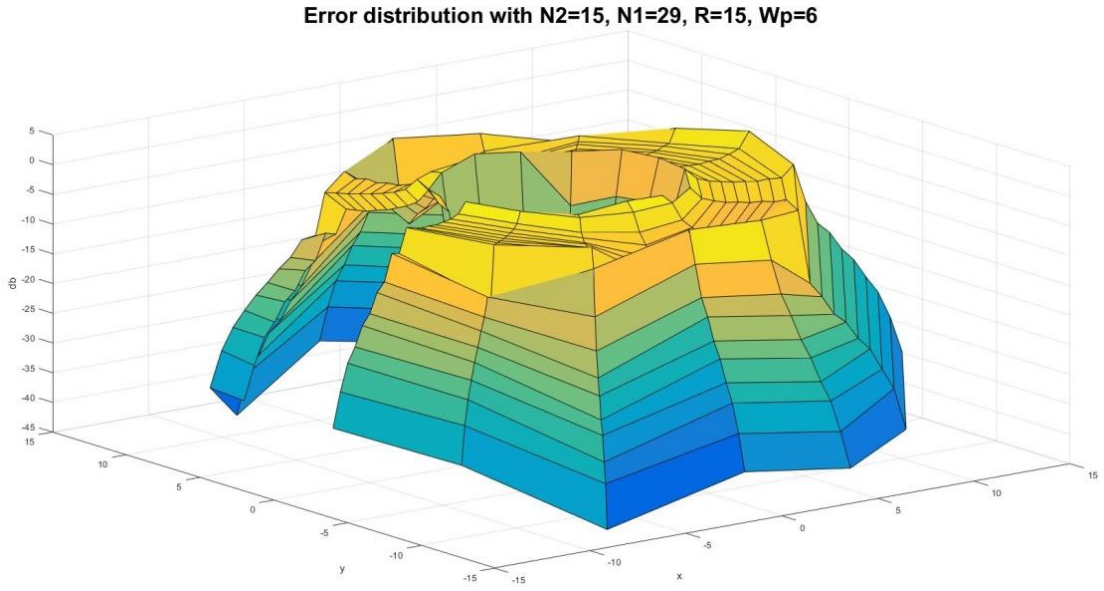

Figure 30 The error distribution of the inverse transform of 'Square Donut' function with R=15, N2=15, N1=29

The maximum value of the error is $Error_{\max} = 2.5647dB$ and this occurs at the center. The average of the error is $Error_{average} = -13.6986dB$. The results for the 2D-IDFT of the Square Donut function are shown for $R = 150$, $N_1 = 290$ in Figure 31 and Figure 32.

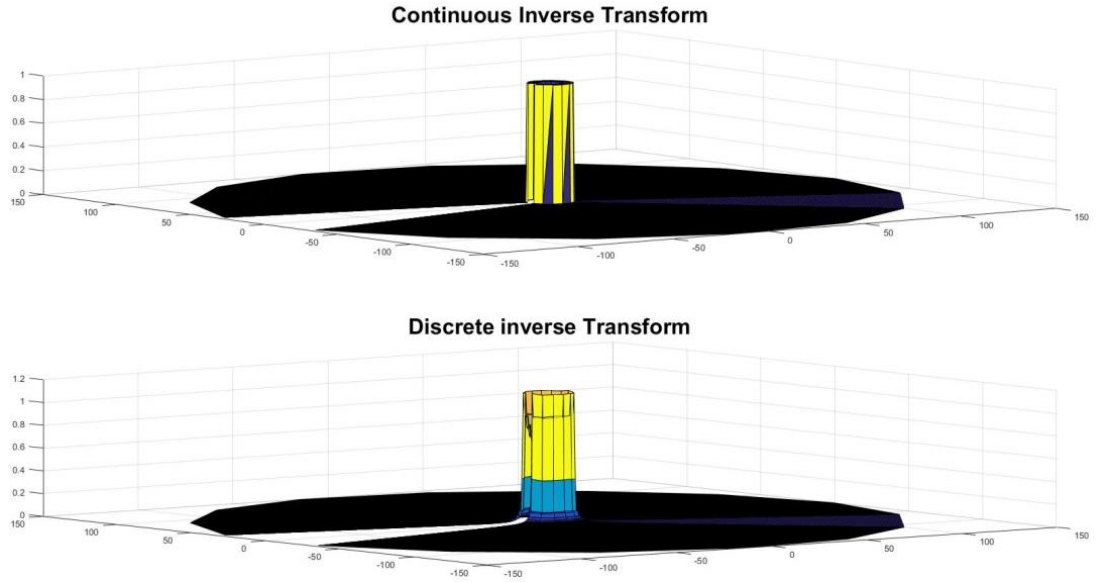

Figure 31 Sampled continuous inverse transform and discrete inverse transform of 'Square Donut' function with R=150, N_2=15, N_1=290

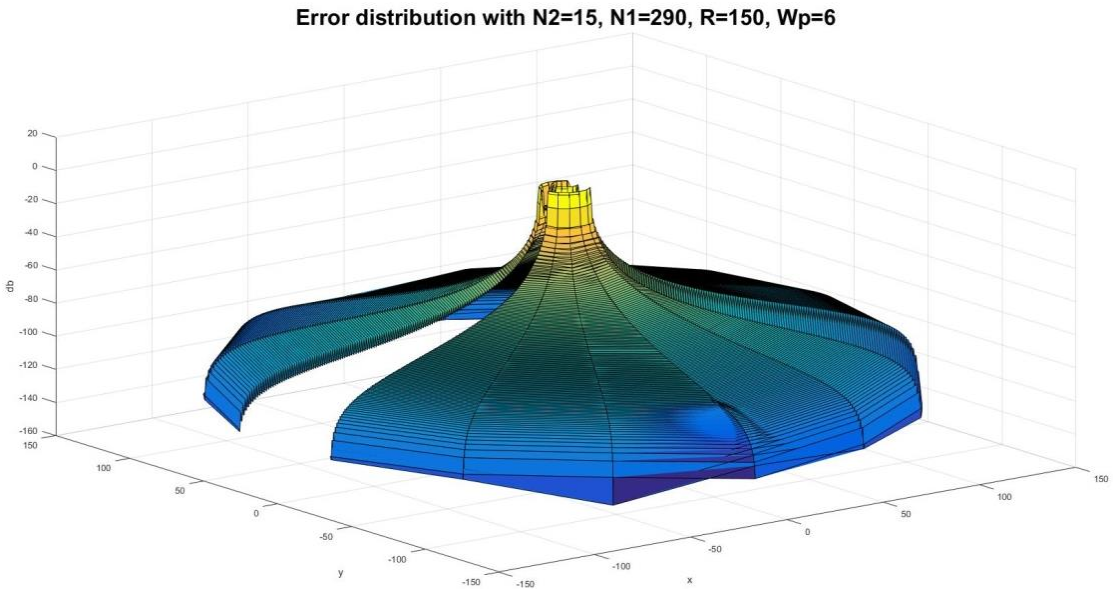

Figure 32 The error distribution of the inverse transform of 'Square Donut' function with R=150, N_2=15, N_1=290

Similar to the forward transform, large errors appear in the center area as expected. The maximum value of the error is $Error_{\max} = 1.5dB$.The average of the error is $Error_{average} = -73dB$. Clearly, with $R = 150$, $N_1 = 290$, a better approximation is obtained.

With $R = 150$, Table 6 shows the errors with respect to different value of N_1 and N_2, from which Figure 33 and Figure 34 show the trend.

Table 6 Error (dB) with different value of N_1 and N_2 of inverse transform of 'Square Donut' function

N2 \ N1	190	240	290	340	390
7	$E_{\max.} = 0.1$ $E_{avg.} = -65.0$	$E_{\max.} = 0.8$ $E_{avg.} = -78.2$	$E_{\max.} = 1.1$ $E_{avg.} = -74.9$	$E_{\max.} = 0.1$ $E_{avg.} = -66.4$	$E_{\max.} = 0.8$ $E_{avg.} = -68.2$

15	$E_{\max.} = 1.3$ $E_{avg.} = -65.3$	$E_{\max.} = 1.9$ $E_{avg.} = -72.0$	$E_{\max.} = 1.5$ $E_{avg.} = -73.0$	$E_{\max.} = 1.2$ $E_{avg.} = -65.4$	$E_{\max.} = 1.7$ $E_{avg.} = -68.7$
31	$E_{\max.} = 3.3$ $E_{avg.} = -65.0$	$E_{\max.} = 2.7$ $E_{avg.} = -62.3$	$E_{\max.} = 2.3$ $E_{avg.} = -63.7$	$E_{\max.} = 2.8$ $E_{avg.} = -62.7$	$E_{\max.} = 2.2$ $E_{avg.} = -64.3$
61	$E_{\max.} = 5.5$ $E_{avg.} = -52.9$	$E_{\max.} = 4.0$ $E_{avg.} = -54.5$	$E_{\max.} = 3.9$ $E_{avg.} = -54.9$	$E_{\max.} = 4.5$ $E_{avg.} = -54.8$	$E_{\max.} = 3.3$ $E_{avg.} = -55.7$
121	$E_{\max.} = 6.4$ $E_{avg.} = -46.5$	$E_{\max.} = 6.2$ $E_{avg.} = -47.6$	$E_{\max.} = 6.8$ $E_{avg.} = -47.0$	$E_{\max.} = 6.2$ $E_{avg.} = -48.3$	$E_{\max.} = 5.7$ $E_{avg.} = -48.9$

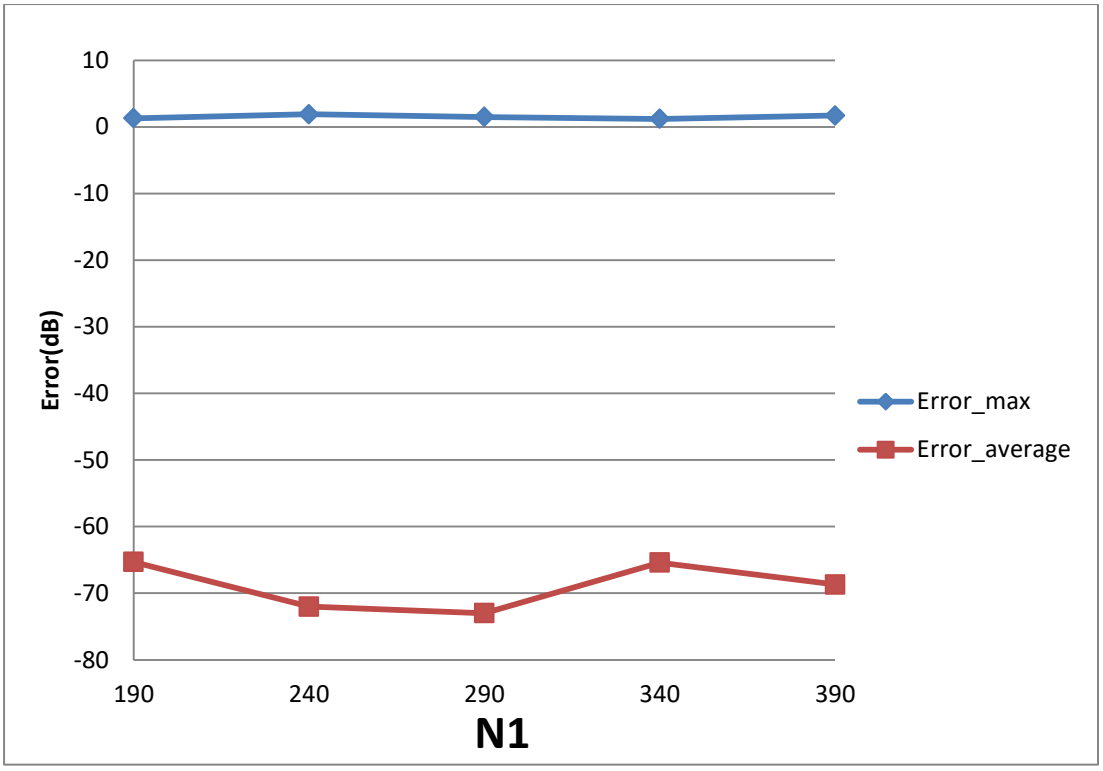

Figure 33 Error of the inverse transform of 'Square Donut' function with fixed N_2 (15) and varying N_1

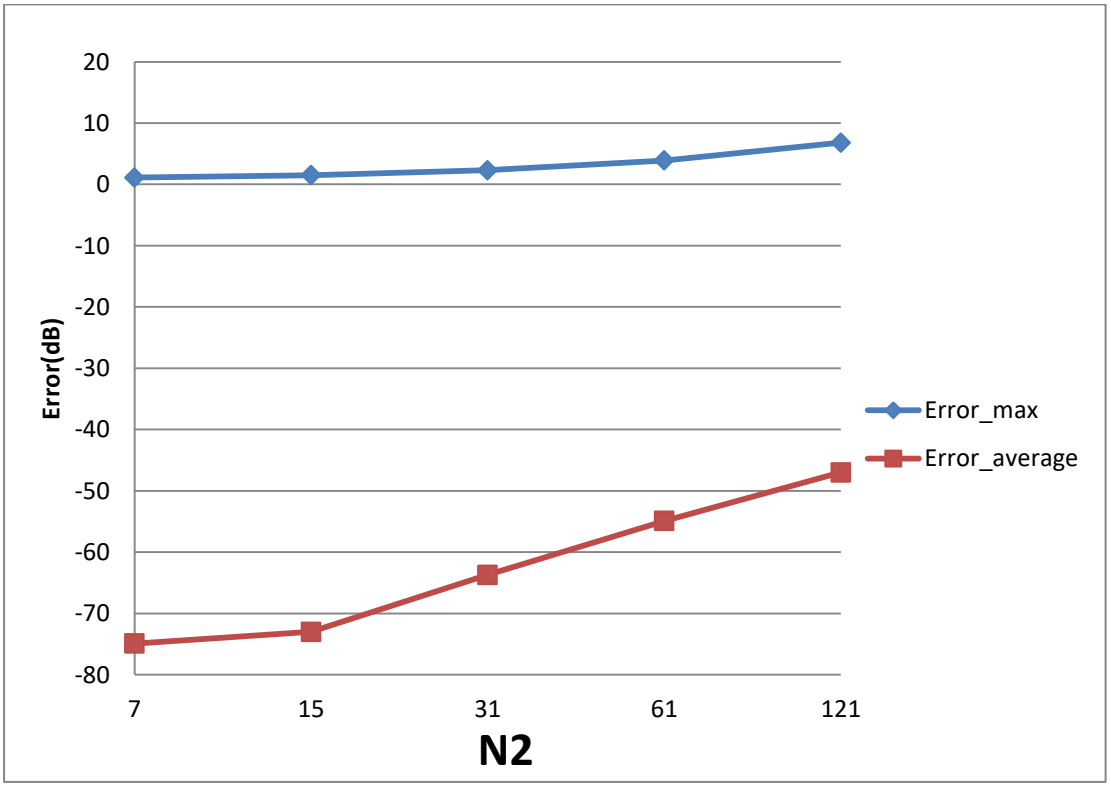

Figure 34 Error of the inverse transform of 'Square Donut' function with fixed N_1 (512) and varying N_2

From Figure 33, when N_1 is less than the minimum value (290) calculated from the sampling theorem, increasing N_1 leads to a better approximation as expected. However, when N_1 is greater than 290, increasing N_1 does not decrease the error as for previous cases. This could be caused by the discontinuity of the function in the space domain. Because with larger value of N_1 , the sampling points will get closer to the discontinuity, which will cause bigger errors. From Figure 34, It can be seen that similar trend (increasing N_2 leads to worse result) with the forward transform is obtained.

Performing 2D-DFT and 2D-IDFT sequentially results in $\varepsilon = 6.7253 \times e^{-14}$ where ε is calculated from equation (6.2) .

6.2.3 Four-term sinusoid & Sinc Function

The third function chosen for evaluation is given by

$$f(r,\theta) = \frac{\sin(ar)}{ar}[3\sin(\theta) + \sin(3\theta) + 4\cos(10\theta) + 12\sin(15\theta)] \tag{6.7}$$

which is a sinc function in the radial direction and a four-term sinusoid in angular direction. The continuous 2D-FT can be calculated from [20]

$$F(\rho,\psi) = \sum_{n=-\infty}^{\infty} 2\pi i^{-n} e^{in\psi} \int_0^{\infty} f_n(r) J_n(\rho r) r dr \tag{6.8}$$

where $f_n(r)$ is the Fourier series of $f(r,\theta)$ and can be written as

$$f_n(r) = \frac{1}{2\pi} \int_{-\pi}^{\pi} f(r,\theta) e^{-in\theta} d\theta \tag{6.9}$$

Since the nth order Hankel transform could be defined as[20]

$$H_n\{f(r)\} = \int_0^{\infty} f(r) J_n(\rho r) r dr \tag{6.10}$$

Equation (6.8) can be written as

$$F(\rho,\psi) = \sum_{n=-\infty}^{\infty} 2\pi i^{-n} e^{in\psi} H_n\{f_n(r)\} \tag{6.11}$$

From the equation (5.6) (the sampling theorem for the angular direction), the highest angular frequency in equation (6.7) results in $N_2 = 31$ needed to reconstruct the signal. Therefore, 31 terms are required to calculate the continuous 2D-FT, which can be written as

$$F(\rho,\psi) = \begin{cases} \dfrac{8\pi\cos(10\psi)\rho^{10}}{a\sqrt{a^2-\rho^2}\left(a+\sqrt{a^2-\rho^2}\right)^{10}}, & \rho < a \\ -\dfrac{6\pi I\sin(\psi)}{a\rho\sqrt{\rho^2+a^2}} + \dfrac{2\pi I\sin\left(3\arcsin\left(\dfrac{a}{\rho}\right)\right)\sin(3\psi)}{\sqrt{\rho^2+a^2}} - \dfrac{8\pi\sin\left(10\arcsin\left(\dfrac{a}{\rho}\right)\right)\cos(10\psi)}{\sqrt{\rho^2+a^2}} \\ + \dfrac{24\pi I\sin\left(15\arcsin\left(\dfrac{a}{\rho}\right)\right)\sin(15\psi)}{\sqrt{\rho^2+a^2}}, & \rho > a \end{cases}$$

(6.12)

The graphs for the original function and its continuous 2D-FT with $a = 5$ are shown in Figure 35

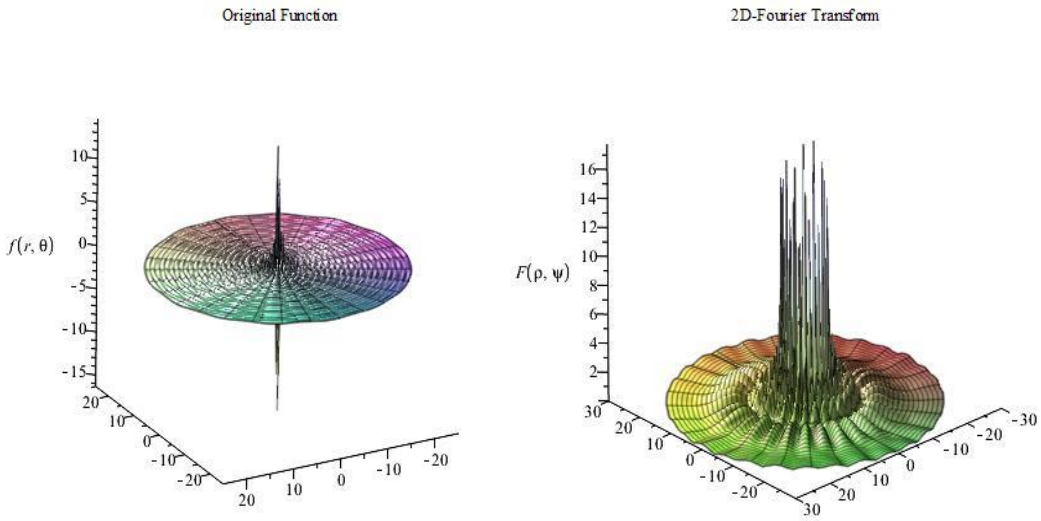

Figure 35 The original function and its 2D-Fourier Transform of 'Four-term sinusoid & Sinc' Function

From Figure 35, the function can be considered as a band-limited function. Therefore equation (3.31) and (3.32) were used to implement the forward and inverse transform.

In the angular direction, the highest frequency term is $12\sin(15\theta)$. From the sampling theorem, the sampling frequency should be at least twice that of the highest

frequency present in the signal. Thus, $N_2 = 41$ is chosen. In the radial direction, from the graphs of the original function and its 2D-FT, it can be assumed that $f(r,\theta)$ is space-limited at $R = 15$ and band-limited at $W_p = 30$. However, since most of the energy in the space domain is located at the origin, a relatively large band limit should be chosen based on the discussion in Chapter 5. Therefore, two cases with $W_p = 90$, $N_1 = 430$ and $W_p = 30$, $N_1 = 144$ are tested.

6.2.3.1 Forward Transform

The results for the forward 2D-DFT of the four-term sinusoid & Sinc function with $W_p = 30$, $N_1 = 144$ are shown in Figure 36 and Figure 37.

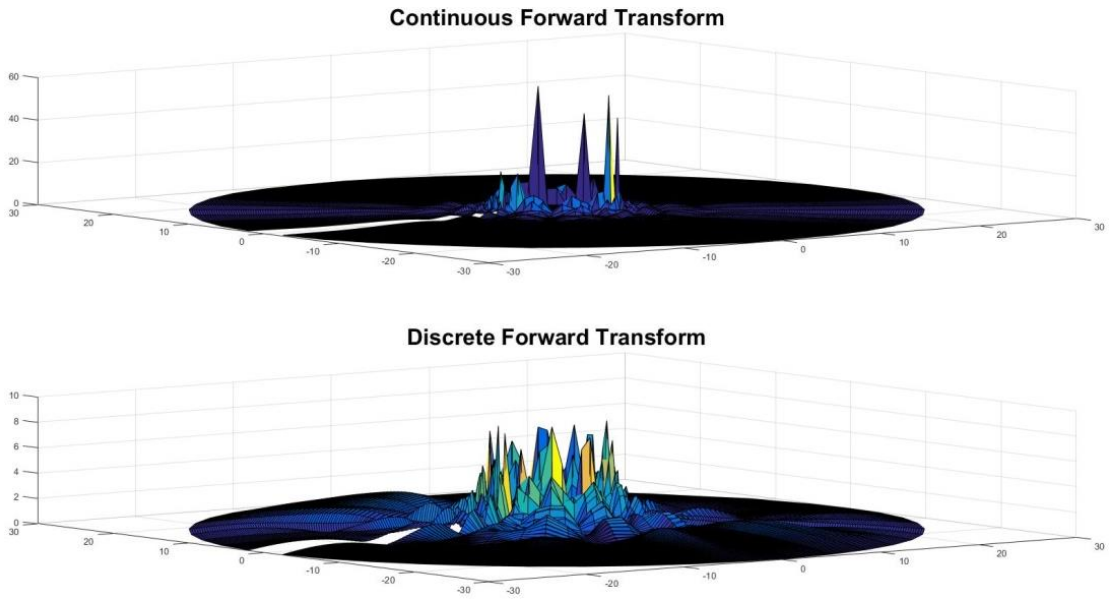

Figure 36 Sampled continuous forward transform and discrete forward transform of 'Four-term sinusoid & Sinc' Function with W_p=30,N_1=144

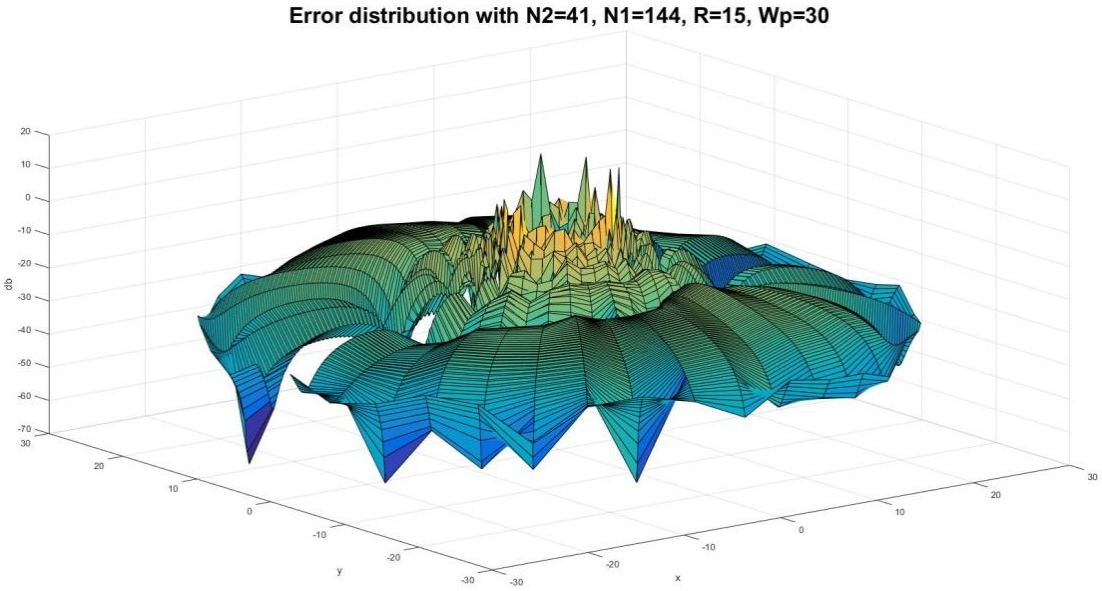

Figure 37 The error distribution of the forward transform of 'Four-term sinusoid & Sinc' Function with W_p=30,N_1=144

The maximum value of the error is $Error_{\max} = 17.0341dB$ and the average of the error is $Error_{average} = -23.1567dB$.

The results for the forward 2D-DFT of Four-term sinusoid & Sinc function with $W_p = 90$, $N_1 = 430$ are shown in Figure 38 and Figure 39.

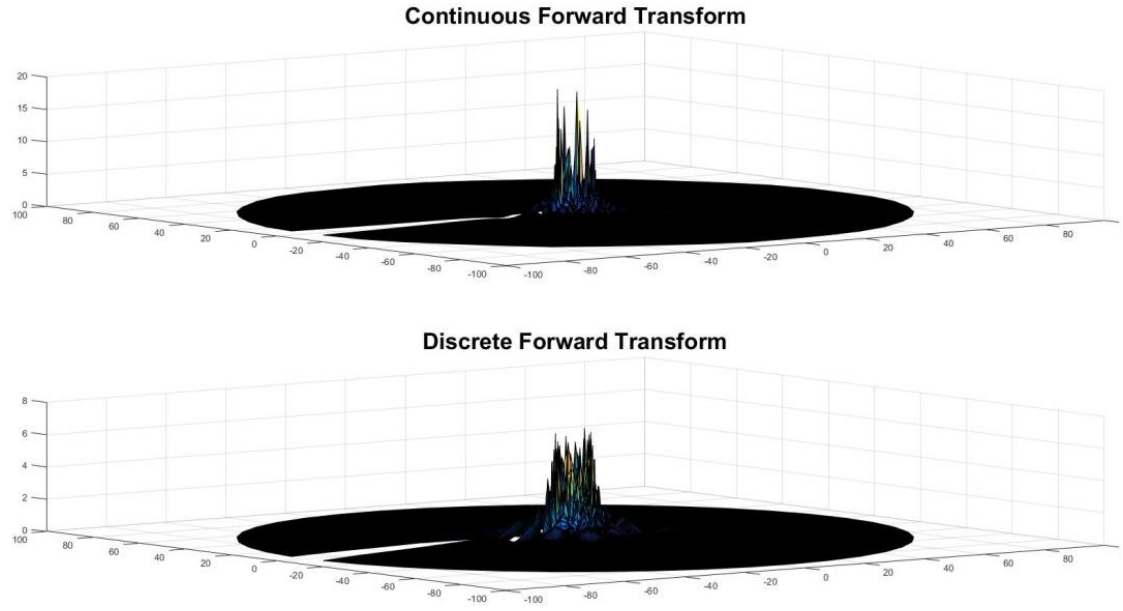

Figure 38 Sampled continuous forward transform and discrete forward transform of 'Four-term sinusoid & Sinc' Function with W_p=90,N_1=430

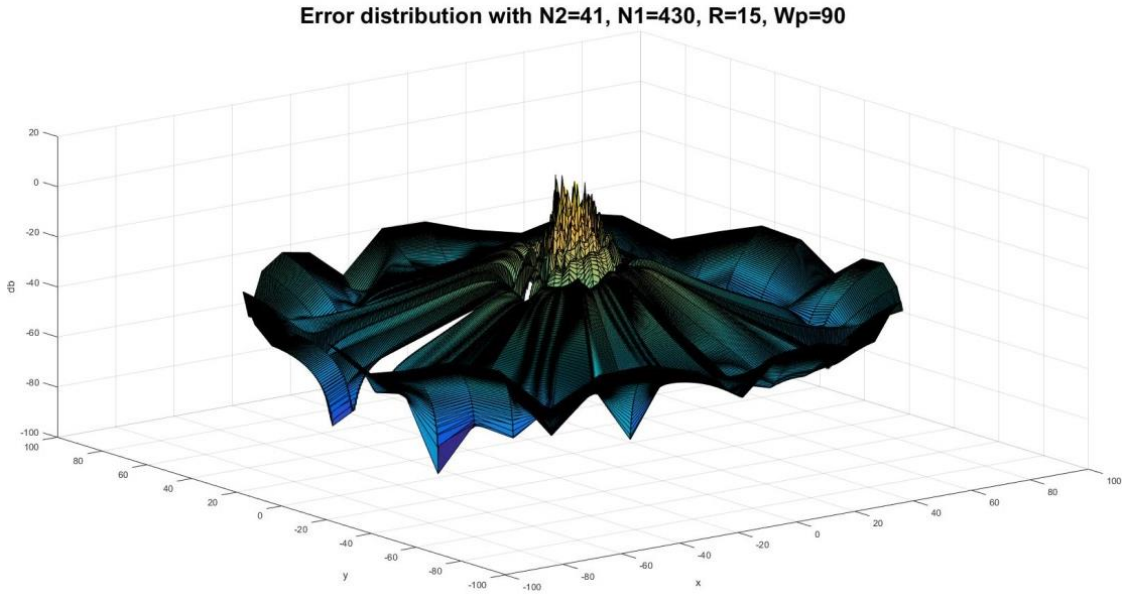

Figure 39 The error distribution of the forward transform of 'Four-term sinusoid & Sinc' Function with W_p=90,N_1=430

From Figure 38, the discrete transform does not approximate the continuous transform properly. This is expected because the function in the frequency domain is discontinuous and the sampling points closed to the discontinuity will result in a very large error. The maximum value of the error is $Error_{\max} = 10.6535dB$ and this occurs where the discontinuities are located. The average of the error is $Error_{average} = -38.7831dB$. It can be observed that the test with $W_p = 90$, $N_1 = 430$ gives a better approximation, which verifies the discussion in Chapter 5.

With $W_p = 90$, $N_1 = 430$, Table 7 shows the errors with respect to different value of N_1 and N_2, from which Figure 40 and Figure 41 show the trend.

Table 7 Error (dB) of the forward transform of 'Four-term sinusoid & Sinc' Function with different value of N1 and N2 of forward transform

N2 \ N1	330	380	430	480	530

11	$E_{\max.} = 4.6$ $E_{avg.} = -33.6$	$E_{\max.} = 7.1$ $E_{avg.} = -33.4$	$E_{\max.} = 3.4$ $E_{avg.} = -33.5$	$E_{\max.} = 9.0$ $E_{avg.} = -35.1$	$E_{\max.} = 2.8$ $E_{avg.} = -35.5$
21	$E_{\max.} = 6.7$ $E_{avg.} = -33.9$	$E_{\max.} = 10.5$ $E_{avg.} = -34.6$	$E_{\max.} = 3.2$ $E_{avg.} = -37.2$	$E_{\max.} = 6.9$ $E_{avg.} = -38.0$	$E_{\max.} = 3.6$ $E_{avg.} = -38.1$
41	$E_{\max.} = 8.5$ $E_{avg.} = -38.7$	$E_{\max.} = 35.1$ $E_{avg.} = -38.9$	$E_{\max.} = 10.7$ $E_{avg.} = -38.8$	$E_{\max.} = 14.6$ $E_{avg.} = -39.8$	$E_{\max.} = 11.1$ $E_{avg.} = -41.3$
81	$E_{\max.} = 9.7$ $E_{avg.} = -34.3$	$E_{\max.} = 32.7$ $E_{avg.} = 35.5$	$E_{\max.} = 14.8$ $E_{avg.} = -36.2$	$E_{\max.} = 22.6$ $E_{avg.} = -37.3$	$E_{\max.} = 14.5$ $E_{avg.} = -37.5$
161	$E_{\max.} = 19.9$ $E_{avg.} = -29.4$	$E_{\max.} = 30.2$ $E_{avg.} = -30.7$	$E_{\max.} = 22.5$ $E_{avg.} = -31.1$	$E_{\max.} = 22.5$ $E_{avg.} = -32.2$	$E_{\max.} = 16.1$ $E_{avg.} = -32.8$

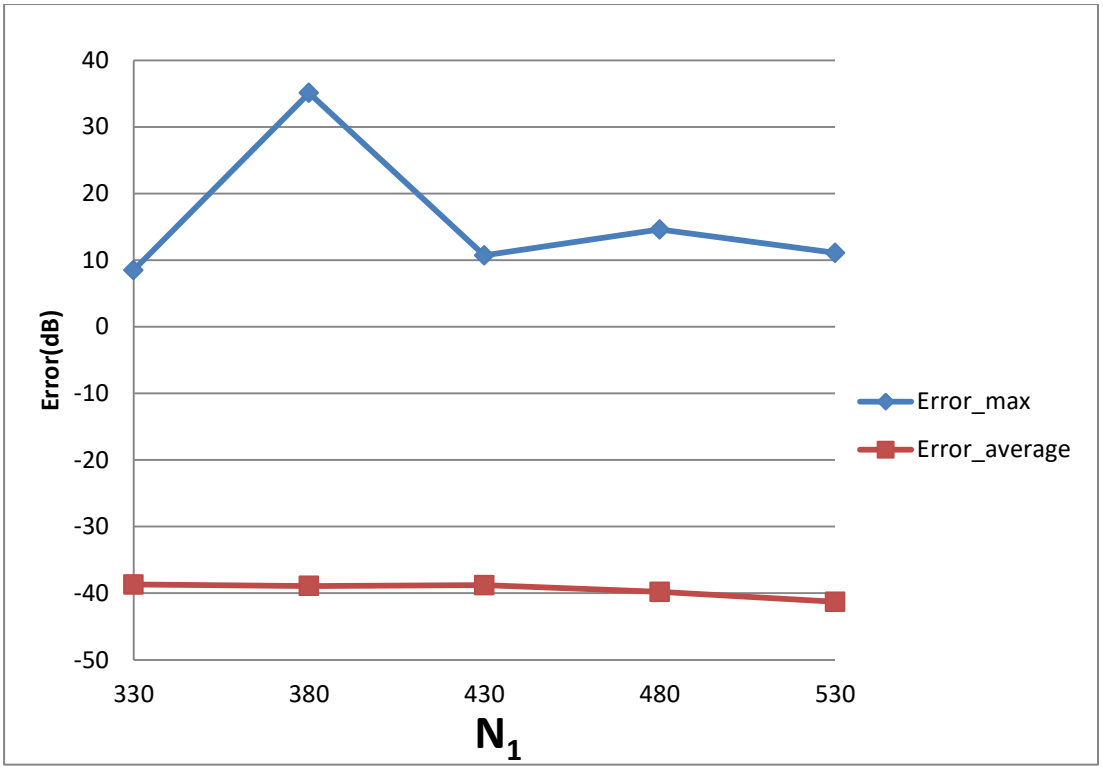

Figure 40 Error of the forward transform of 'Four-term sinusoid & Sinc' Function with fixed N2 (41) and varying N1

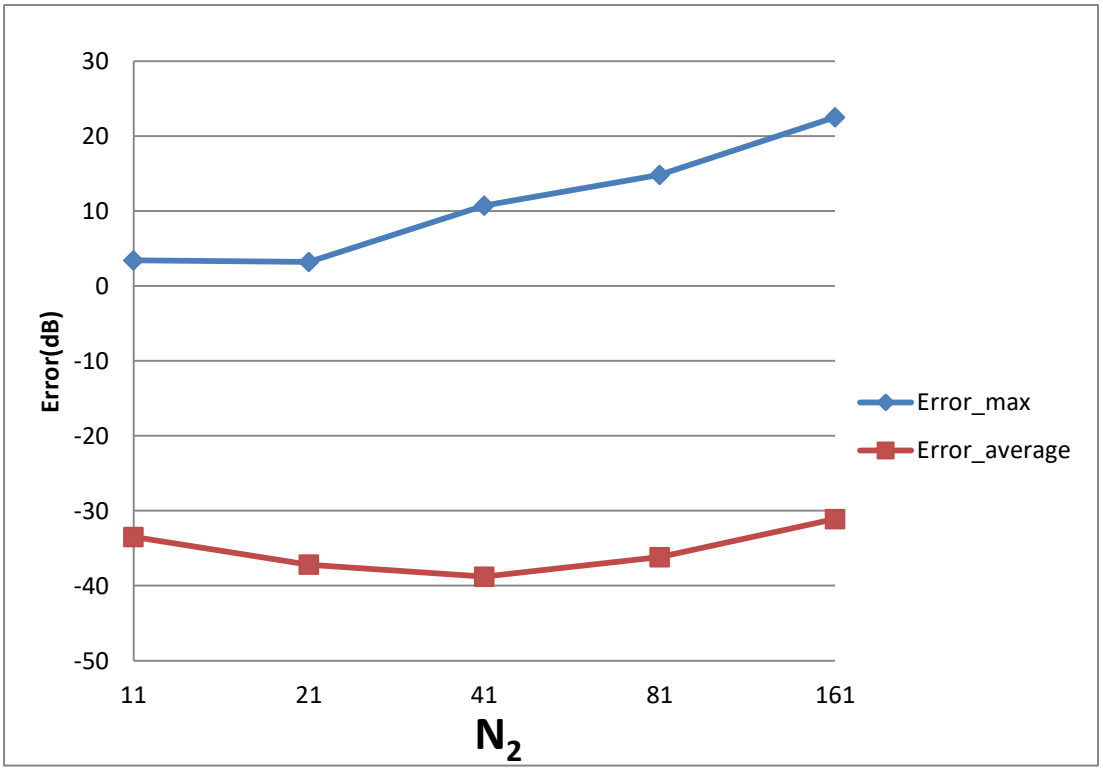

Figure 41 Error of the forward transform of 'Four-term sinusoid & Sinc' Function with fixed N1 (512) and varying N2

From Figure 40, increasing N_1 alone tends improve the average error. The maximum error does not change with N_1, which is reasonable because of the discontinuity of the function in the frequency domain.

From Figure 41, increasing N_2 leads to $Error_{\max}$ and $Error_{average}$ first improving and then worsening. This is reasonable because when N_2 is less than the minimum requirement of 31 from sampling theorem, the test result is actually affected by both sampling point density (from the sampling theorem) and grid coverage (discussed in Chapter 5). Increasing N_2 should give better results from the point of view of the sampling theorem but worse grid coverage. The result from the combined effects is dependent on the function properties. In the specific case of this function, when N_2 is bigger than 31, implying that the sampling theorem has been satisfied, the result gets worse with increasing N_2.

6.2.3.2 Inverse Transform

The results for the forward 2D-IDFT of Four-term sinusoid & Sinc function with $W_p = 30$, $N_1 = 144$ are shown in Figure 42 and Figure 43.

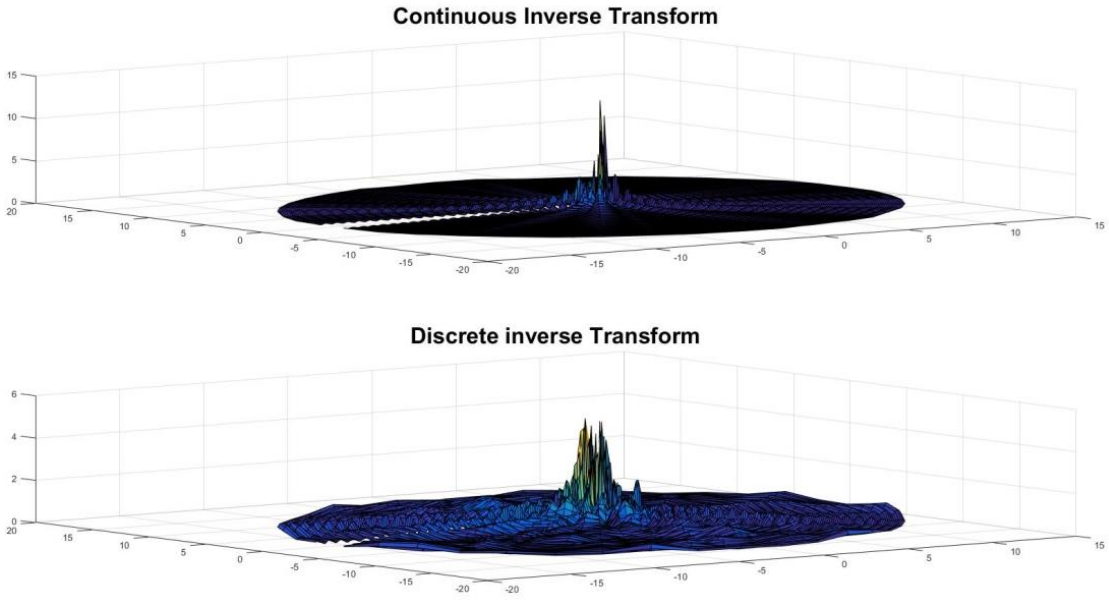

Figure 42 Sampled continuous inverse transform and discrete inverse transform of 'Four-term sinusoid & Sinc' Function with W_p=30,N_1=144

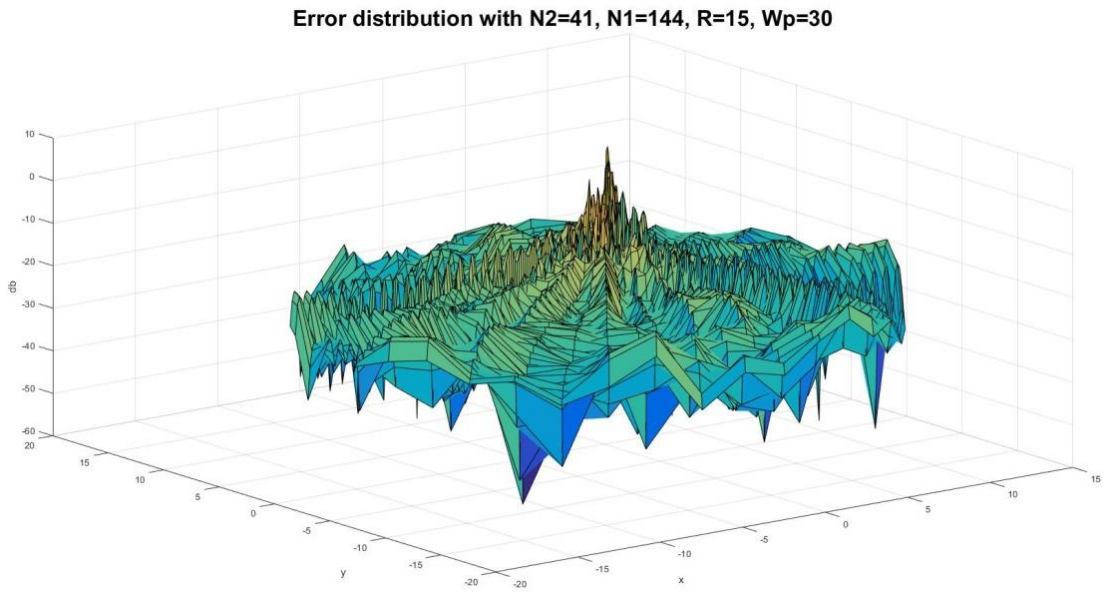

Figure 43 The error distribution of the inverse transform of 'Four-term sinusoid & Sinc' Function with W_p=30,N_1=144

The maximum value of the error is $Error_{\max} = 9.7444dB$ and the average of the error is $Error_{average} = -23.6397dB$.

The results for the 2D-IDFT of Four-term sinusoid & Sinc function with $W_p = 90$, $N_1 = 430$ are shown in Figure 44 and Figure 45.

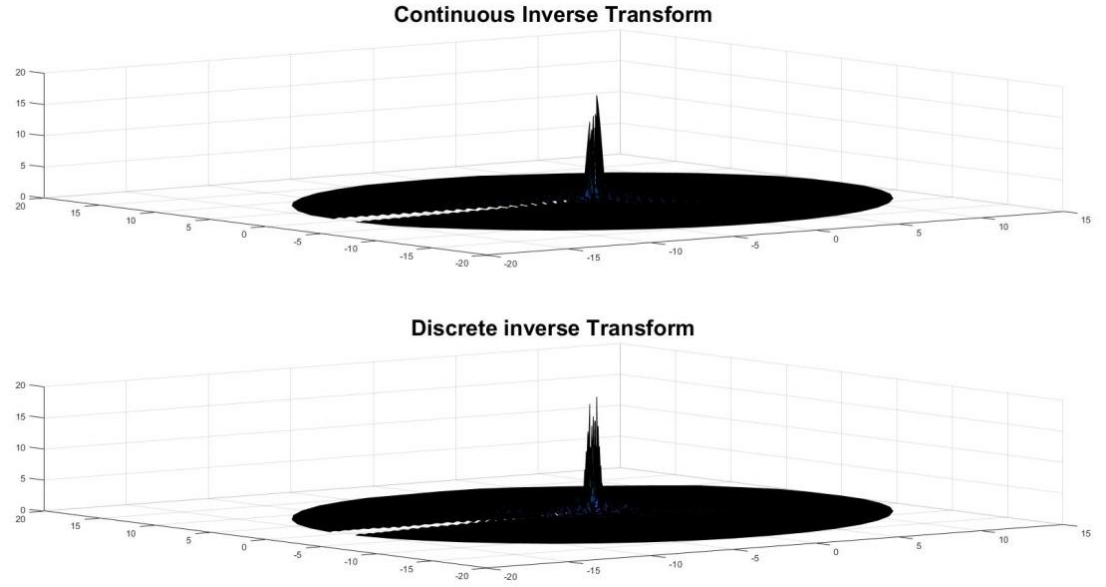

Figure 44 Sampled continuous inverse transform and discrete inverse transform of 'Four-term sinusoid & Sinc' Function with W_p=90,N_1=430

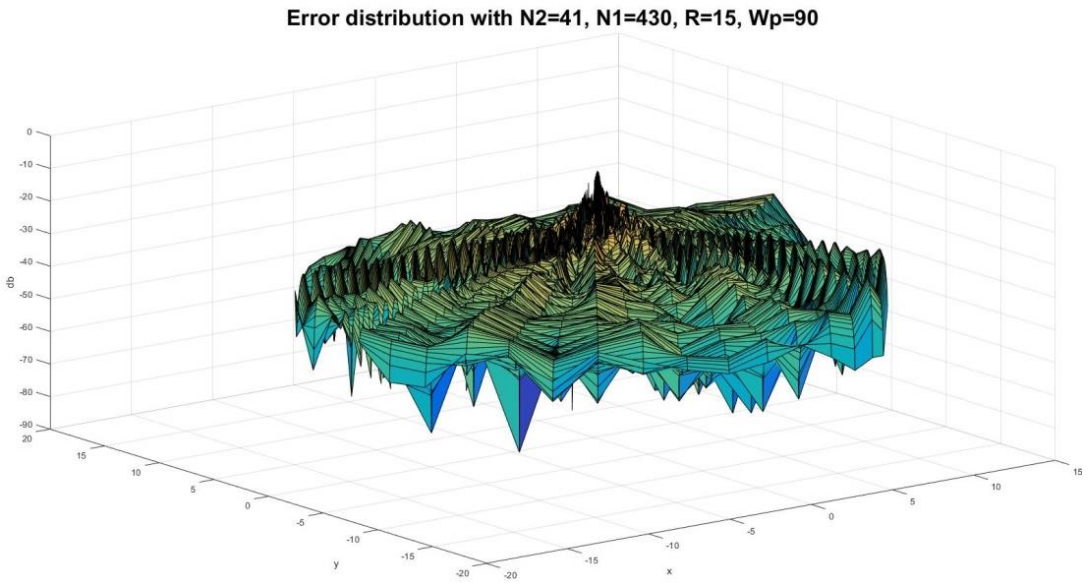

Figure 45 The error distribution of the inverse transform of 'Four-term sinusoid & Sinc' Function with W_p=90,N_1=430

The maximum value of the error is $Error_{\max} = -8.6734dB$.The average of the error is $Error_{average} = -37.8119dB$. It can be observed that the test with $W_p = 90$, $N_1 = 430$ gives a better approximation, which verifies the discussion in Chapter 5.

With $W_p = 90$, $N_1 = 430$, Table 8 shows the errors with respect to different value of N_1 and N_2, from which Figure 46 and Figure 47 show the trend.

Table 8 Error (dB) of inverse transform of 'Four-term sinusoid & Sinc' Function with different value of N_1 and N_2

N2 \ N1	330	380	430	480	530
11	$E_{\max.} = 0.1$ $E_{avg.} = -43.7$	$E_{\max.} = 0.1$ $E_{avg.} = -43.7$	$E_{\max.} = 0.1$ $E_{avg.} = -46.6$	$E_{\max.} = 0.1$ $E_{avg.} = -45.6$	$E_{\max.} = 0.1$ $E_{avg.} = -48.1$

21	$E_{\max.} = 0.7$ $E_{avg.} = -38.3$	$E_{\max.} = 0.7$ $E_{avg.} = -38.0$	$E_{\max.} = 0.6$ $E_{avg.} = -40.4$	$E_{\max.} = 0.6$ $E_{avg.} = -40.6$	$E_{\max.} = 0.7$ $E_{avg.} = -42.2$
41	$E_{\max.} = -9.0$ $E_{avg.} = -35.9$	$E_{\max.} = -8.5$ $E_{avg.} = -24.7$	$E_{\max.} = -8.7$ $E_{avg.} = -37.8$	$E_{\max.} = -8.8$ $E_{avg.} = -38.2$	$E_{\max.} = -8.6$ $E_{avg.} = -39.0$
81	$E_{\max.} = -4.5$ $E_{avg.} = -35.7$	$E_{\max.} = -4.7$ $E_{avg.} = -26.5$	$E_{\max.} = -4.5$ $E_{avg.} = -37.5$	$E_{\max.} = -4.6$ $E_{avg.} = -36.2$	$E_{\max.} = -4.5$ $E_{avg.} = -39.0$
161	$E_{\max.} = 0.8$ $E_{avg.} = -35.6$	$E_{\max.} = 0.7$ $E_{avg.} = -32.5$	$E_{\max.} = 0.7$ $E_{avg.} = -36.6$	$E_{\max.} = 0.7$ $E_{avg.} = -37.2$	$E_{\max.} = 0.7$ $E_{avg.} = -39.2$

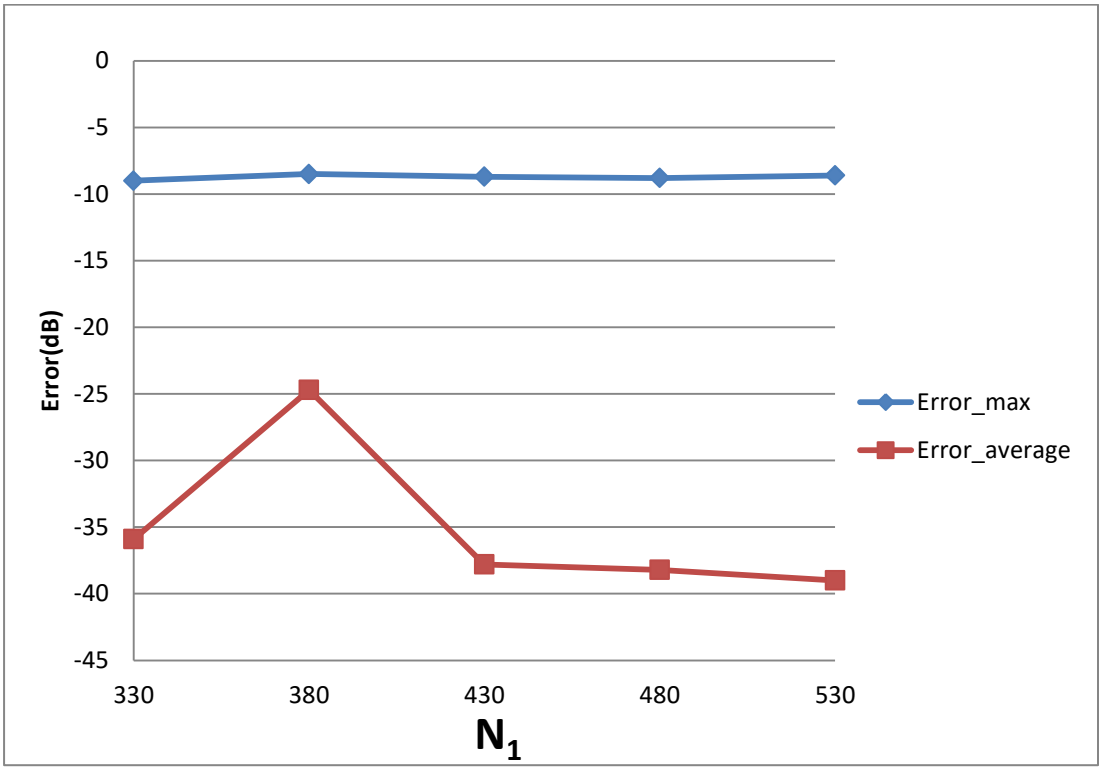

Figure 46 Error of inverse transform of 'Four-term sinusoid & Sinc' Function with fixed N_2 (41) and varying N_1

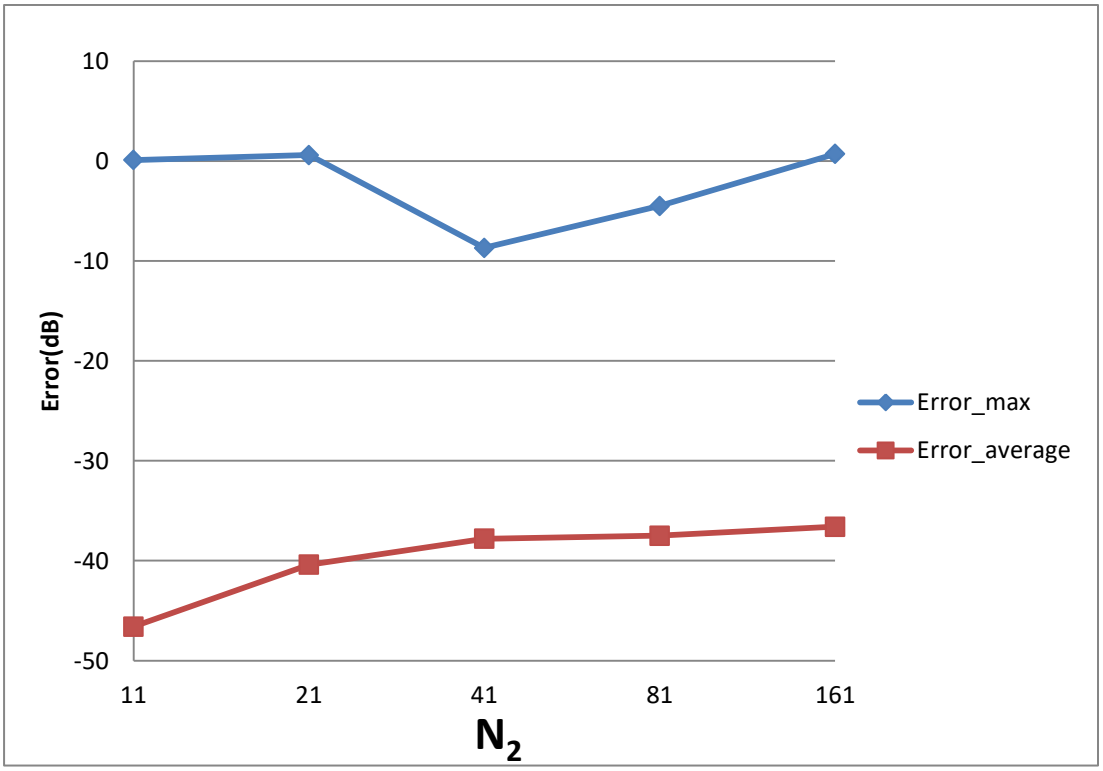

Figure 47 Error of inverse transform of 'Four-term sinusoid & Sinc' Function with fixed N_1 (512) and varying N_2

From Figure 46, it can be observed that the increasing N_1 separately improves the average errors as was expected. However, $N_1 = 380$ gives an apparently worse average error than other points. This could be caused by the discontinuity of the function in the frequency domain. Changing to $N_1 = 381$, the average error becomes -37.0 which proves that the large error is caused by discontinuity.

From Figure 47, increasing N_2 does not lead to worse results which is different from previous cases. However, from Figure 35 it can be seen that the function in the frequency domain does not have much information in the center area. So, even though increasing N_2 causes a bigger hole in the center, as discussed in Chapter 5, it does not lead to losing much energy which explains why Figure 47 shows a different trend from the previous cases.

Performing 2D-DFT and 2D-IDFT sequentially results in $\varepsilon = 1.3117 \times e^{-12}$ where ε is calculated by equation (6.2) .

6.2.4 Four-term sinusoid and modified exponential

For the next test function, the function is given by

$$f(r,\theta) = \frac{\mathrm{e}^{-ar}}{r}[3\sin(\theta) + \sin(3\theta) + 4\cos(10\theta) + 12\sin(15\theta)] \qquad (6.13)$$

Its continuous 2D-FT can be calculated as

$$F(\rho,\psi) = -6\pi i \sin(\psi)\frac{\sqrt{\rho^2+a^2}-a}{\rho\sqrt{\rho^2+a^2}} + 2\pi i \sin(3\psi)\frac{(\sqrt{\rho^2+a^2}-a)^3}{\rho^3\sqrt{\rho^2+a^2}}$$
$$-8\pi\cos(10\psi)\frac{(\sqrt{\rho^2+a^2}-a)^{10}}{\rho^{10}\sqrt{\rho^2+a^2}} + 24\pi i \sin(15\psi)\frac{(\sqrt{\rho^2+a^2}-a)^{15}}{\rho^{15}\sqrt{\rho^2+a^2}}$$
$$(6.14)$$

The graphs for the original function and its continuous 2D-FT are shown in Figure 48.

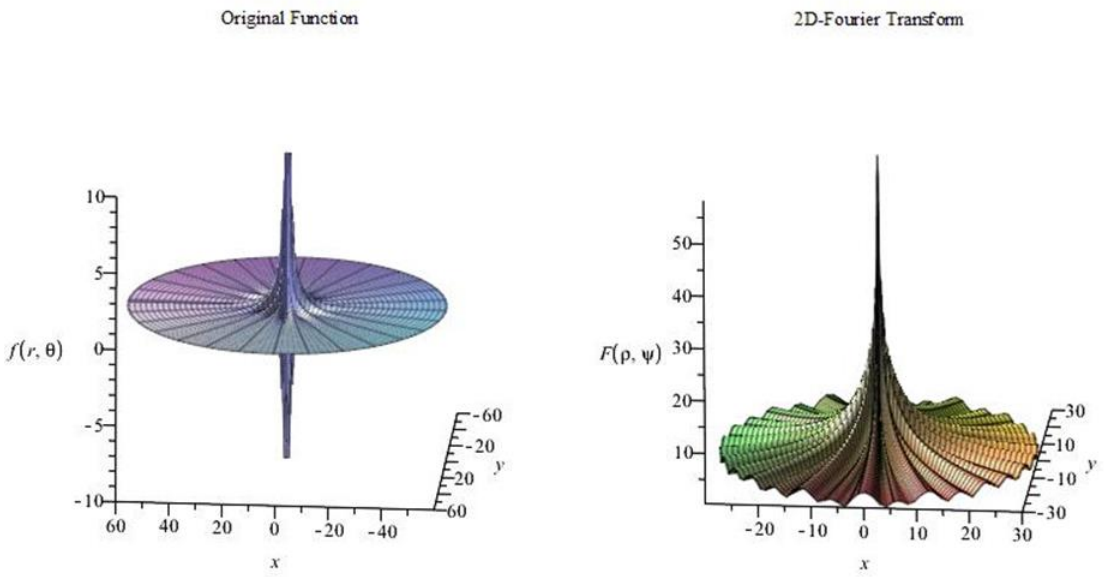

Figure 48The original function and 2D-Fourier Transform of 'Four-term Sinusoid & Modified Exponential' function

From Figure 48, it can be observed that the function has a spike in both domains, which is a more difficult scenario based on the discussion in Chapter 5. In this case, the function can be assumed as space-limited or band-limited. This function will be tested as being space-limited and band-limited.

From graph of the original function and its 2D-DFT, it can be assumed that $f(r,\theta)$ is effectively space-limited from $R=20$ and $F(\rho,\psi)$ is effectively band-limited with $W_p=15$,which gives $j_{0N_1}\approx 300$. This results in $N_1=96.$ However, since the function explodes at the center area in both domains, relatively large values of R and W_p should give a better approximation. Therefore, another case with $R=40$, $W_p=30$ is tested. In this case, $N_1=383$ is chosen.

In the angular direction, the highest frequency term is $12\sin(15\theta)$. From the sampling theorem, the sampling frequency should be at least twice of the highest frequency of signal. Thus $N_2=41$ is chosen.

6.2.4.1 Test as a space limited function

6.2.4.1.1 Forward Transform

Here, the function is tested as a space limited function and equation (3.28) and (3.29) are used to proceed with the forward and inverse transform in sequence.

The results for the 2D-DFT of the Four-term sinusoid & Modified exponential function with $R = 20, W_p = 15, N_1 = 96$ are shown in Figure 49 and Figure 50.

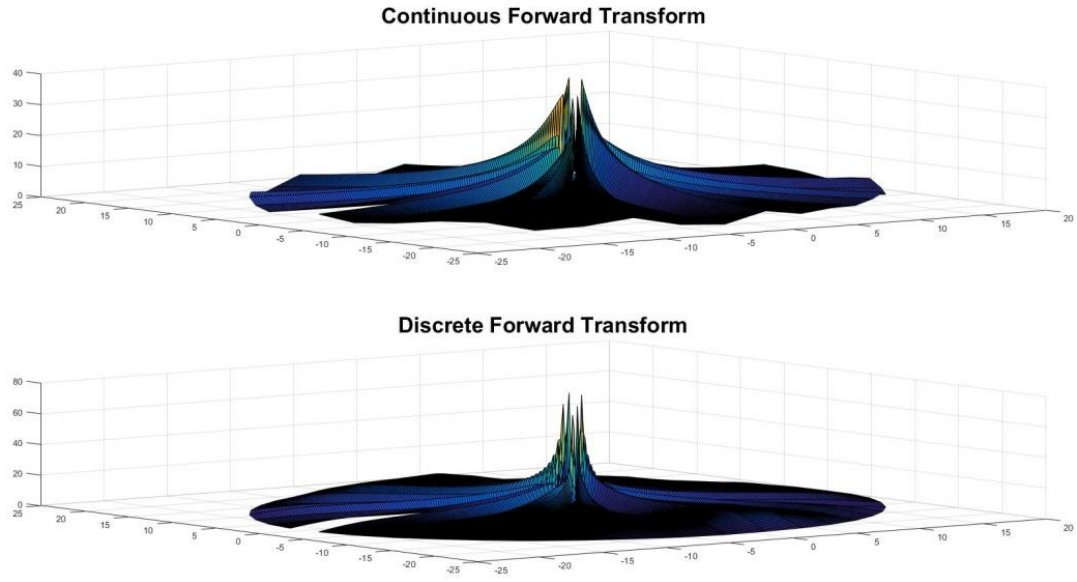

Figure 49 Continuous forward transform and discrete forward transform of 'Four-term Sinusoid & Modified Exponential' function with R=20, W_p=15, N_1=96(test as a space limited function)

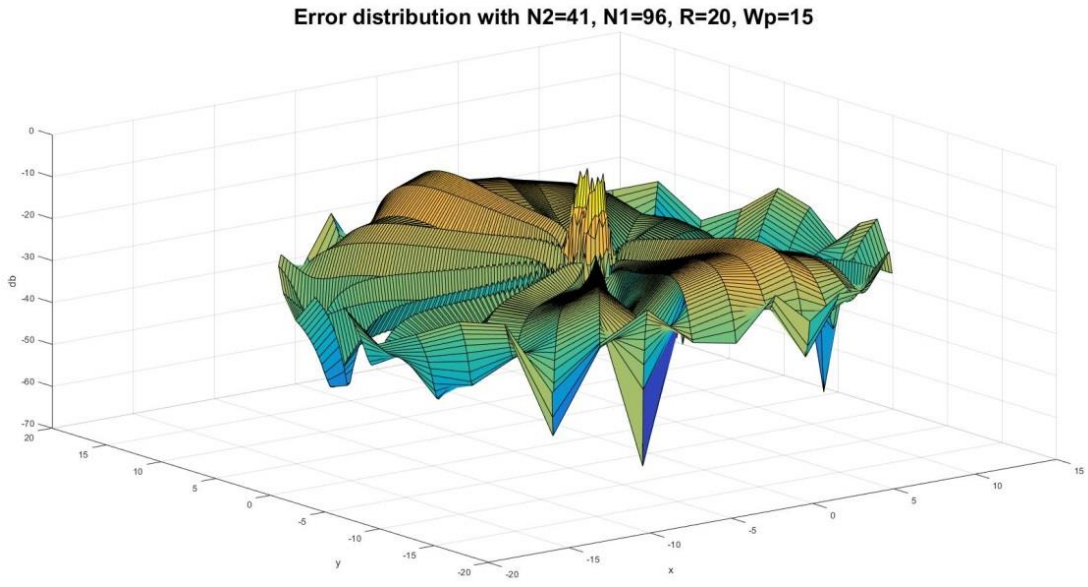

Figure 50 The error distribution of the forward transform of 'Four-term Sinusoid & Modified Exponential' function with R=20, W_p=15, N_1=96(test as a space limited function)

From Figure 50, it can be observed that the error gets larger at the center, which is as expected because the sampling grid shows that the sampling points cannot reach the origin. The maximum value of the error is $Error_{\max} = -6.6128dB$ and it happens at the center. The average of the error is $Error_{average} = -29.4738dB$.

The results with $R = 40, W_p = 30, N_1 = 383$ are shown in Figure 51 and Figure 52.

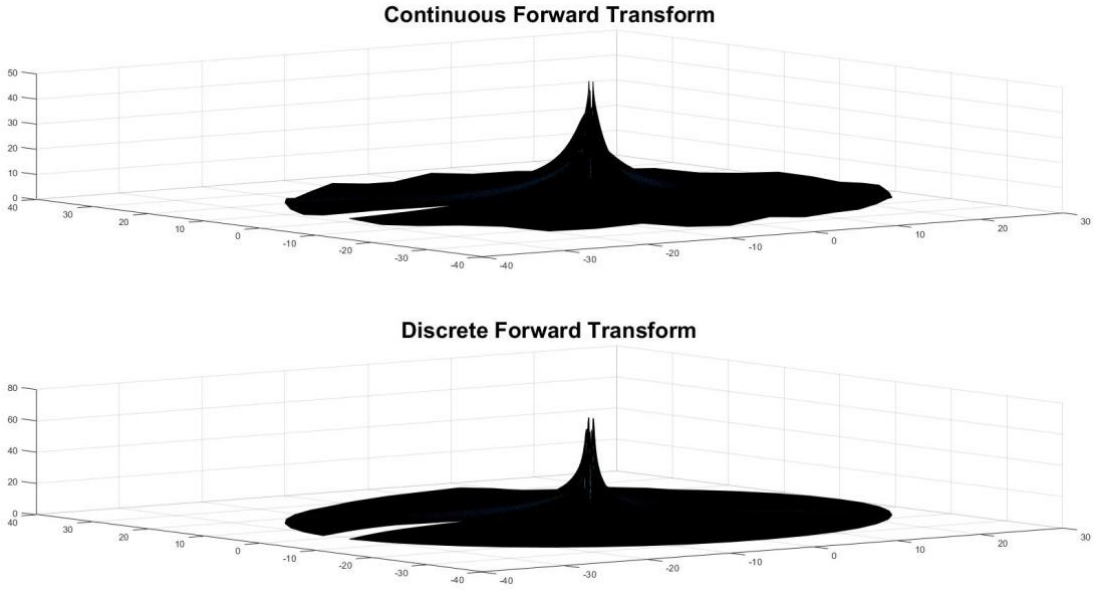

Figure 51 Continuous forward transform and discrete forward transform of 'Four-term Sinusoid & Modified Exponential' function with R=40, W_p=30, N_1=383(test as a space limited function)

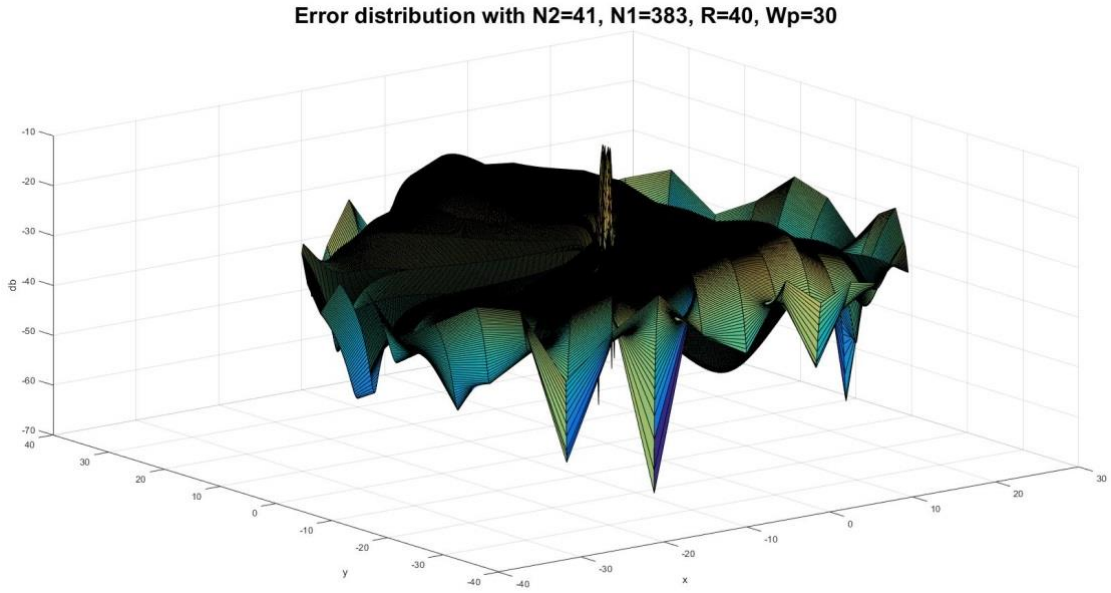

Figure 52 The error distribution of the forward transform of 'Four-term Sinusoid & Modified Exponential' function with R=40, W_p=30, N_1=383(test as a space limited function)

The maximum value of the error is $Error_{\max} = -10.1535dB$ and this occurs at the center area. The average of the error is $Error_{average} = -32.7619dB$. It shows a better result than the previous case. Table 9 shows the errors with respect to different value of N_1 and N_2, from which Figure 53 and Figure 54 show the trend.

Table 9 Error (dB) of forward transform of 'Four-term sinusoid & Modified Exponential' Function with different value of N_1 and N_2 (test as a space limited function)

N2 \ N1	283	333	383	433	483
11	$E_{\max.} = -0.8$ $E_{avg.} = -23.6$	$E_{\max.} = -0.8$ $E_{avg.} = -24.8$	$E_{\max.} = -0.8$ $E_{avg.} = -26.0$	$E_{\max.} = -0.8$ $E_{avg.} = -27.0$	$E_{\max.} = -0.9$ $E_{avg.} = -27.8$
21	$E_{\max.} = -2.6$ $E_{avg.} = -21.4$	$E_{\max.} = -2.7$ $E_{avg.} = -22.6$	$E_{\max.} = -2.7$ $E_{avg.} = -23.7$	·· $E_{avg.} = -24.7$	$E_{\max.} = -2.8$ $E_{avg.} = -25.6$

41	$E_{max.} = -10.6$ $E_{avg.} = -30.2$	$E_{max.} = -10.3$ $E_{avg.} = -31.6$	$E_{max.} = -10.1$ $E_{avg.} = -32.8$	$E_{max.} = -10.0$ $E_{avg.} = -33.8$	$E_{max.} = -9.9$ $E_{avg.} = -34.7$
81	$E_{max.} = -6.3$ $E_{avg.} = -30.4$	$E_{max.} = -6.2$ $E_{avg.} = -31.8$	$E_{max.} = -6.2$ $E_{avg.} = -33.0$	$E_{max.} = -6.0$ $E_{avg.} = -34.0$	$E_{max.} = -6.0$ $E_{avg.} = -35.0$
161	$E_{max.} = -3.0$ $E_{avg.} = -27.7$	$E_{max.} = -2.9$ $E_{avg.} = -29.0$	$E_{max.} = -2.9$ $E_{avg.} = -30.2$	$E_{max.} = -2.8$ $E_{avg.} = -31.3$	$E_{max.} = -2.8$ $E_{avg.} = -32.2$

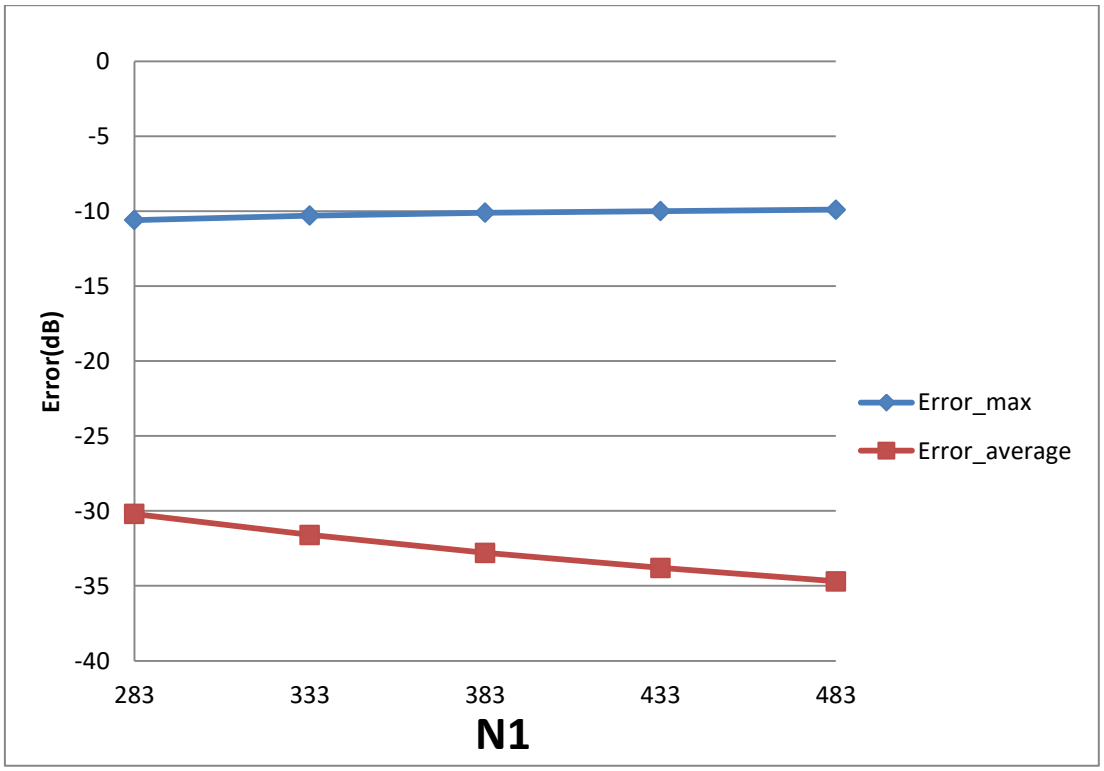

Figure 53 Error of forward transform for 'Four-term sinusoid & Modified Exponential' Function with fixed N_2 (41) and varying N_1 (test as a space limited function)

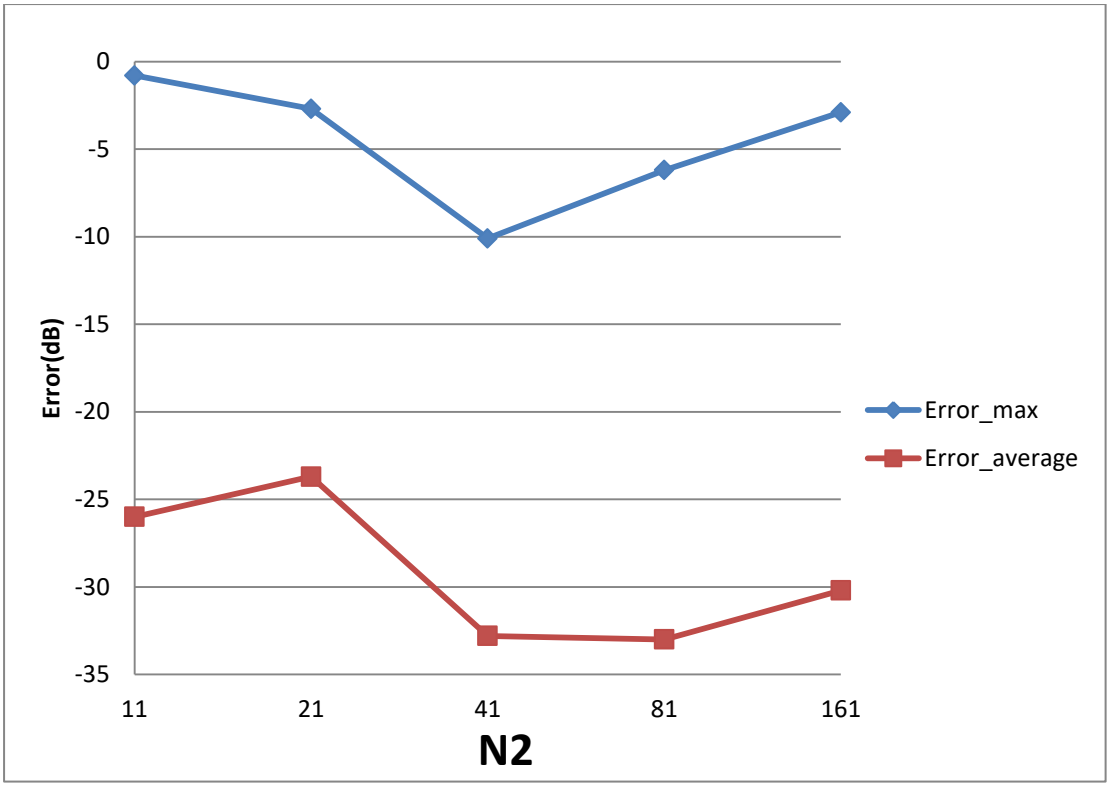

Figure 54 Error of forward transform for 'Four-term sinusoid & Modified Exponential' Function with fixed N_1 (383) and varying N_2 (test as a space limited function)

From Figure 53, increasing N_1 alone does not change the maximum error very much but improves the average error significantly. From Figure 54, before the minimum sampling points criteria (two times of the highest frequency) is satisfied, the error is large. After the criteria is satisfied, increasing N_2 leads to larger $Error_{\max}$ and $Error_{average}$, as in previous cases.

6.2.4.1.2 Inverse Transform

The results for the 2D-IDFT of the Four-term sinusoid & Modified exponential function with $R = 20, W_p = 15, N_1 = 96$ are shown in Figure 55 and Figure 56.

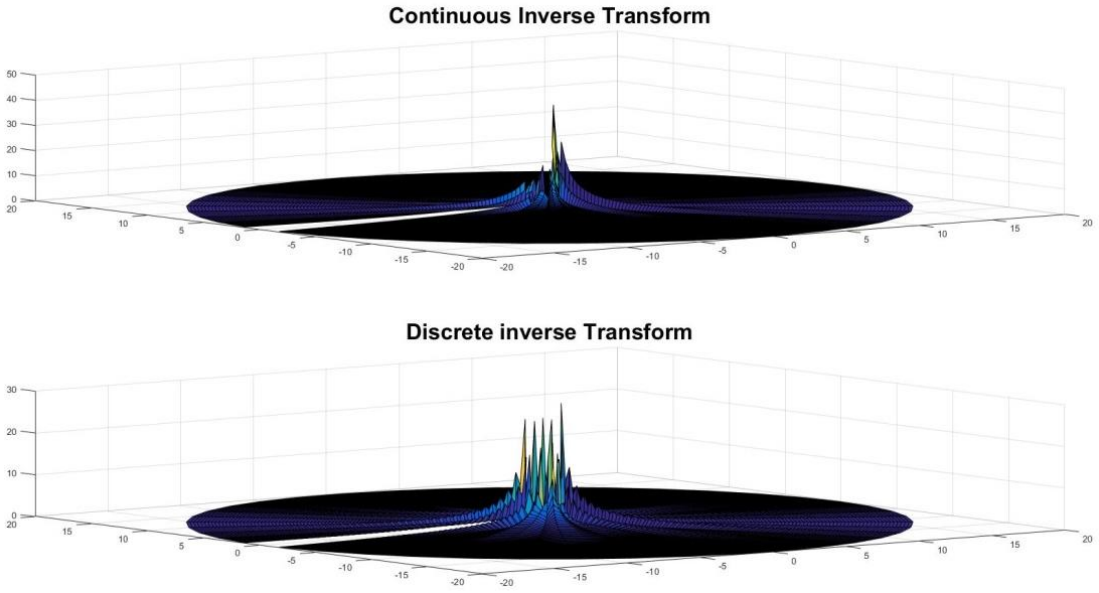

Figure 55 Continuous inverse transform and discrete inverse transform of 'Four-term Sinusoid & Modified Exponential' function with R=20, W_p=15, N_1=96(test as a space limited function)

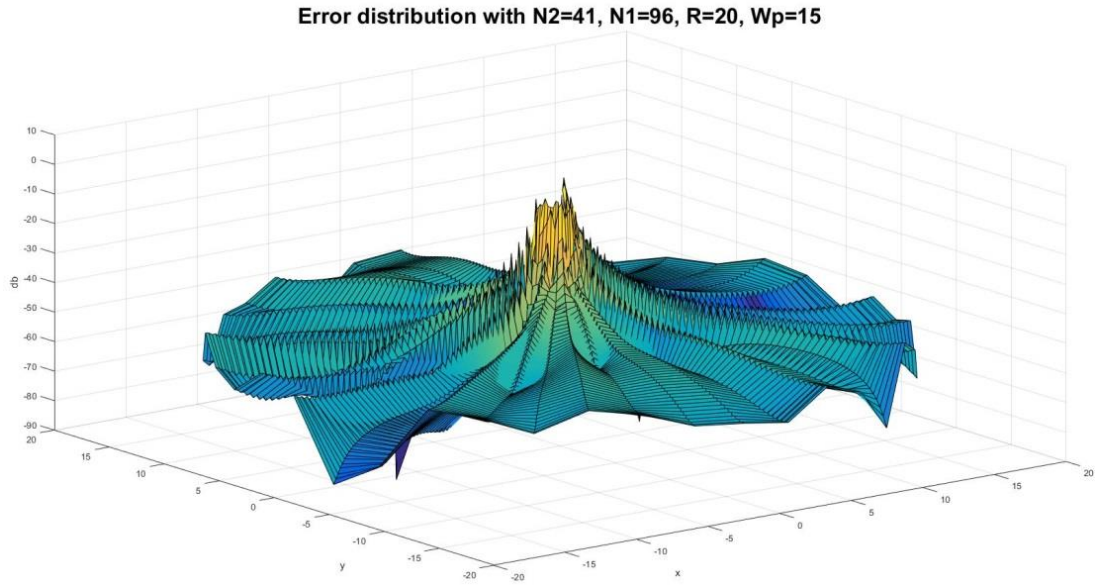

Figure 56 The error distribution of the inverse transform of 'Four-term Sinusoid & Modified Exponential' function with R=20, W_p=15, N_1=96(test as a space limited function)

Similar to the forward transform, large errors appear at center area as expected. The maximum value of the error is $Error_{\max} = 0.5211dB$ .The average of the error is $Error_{average} = -49.8349dB$.

The results with $R = 40, W_p = 30, N_1 = 383$ are shown in Figure 57 and Figure 58.

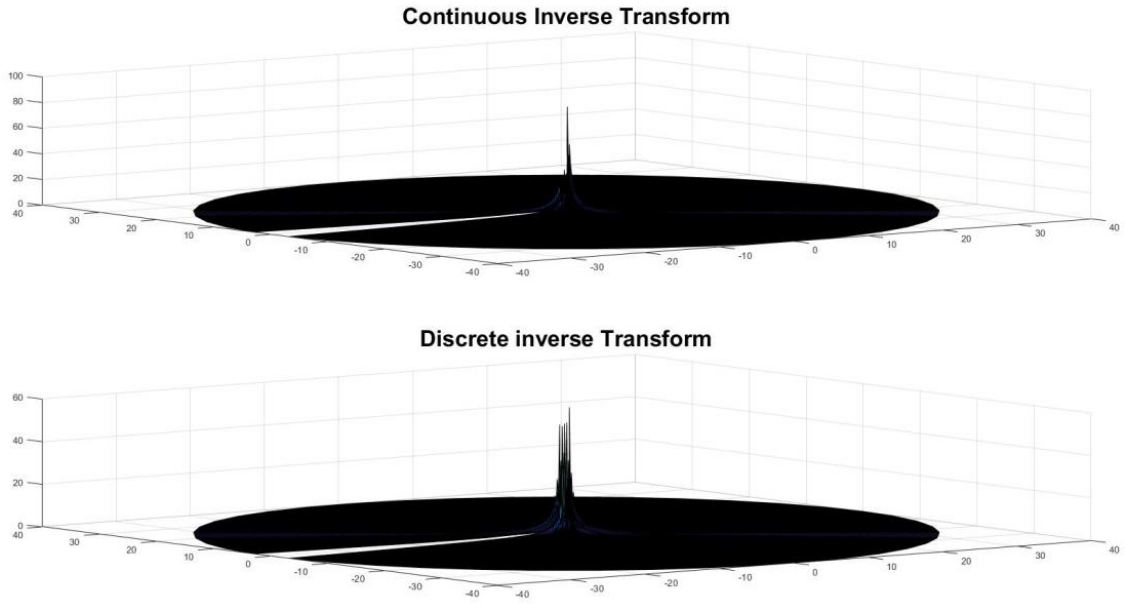

Figure 57 Continuous inverse transform and discrete forward transform of 'Four-term Sinusoid & Modified Exponential' function with R=40, W_p=30, N_1=383(test as a space limited function)

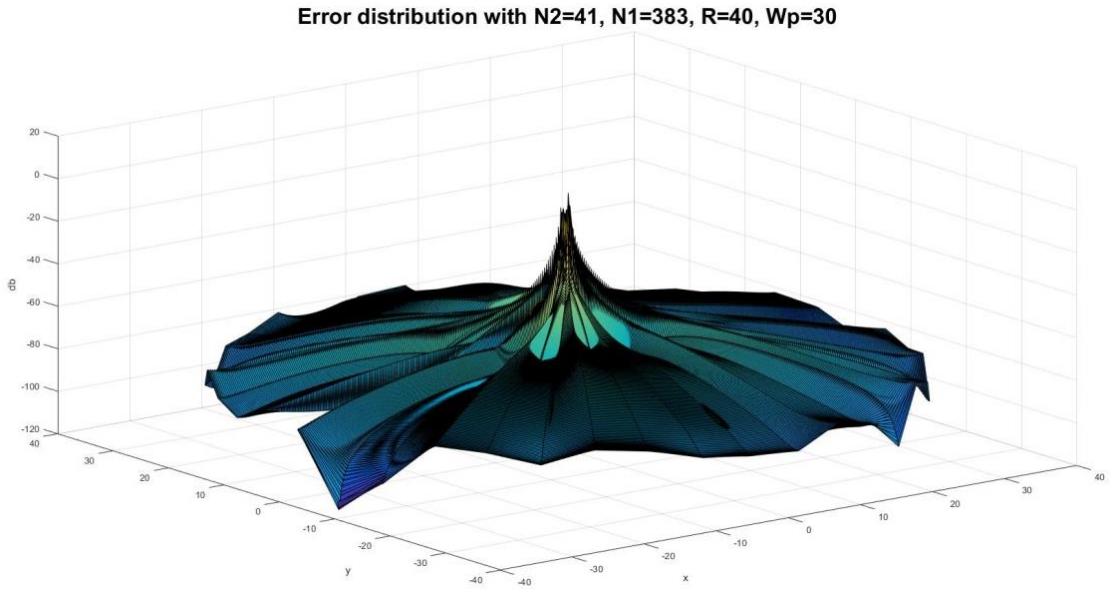

Figure 58 The error distribution of the forward transform of 'Four-term Sinusoid & Modified Exponential' function with R=40, W_p=30, N_1=383 (test as a space limited function)

The maximum value of the error is $Error_{\max} = 0.5579dB$ and this occurs at the center. The average of the error is $Error_{average} = -68.7317dB$. This is a better result than the previous case. Table 10 shows the errors with respect to different values of N_1 and N_2, from which Figure 59 and Figure 60 a show the trend.

Table 10 Error (dB) of inverse transform of 'Four-term sinusoid & Modified Exponential' Function with different value of N_1 and N_2(test as a space limited function)

N2 \ N1	283	333	383	433	483
11	$E_{\max.}=1.1$ $E_{avg.}=-60.5$	$E_{\max.}=1.0$ $E_{avg.}=-62.1$	$E_{\max.}=1.0$ $E_{avg.}=-63.4$	$E_{\max.}=0.9$ $E_{avg.}=-64.6$	$E_{\max.}=0.9$ $E_{avg.}=-65.6$
21	$E_{\max.}=6.9$ $E_{avg.}=-57.1$	$E_{\max.}=6.8$ $E_{avg.}=-58.6$	$E_{\max.}=6.8$ $E_{avg.}=-59.9$	$E_{\max.}=6.7$ $E_{avg.}=-61.0$	$E_{\max.}=6.7$ $E_{avg.}=-61.9$
41	$E_{\max.}=0.6$ $E_{avg.}=-65.9$	$E_{\max.}=0.6$ $E_{avg.}=-67.4$	$E_{\max.}=0.6$ $E_{avg.}=-68.7$	$E_{\max.}=0.5$ $E_{avg.}=-69.9$	$E_{\max.}=0.5$ $E_{avg.}=-70.9$
81	$E_{\max.}=2.7$ $E_{avg.}=-65.3$	$E_{\max.}=2.6$ $E_{avg.}=-66.9$	$E_{\max.}=2.5$ $E_{avg.}=-68.2$	$E_{\max.}=2.5$ $E_{avg.}=-69.4$	$E_{\max.}=2.4$ $E_{avg.}=-70.4$
161	$E_{\max.}=0.5$ $E_{avg.}=-62.3$	$E_{\max.}=0.4$ $E_{avg.}=-64.9$	$E_{\max.}=0.2$ $E_{avg.}=-66.3$	$E_{\max.}=0.1$ $E_{avg.}=-67.5$	$E_{\max.}=0.0$ $E_{avg.}=-68.6$

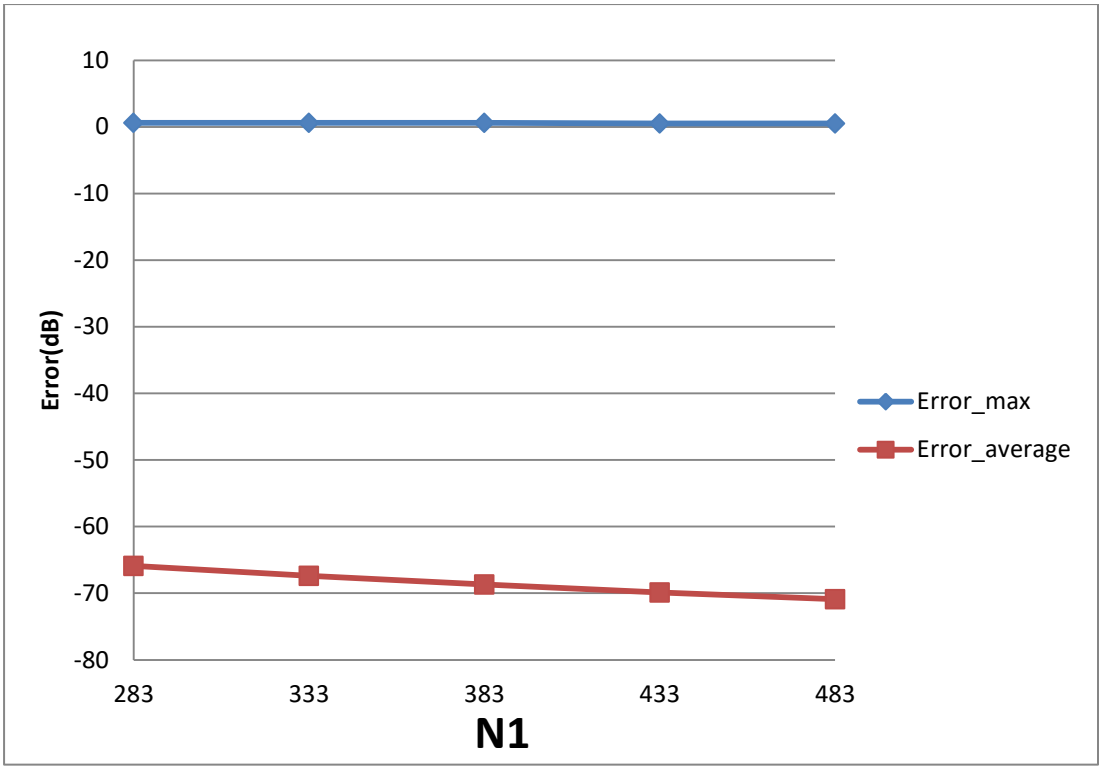

Figure 59 Error of inverse transform for 'Four-term sinusoid & Modified Exponential' Function with fixed N_2 (41) and varying N_1 (test as a space limited function)

.

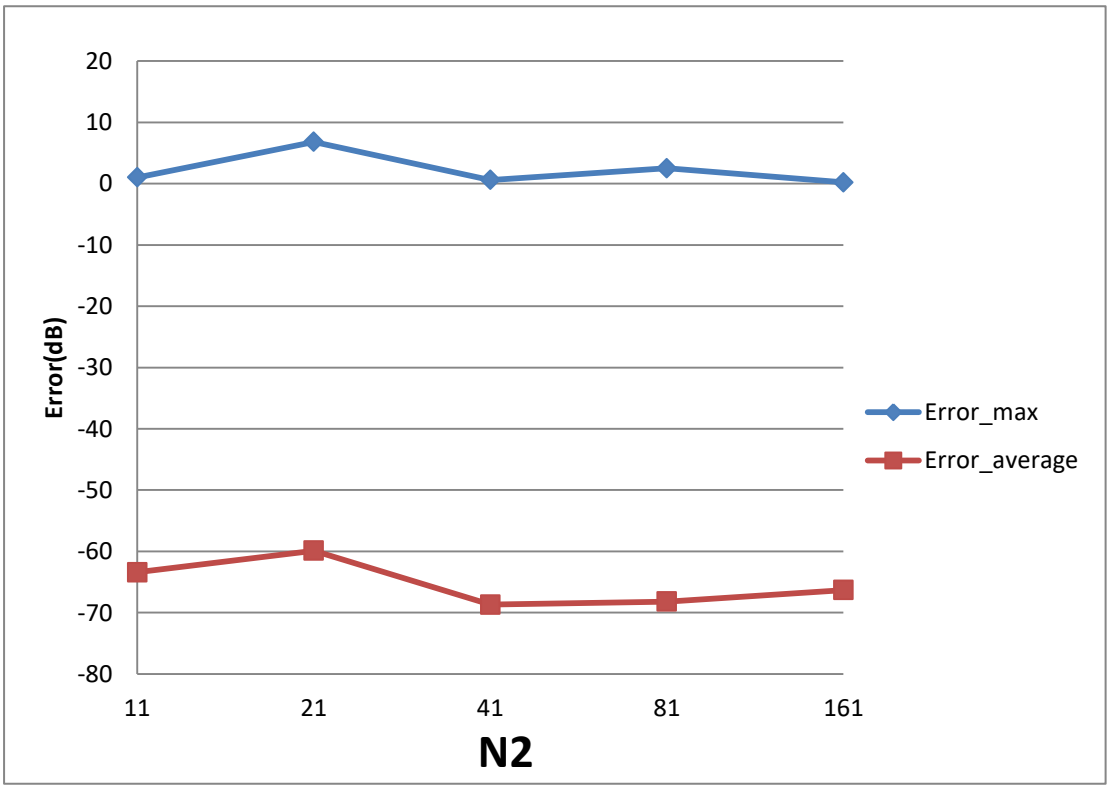

Figure 60 Error of inverse transform for 'Four-term sinusoid & Modified Exponential' Function with fixed N_1 (383) and varying N_2 (test as a space limited function)

A similar trend to the forward transform is obtained. Performing 2D-DFT and 2D-IDFT results in $\varepsilon = 1.421 \times e^{-12}$, where ε is calculated by equation (6.2) .

6.2.4.2 Test as a band-limited function

6.2.4.2.1 Forward Transform

The function will be tested as a band-limit function. Therefore equation (3.31) and (3.32) are used to proceed with the forward and inverse transform.

The results for the 2D-IDFT of the Four-term sinusoid & Modified exponential function with $R = 20, W_p = 15, N_1 = 96$ are shown in Figure 61 and Figure 62.

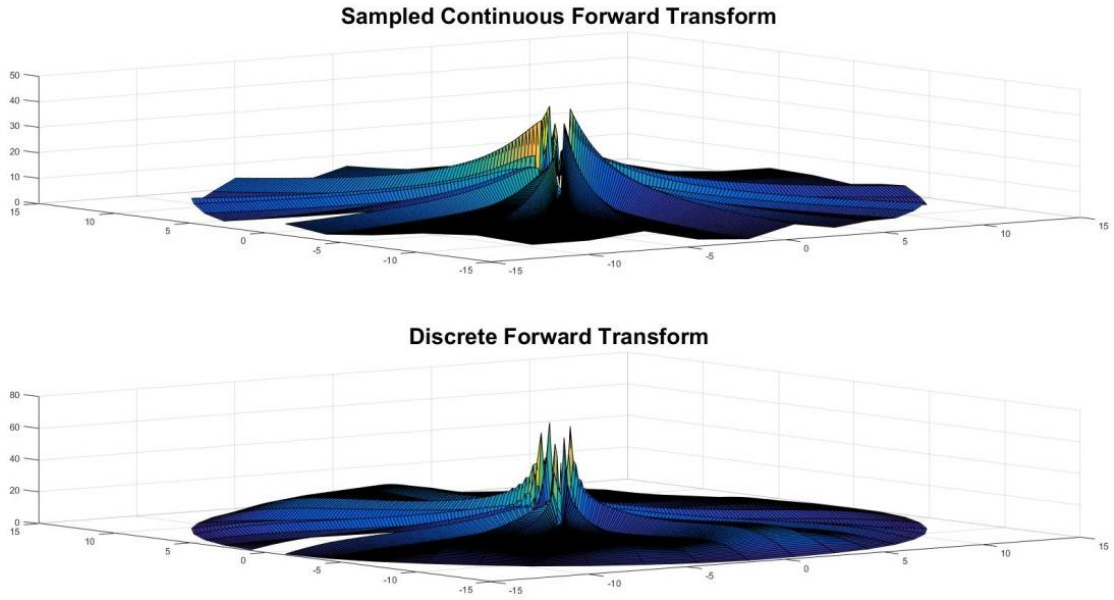

Figure 61 Continuous forward transform &. Discrete forward transform of 'Four-term Sinusoid & Modified Exponential' function with R=20, W_p=15, N_1=96(test as a band limited function)

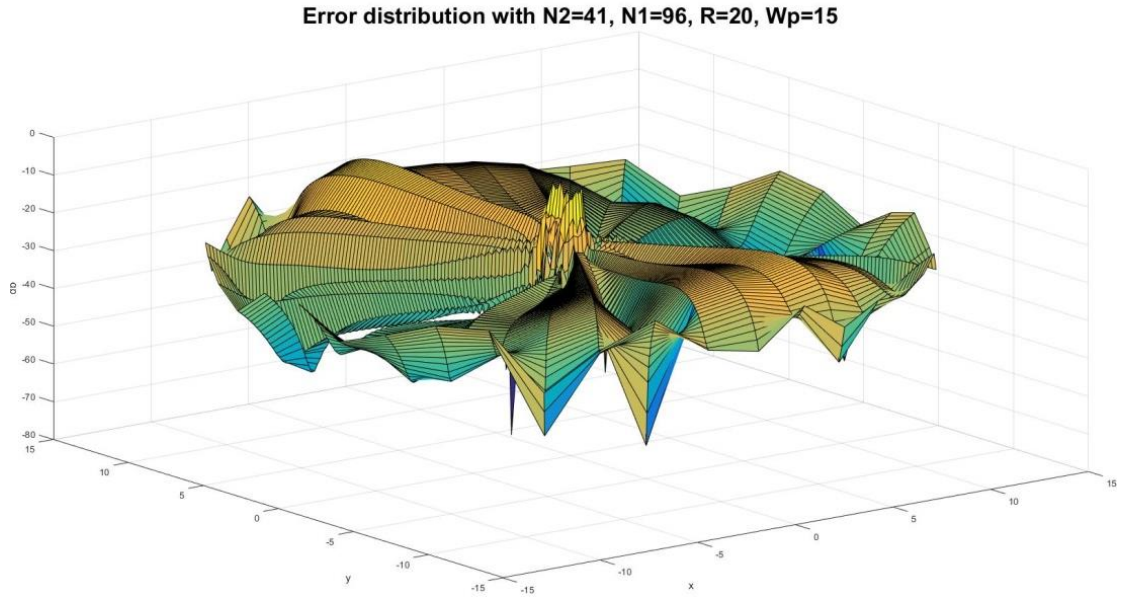

Figure 62 The error distribution of the forward transform of 'Four-term Sinusoid & Modified Exponential' function with R=20, W_p=15, N_1=96(test as a band limited function)

The maximum value of the error is $Error_{\max} = -7.8789dB$ and this occurs at the center. The average of the error is $Error_{average} = -29.0278dB$.

The results with $R = 40$, $W_p = 30$, $N_1 = 383$ are shown in Figure 63 and Figure 64.

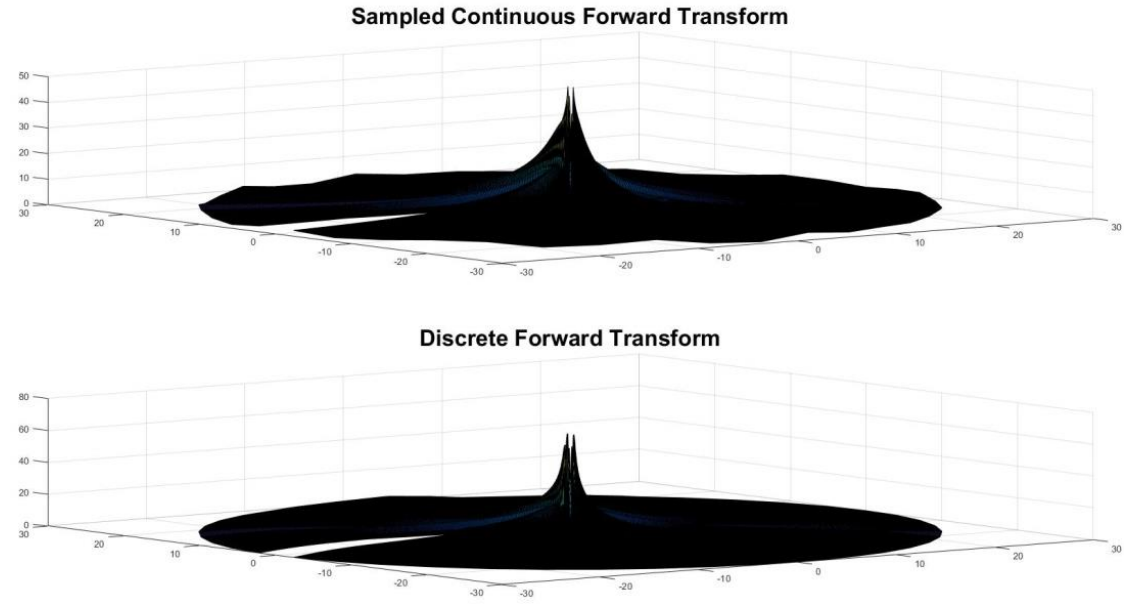

Figure 63 Continuous forward transform and discrete forward transform of 'Four-term Sinusoid & Modified Exponential' function with R=40, W_p=30, N_1=383 (test as a band limited function)

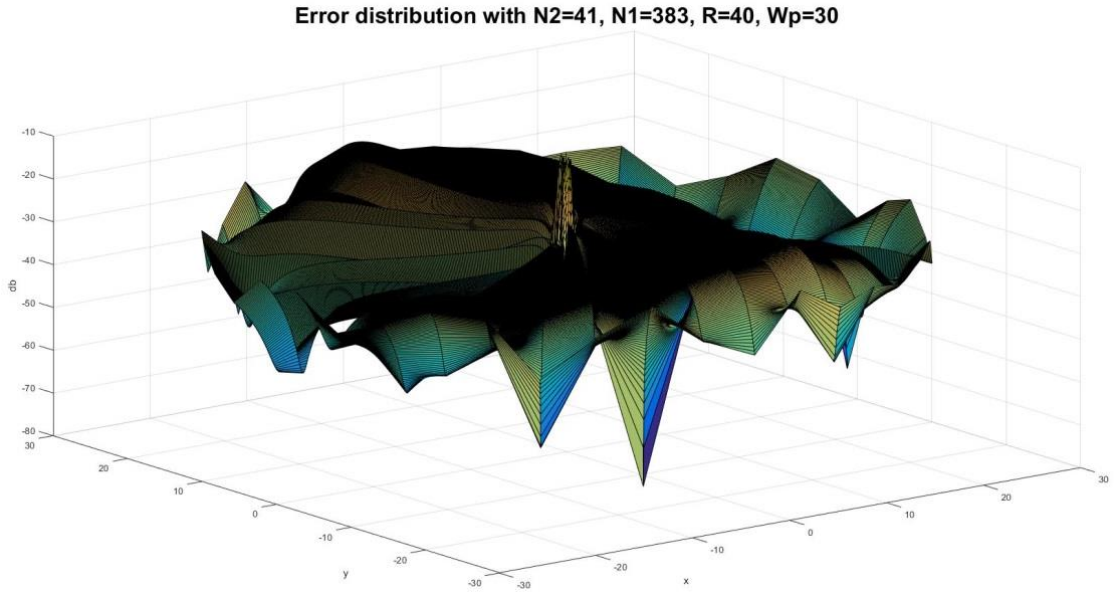

Figure 64 The error distribution of the forward transform of 'Four-term Sinusoid & Modified Exponential' function with R=40, W_p=30, N_1=383(test as a band limited function)

The maximum value of the error is $Error_{\max} = -10.6392dB$ and this occurs at the center. The average of the error is $Error_{average} = -32.6585dB$. Table 11 shows the errors with respect to different values of N_1 and N_2, from which Figure 65 and Figure 66 show the trend.

Table 11 Error (dB) of forward transform of 'Four-term sinusoid & Modified Exponential' Function with different value of N_1 and N_2 (test as a band limited function)

N2 \ N1	283	333	383	433	483
11	$E_{\max.} = -0.4$ $E_{avg.} = -27.8$	$E_{\max.} = -0.6$ $E_{avg.} = -27.0$	$E_{\max.} = -0.8$ $E_{avg.} = -26.0$	$E_{\max.} = -0.7$ $E_{avg.} = -25.0$	$E_{\max.} = -0.5$ $E_{avg.} = -24.1$
21	$E_{\max.} = -2.3$ $E_{avg.} = -25.2$	$E_{\max.} = -2.5$ $E_{avg.} = -24.1$	$E_{\max.} = -2.7$ $E_{avg.} = -23.5$	$E_{\max.} = -2.5$ $E_{avg.} = -22.9$	$E_{\max.} = -1.6$ $E_{avg.} = -21.5$

41	$E_{max.} = -3.7$ $E_{avg.} = -28.7$	$E_{max.} = -6.6$ $E_{avg.} = -30.3$	$E_{max.} = -10.6$ $E_{avg.} = -32.7$	$E_{max.} = -11.1$ $E_{avg.} = -31.8$	$E_{max.} = -4.5$ $E_{avg.} = -28.2$
81	$E_{max.} = -3.5$ $E_{avg.} = -32.3$	$E_{max.} = -5.3$ $E_{avg.} = -34.2$	$E_{max.} = -6.2$ $E_{avg.} = -31.3$	$E_{max.} = -6.4$ $E_{avg.} = -28.4$	$E_{max.} = -6.2$ $E_{avg.} = -25.4$
161	$E_{max.} = -3.4$ $E_{avg.} = -34.1$	$E_{max.} = -3.1$ $E_{avg.} = -31.6$	$E_{max.} = -2.7$ $E_{avg.} = -28.1$	$E_{max.} = -2.5$ $E_{avg.} = -25.0$	$E_{max.} = -1.7$ $E_{avg.} = -22.5$

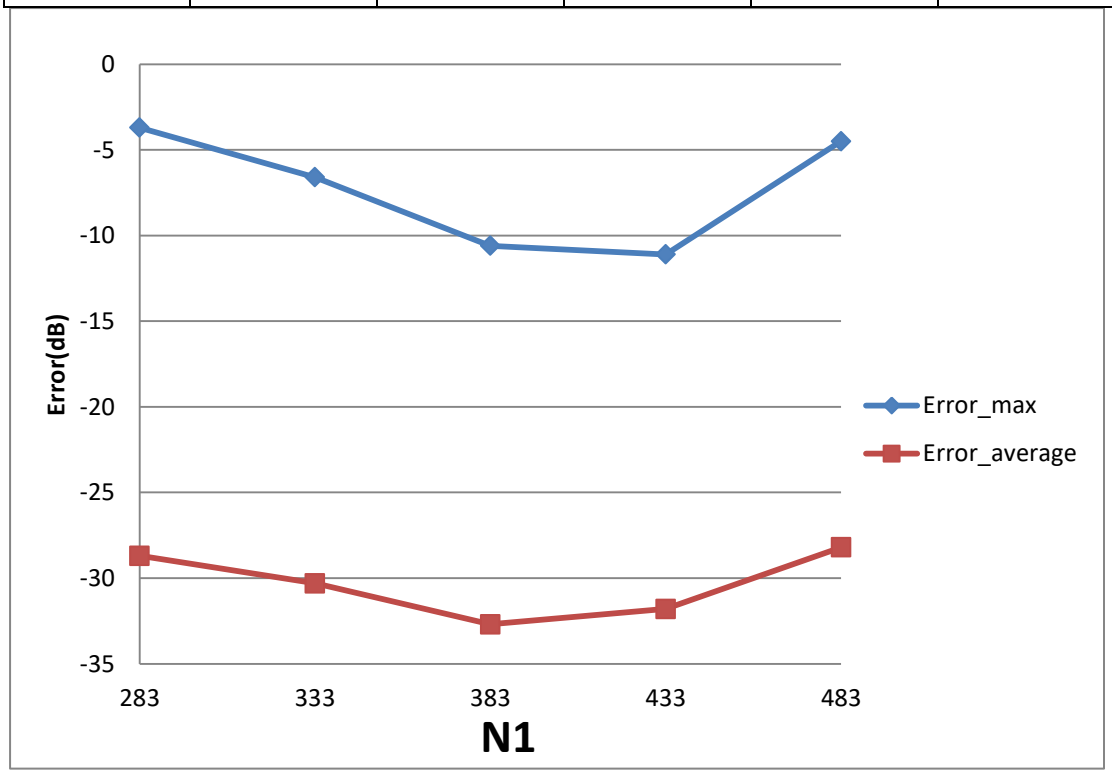

Figure 65 Error of forward transform for 'Four-term sinusoid & Modified Exponential' Function with fixed N_2 (41) and varying N_1 (test as a band limited function)

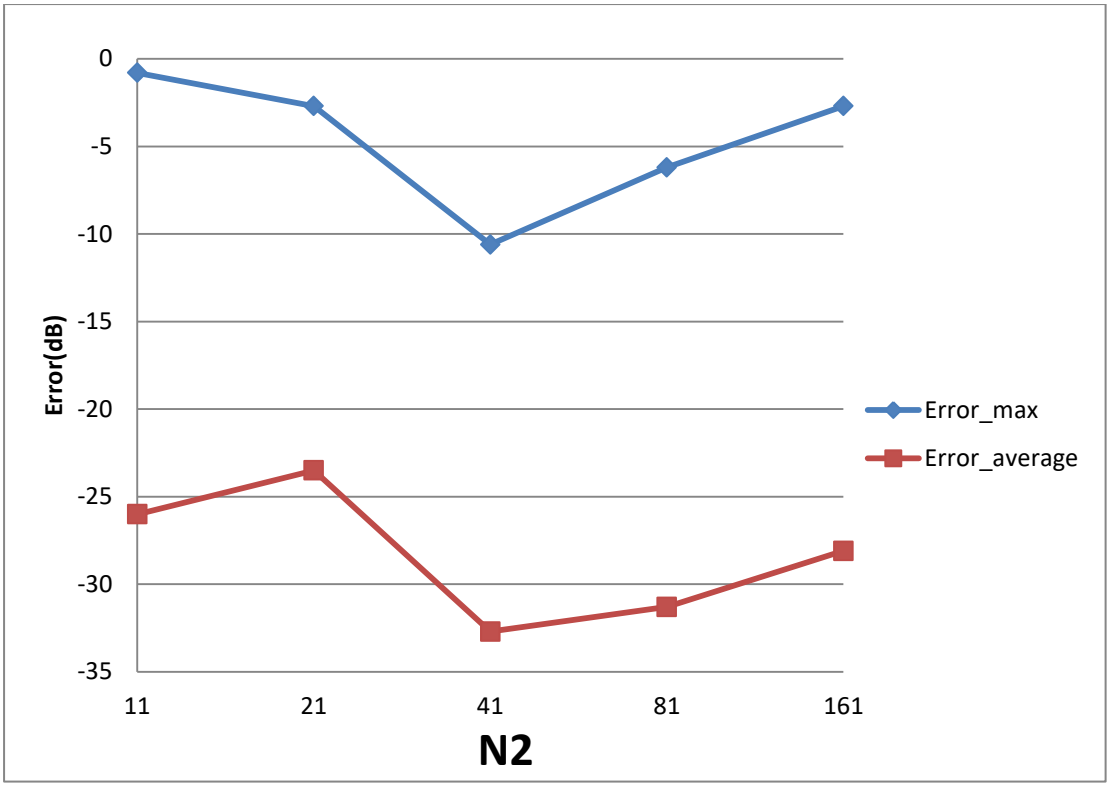

Figure 66 Error of forward transform for 'Four-term sinusoid & Modified Exponential' Function with fixed N_1 (383) and varying N_2 (test as a band limited function)

6.2.4.2.2 Inverse Transform

The results for the 2D-IDFT of the Four-term sinusoid & Modified exponential function with $R = 20, W_p = 15, N_1 = 96$ are shown in Figure 67 and Figure 68.

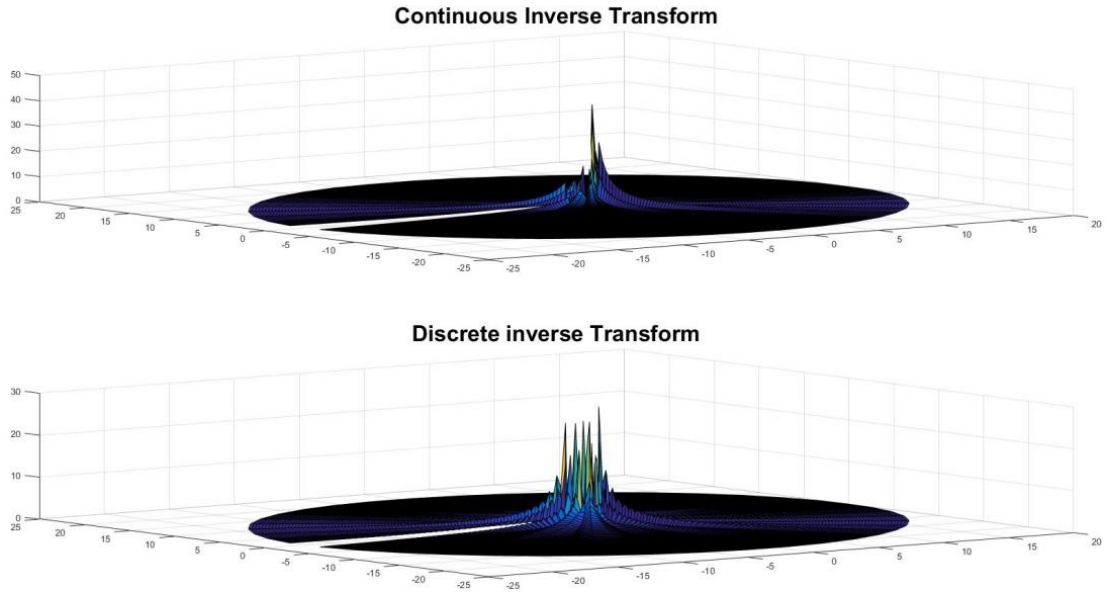

Figure 67 Continuous inverse transform and discrete inverse transform of 'Four-term Sinusoid & Modified Exponential' function with R=20, W_p=15, N_1=96 (test as a band limited function)

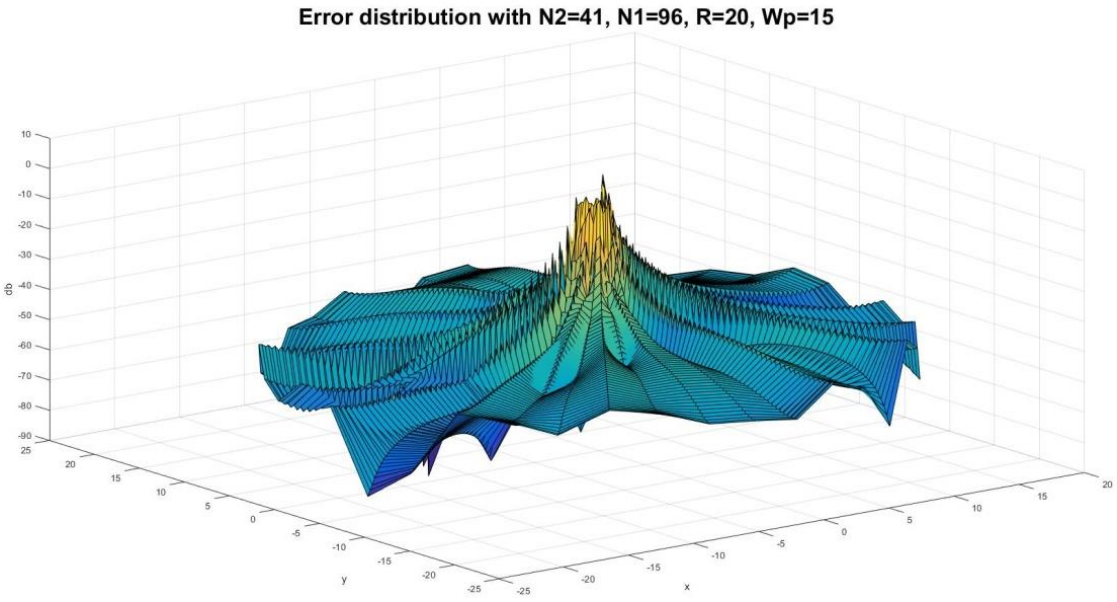

Figure 68 The error distribution of the inverse transform of 'Four-term Sinusoid & Modified Exponential' function with R=20, W_p=15, N_1=96 (test as a band limited function)

The maximum value of the error is $Error_{\max} = 1.1244 dB$.The average of the error is $Error_{average} = -49.8759 dB$.

The results with $R = 40, W_p = 30, N_1 = 383$ are shown in Figure 69 and Figure 70.

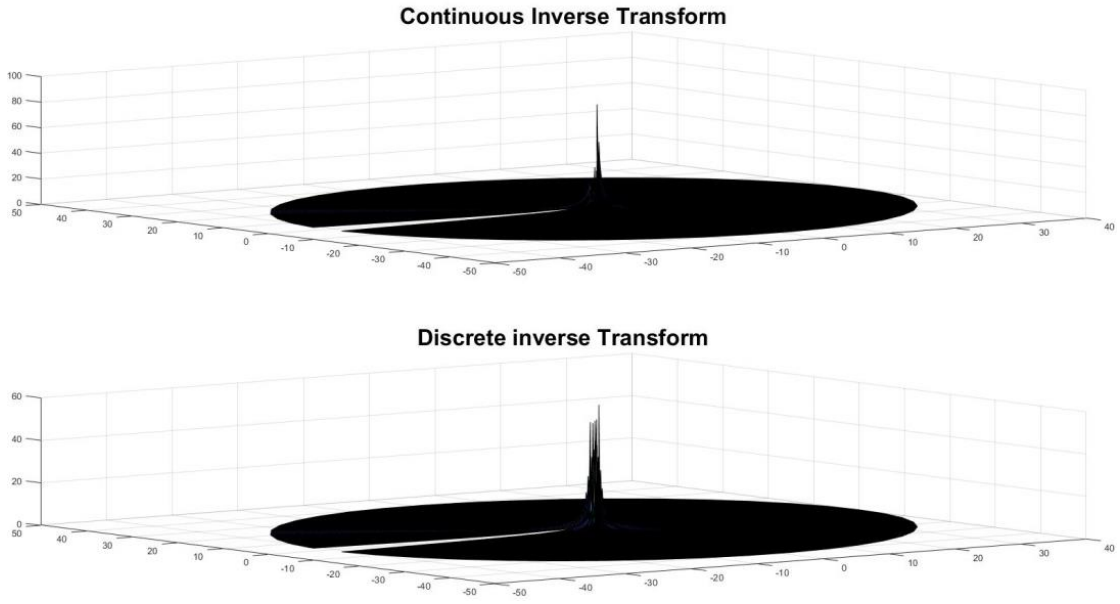

Figure 69 Continuous inverse transform and discrete forward transform of 'Four-term Sinusoid & Modified Exponential' function with R=40, W_p=30, N_1=383(test as a band limited function)

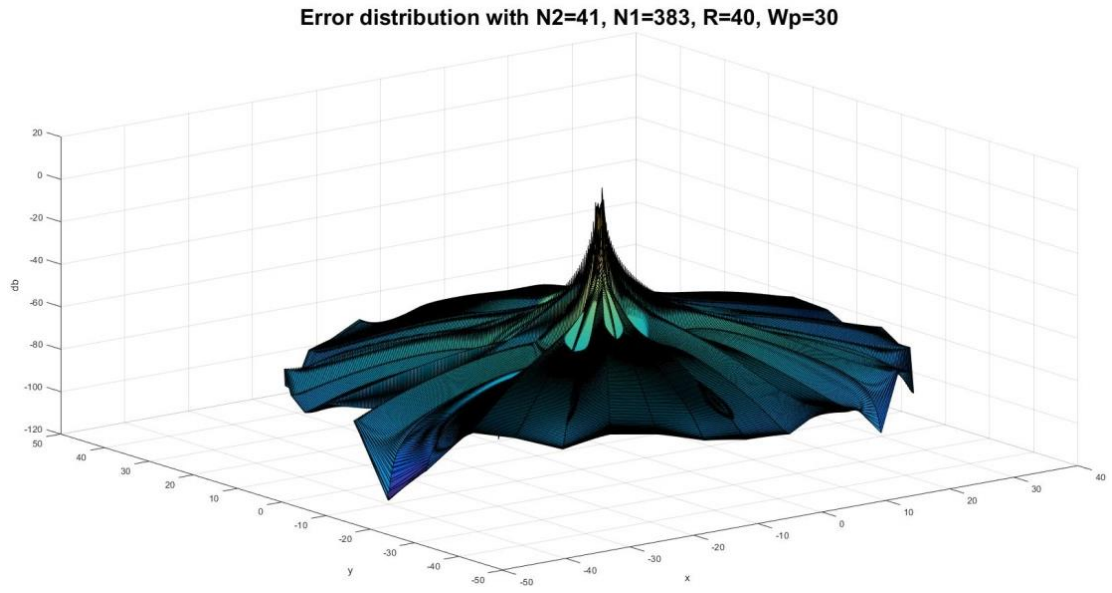

Figure 70 The error distribution of the forward transform of 'Four-term Sinusoid & Modified Exponential' function with R=40, W_p=30, N_1=383(test as a band limited function)

The maximum value of the error is $Error_{\max} = 0.7066dB$ and this occurs at the center. The average of the error is $Error_{average} = -68.9100dB$. Table 12 shows the errors with respect to different value of N_1 and N_2, from which Figure 71 and Figure 72 show the trend.

Table 12 Error (dB) of inverse transform of 'Four-term sinusoid & Modified Exponential' Function with different value of N_1 and N_2(test as a band limited function)

N2 \ N1	283	333	383	433	483
11	$E_{\max.} = 8.6$ $E_{avg.} = -72.4$	$E_{\max.} = 8.6$ $E_{avg.} = -74.5$	$E_{\max.} = 8.6$ $E_{avg.} = -76.4$	$E_{\max.} = 8.6$ $E_{avg.} = -78.0$	$E_{\max.} = 8.6$ $E_{avg.} = -79.4$
21	$E_{\max.} = 10.7$ $E_{avg.} = -73.3$	$E_{\max.} = 10.7$ $E_{avg.} = -75.4$	$E_{\max.} = 10.7$ $E_{avg.} = -77.3$	$E_{\max.} = 10.7$ $E_{avg.} = -78.8$	$E_{\max.} = 10.7$ $E_{avg.} = -80.2$
41	$E_{\max.} = 6.4$ $E_{avg.} = -75.0$	$E_{\max.} = 6.4$ $E_{avg.} = -77.1$	$E_{\max.} = 6.4$ $E_{avg.} = -79.0$	$E_{\max.} = 6.4$ $E_{avg.} = -80.5$	$E_{\max.} = 6.4$ $E_{avg.} = -81.9$
81	$E_{\max.} = 9.0$ $E_{avg.} = -75.5$	$E_{\max.} = 9.0$ $E_{avg.} = -77.6$	$E_{\max.} = 9.0$ $E_{avg.} = -79.4$	$E_{\max.} = 9.0$ $E_{avg.} = -81.3$	$E_{\max.} = 8.9$ $E_{avg.} = -82.5$
161	$E_{\max.} = 6.4$ $E_{avg.} = -75.2$	$E_{\max.} = 6.4$ $E_{avg.} = -77.4$	$E_{\max.} = 6.4$ $E_{avg.} = -79.2$	$E_{\max.} = 6.4$ $E_{avg.} = -80.8$	$E_{\max.} = 6.4$ $E_{avg.} = -82.2$

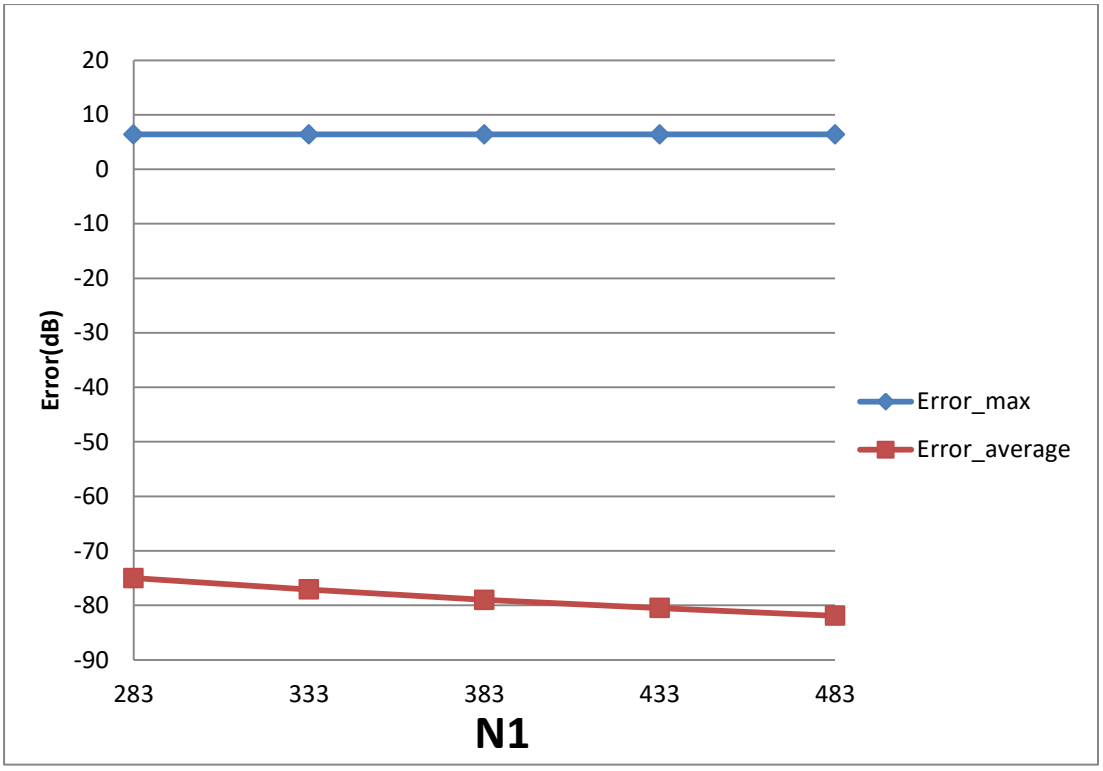

Figure 71 Error of inverse transform for 'Four-term sinusoid & Modified Exponential' Function with fixed N_2 (41) and varying N_1 (test as a band limited function)

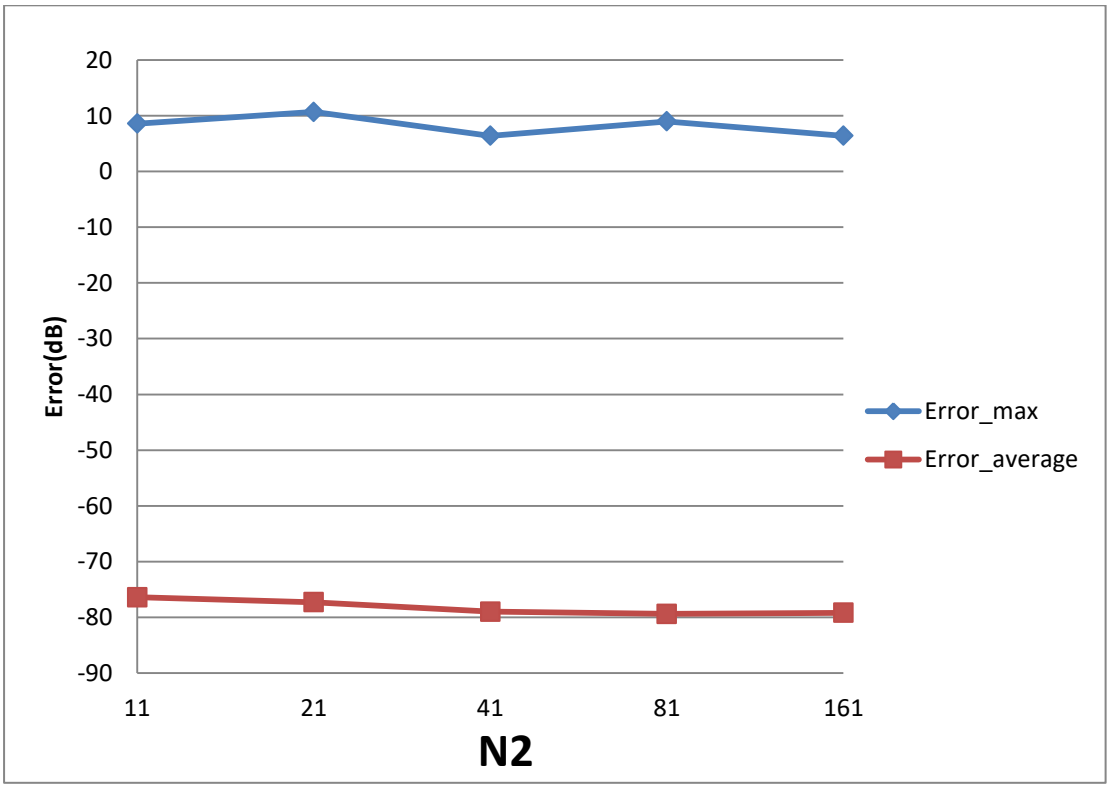

Figure 72 Error of inverse transform for 'Four-term sinusoid & Modified Exponential' Function with fixed N_1 (383) and varying N_2 (test as a band limited function)

Performing 2D-DFT and 2D-IDFT sequentially results in $\varepsilon = 1.4004 \times e^{-12}$ where ε is calculated by equation (6.2) .

It could be observed that testing the function as a space limited function and a band limited function shows similar approximations and that both are good. This demonstrates that both definitions defined for space limited function and band limited functions can be used to approximate the continuous function.

6.2.5 Square & Modified exponential

The next test case is chosen as

$$f(r,\theta) = \begin{cases} \dfrac{e^{-ar}}{r} & -\dfrac{\pi}{2} \le \theta \le \dfrac{\pi}{2} \\ 0 & -\pi \le \theta \le -\dfrac{\pi}{2}, \dfrac{\pi}{2} \le \theta \le \pi \end{cases} \tag{6.15}$$

This test function has different properties from the previous cases in that the function in the angular direction is a square wave whose Fourier series has an infinite number of terms. Therefore, to calculate the closed form of 2D-Fourier Transform, it is necessary to truncate the Fourier series at a large enough Fourier coefficient so that most of the energy is covered. It is calculated that 41 terms in the Fourier series captures 98.99% energy, and this is used to calculate the closed form 2D-Fourier Transform as

$$F(\rho,\psi)=\frac{\pi}{\sqrt{\rho^2+1}}-\frac{4I(\sqrt{\rho^2+1}-1)\cos(\psi)}{\rho\sqrt{\rho^2+1}}-\frac{\frac{4}{3}I(\sqrt{\rho^2+1}-1)^3\cos(3\psi)}{\rho^3\sqrt{\rho^2+1}}$$
$$-\frac{\frac{4}{5}I(\sqrt{\rho^2+1}-1)^5\cos(5\psi)}{\rho^5\sqrt{\rho^2+1}}-\frac{\frac{4}{7}I(\sqrt{\rho^2+1}-1)^7\cos(7\psi)}{\rho^7\sqrt{\rho^2+1}}$$
$$-\frac{\frac{4}{9}I(\sqrt{\rho^2+1}-1)^9\cos(9\psi)}{\rho^9\sqrt{\rho^2+1}}-\frac{\frac{4}{11}I(\sqrt{\rho^2+1}-1)^{11}\cos(11\psi)}{\rho^{11}\sqrt{\rho^2+1}}$$
$$-\frac{\frac{4}{13}I(\sqrt{\rho^2+1}-1)^{13}\cos(13\psi)}{\rho^{13}\sqrt{\rho^2+1}}-\frac{\frac{4}{15}I(\sqrt{\rho^2+1}-1)^{15}\cos(15\psi)}{\rho^{15}\sqrt{\rho^2+1}}$$
$$-\frac{\frac{4}{17}I(\sqrt{\rho^2+1}-1)^{17}\cos(17\psi)}{\rho^{17}\sqrt{\rho^2+1}}-\frac{\frac{4}{19}I(\sqrt{\rho^2+1}-1)^{19}\cos(19\psi)}{\rho^{19}\sqrt{\rho^2+1}}$$

(6.16)

The original function and its 2D-Fourier Transform are plotted by Maple and shown in Figure 73.

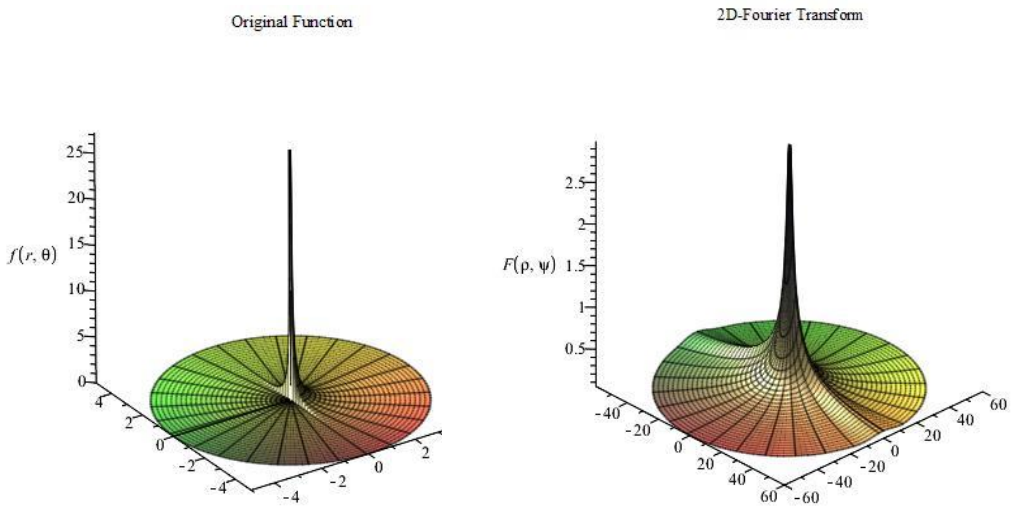

Figure 73 The Original Function and its 2D-Fourier Transform for the 'Square & Modified exponential' function

In the angular direction, since the function was truncated at 41 terms of Fourier series, N_2 needs to be at least 41.

From Figure 73, it can be seen that the function is effectively space limited at $R = 5$ and effectively band limited at $W_p = 40$. However, the functions in both domains explode at the center. Hence, relatively large values of R and W_p need to be selected. In the test, $R = 30$ and $W_p = 50$ are used which gives $N_1 = 478$. The function is tested as space limited function using Equation (3.28) and (3.29).

In this case, relatively large values of N_2 need to be selected since the functions in both domains explode at the center. Based on the discussion in Chapter 5, this test function could be considered one of the worst possible scenarios.

6.2.5.1 Forward Transform

The results for the 2D-DFT of Square & Modified exponential function are shown in Figure 74 and Figure 75.

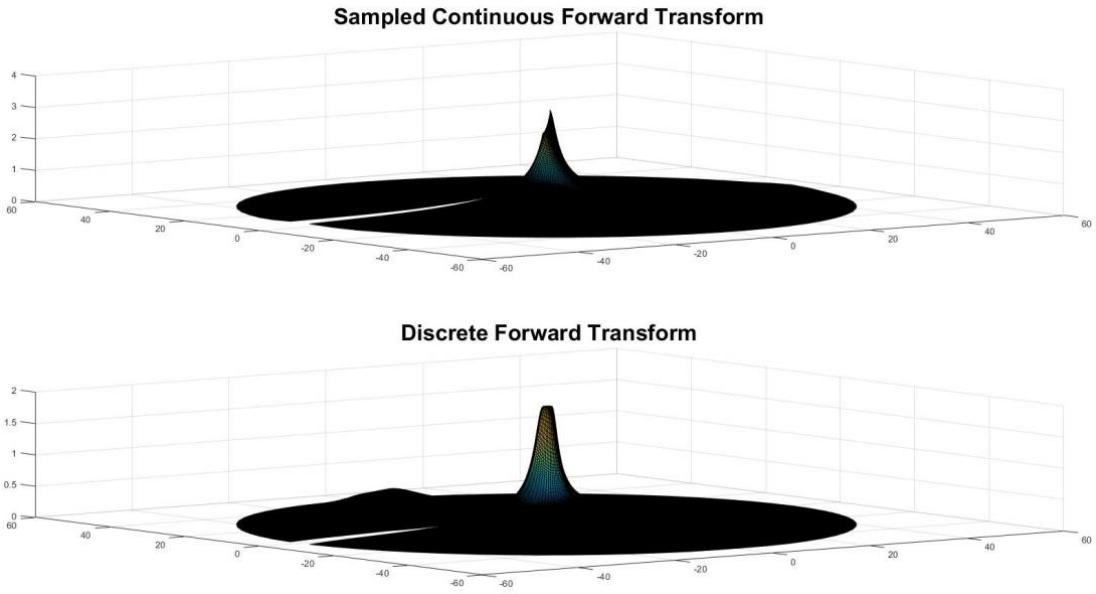

Figure 74 Continuous forward transform and discrete forward transform of 'Square&Modified Exponential' function with N_2=61,N_1=478,R=30,W_p=50

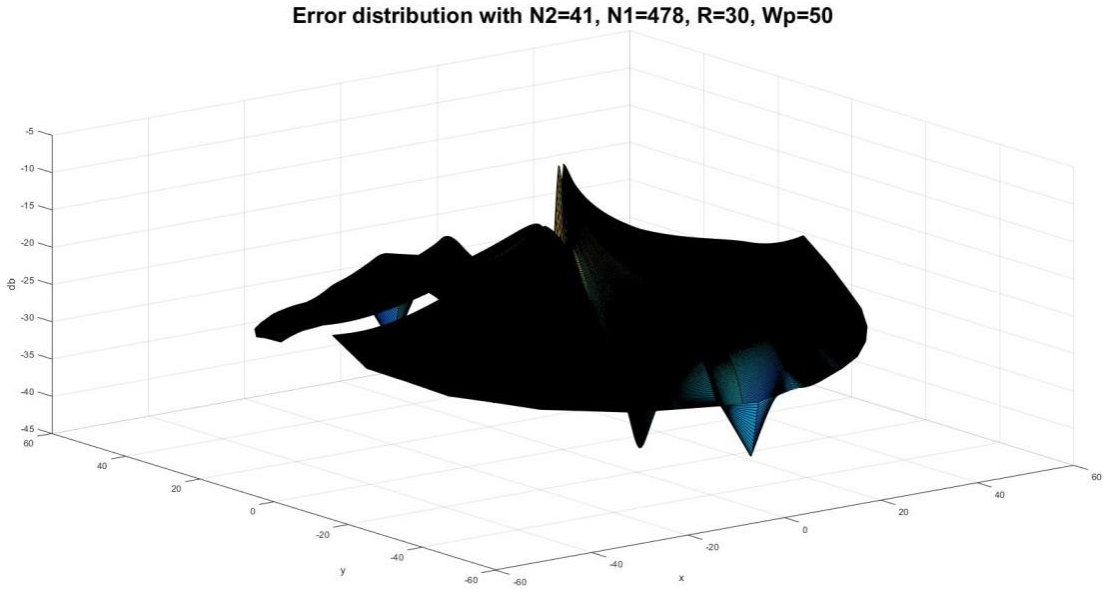

Figure 75 The error distribution of the forward transform of 'Square&Modified Exponential' function with N_2=61,N_1=478,R=30,W_p=50

The maximum value of the error is $Error_{\max} = -3.4905dB$ and it happens at the center area. The average of the error is $Error_{average} = -21.6574dB$. Table 13 shows the errors with respect to different values of N_1 and N_2, from which Figure 76 and Figure 77 show the trend.

Table 13 Error (dB) of forward transform of 'Square & Modified Exponential' function with different values of N_1 and N_2

N2 \ N1	378	428	478	528	578
21	$E_{\max.} = -10.7$ $E_{avg.} = -23.6$	$E_{\max.} = -11.4$ $E_{avg.} = -24.9$	$E_{\max.} = -11.9$ $E_{avg.} = -26.0$	$E_{\max.} = -12.3$ $E_{avg.} = -27.0$	$E_{\max.} = -12.6$ $E_{avg.} = -27.9$
41	$E_{\max.} = -4.9$ $E_{avg.} = -20.7$	$E_{\max.} = -5.9$ $E_{avg.} = -22.1$	$E_{\max.} = -6.7$ $E_{avg.} = -23.3$	$E_{\max.} = -7.2$ $E_{avg.} = -24.3$	$E_{\max.} = -7.5$ $E_{avg.} = -25.3$

61	$E_{max.} = -1.6$ $E_{avg.} = -18.9$	$E_{max.} = -2.6$ $E_{avg.} = -20.4$	$E_{max.} = -3.5$ $E_{avg.} = -21.7$	$E_{max.} = -4.3$ $E_{avg.} = -22.8$	$E_{max.} = -5.0$ $E_{avg.} = -23.8$
81	$E_{max.} = 0.7$ $E_{avg.} = -17.6$	$E_{max.} = -0.3$ $E_{avg.} = -19.1$	$E_{max.} = -1.2$ $E_{avg.} = -20.5$	$E_{max.} = -2.0$ $E_{avg.} = -21.6$	$E_{max.} = -2.7$ $E_{avg.} = -22.8$
101	$E_{max.} = 2.5$ $E_{avg.} = -16.6$	$E_{max.} = 1.5$ $E_{avg.} = -18.1$	$E_{max.} = 0.6$ $E_{avg.} = -19.5$	$E_{max.} = -0.2$ $E_{avg.} = -20.7$	$E_{max.} = -0.9$ $E_{avg.} = -21.8$

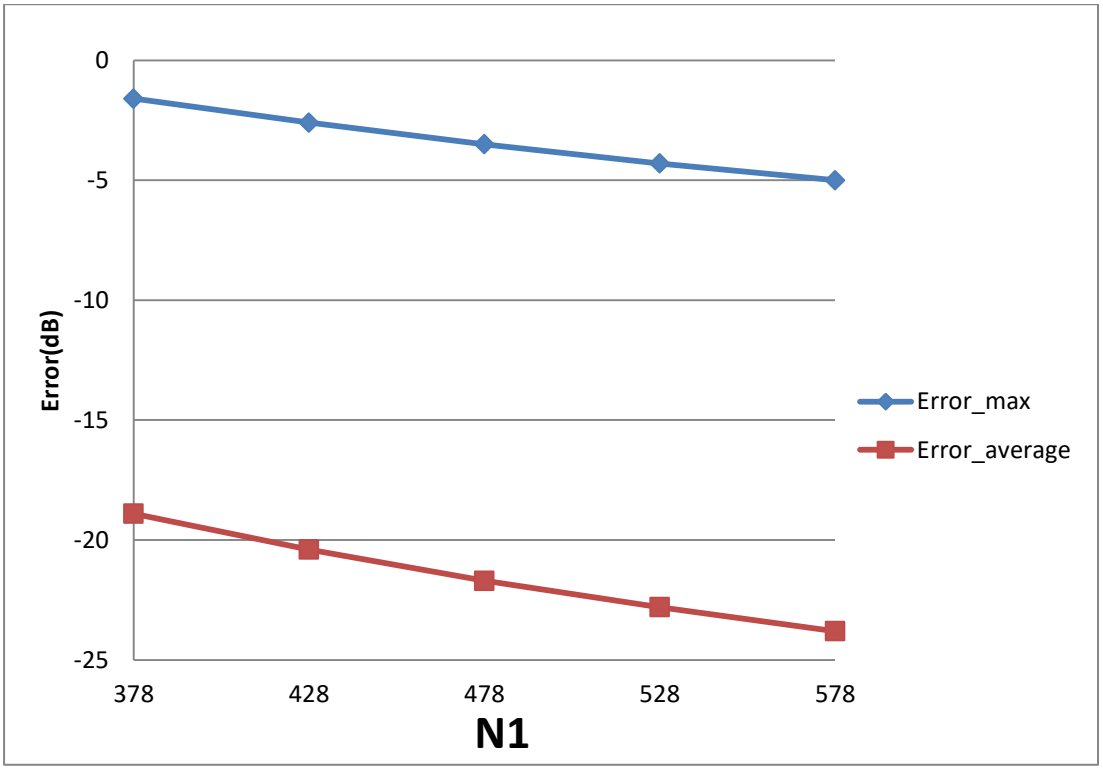

Figure 76 Error of forward transform for 'Square & Modified Exponential' function with fixed N_2 (61) and varying N_1

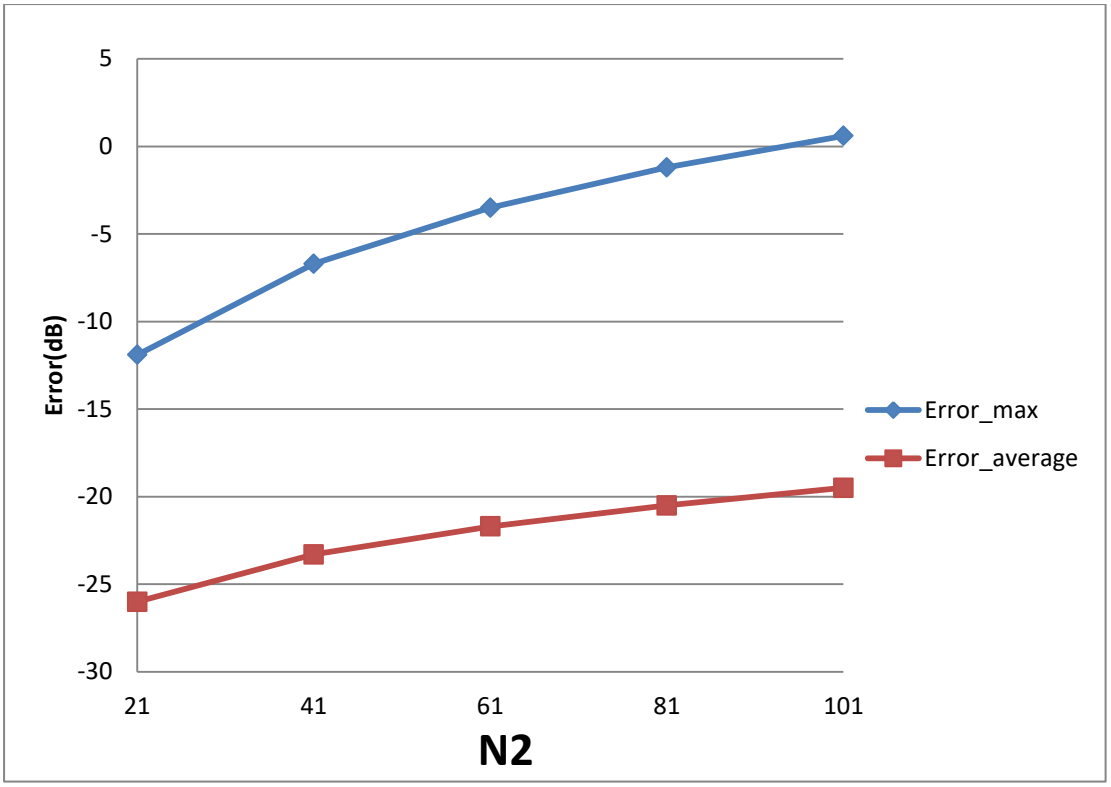

Figure 77 Error of forward transform for 'Square & Modified Exponential' function with fixed N_1 (478) and varying N_2

It can be observed from Figure 76 and Figure 77that this function shows a larger error than the previous cases, however the trend is similar in that increasing N_1 separately gives less error, while increasing N_2 results in a larger error.

6.2.5.2 Inverse Transform

The results for the 2D-IDFT of the Square & Modified exponential function are shown in Figure 78 and Figure 79.

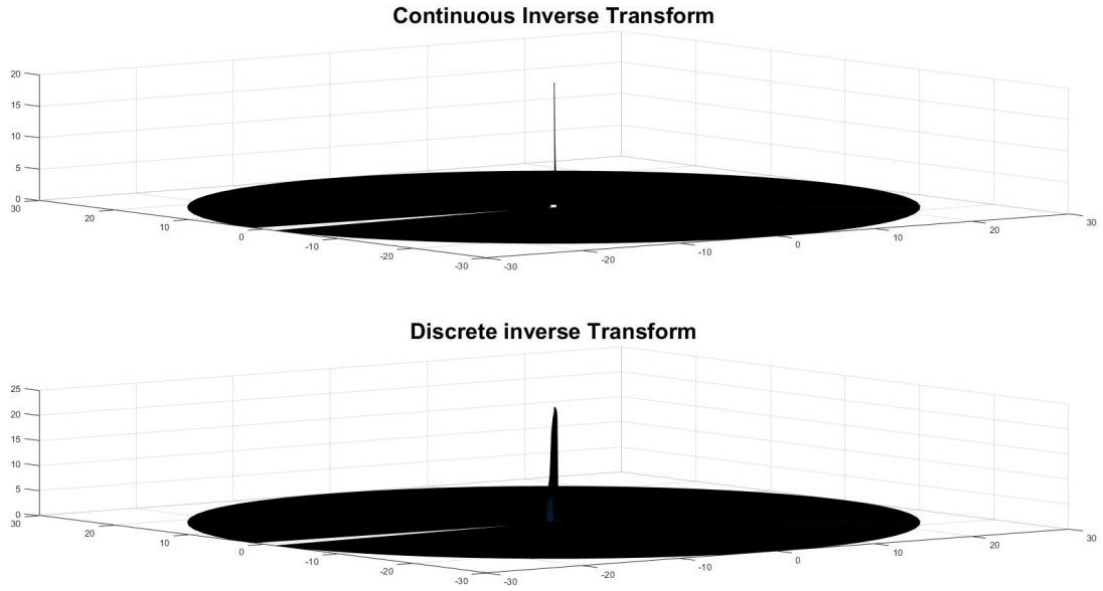

Figure 78 Continuous inverse transform and discrete inverse transform of Square&Modified Exponential function with N_2=61,N_1=478,R=30,W_p=50

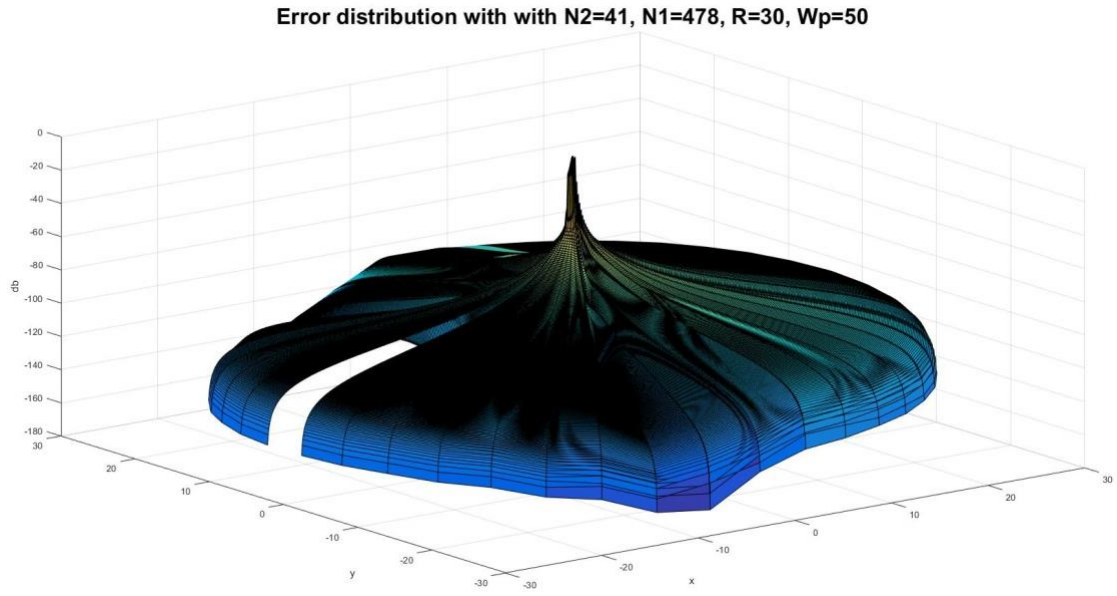

Figure 79 The error distribution of the inverse transform of Square&Modified Exponential function with N_2=61,N_1=478,R=30,W_p=50

Table 5 shows the errors with respect to different value of N_1 and N_2, from which Figure 80 and Figure 81 show the trend.

Table 14 Error (dB) of inverse transform of 'Square & Modified Exponential' function with different values of N_1 and N_2

N2 \ N1	378	428	478	528	578
21	$E_{\max.} = -3.7$ $E_{avg.} = -89.5$	$E_{\max.} = -3.8$ $E_{avg.} = -91.0$	$E_{\max.} = -3.8$ $E_{avg.} = -92.2$	$E_{\max.} = -3.8$ $E_{avg.} = -93.4$	$E_{\max.} = -3.8$ $E_{avg.} = -94.4$
41	$E_{\max.} = -2.3$ $E_{avg.} = -87.3$	$E_{\max.} = -2.3$ $E_{avg.} = -88.8$	$E_{\max.} = -2.4$ $E_{avg.} = -90.1$	$E_{\max.} = -2.4$ $E_{avg.} = -91.2$	$E_{\max.} = -2.4$ $E_{avg.} = -92.3$
61	$E_{\max.} = -1.7$ $E_{avg.} = -85.7$	$E_{\max.} = -1.8$ $E_{avg.} = -87.2$	$E_{\max.} = -1.8$ $E_{avg.} = -88.5$	$E_{\max.} = -1.8$ $E_{avg.} = -89.6$	$E_{\max.} = -1.8$ $E_{avg.} = -90.6$
81	$E_{\max.} = -1.4$ $E_{avg.} = -84.5$	$E_{\max.} = -1.4$ $E_{avg.} = -85.9$	$E_{\max.} = -1.4$ $E_{avg.} = -87.2$	$E_{\max.} = -1.5$ $E_{avg.} = -88.3$	$E_{\max.} = -1.5$ $E_{avg.} = -89.4$
101	$E_{\max.} = 2.0$ $E_{avg.} = -67.2$	$E_{\max.} = 1.9$ $E_{avg.} = -68.4$	$E_{\max.} = 1.8$ $E_{avg.} = -69.4$	$E_{\max.} = 1.8$ $E_{avg.} = -70.4$	$E_{\max.} = 1.7$ $E_{avg.} = -71.2$

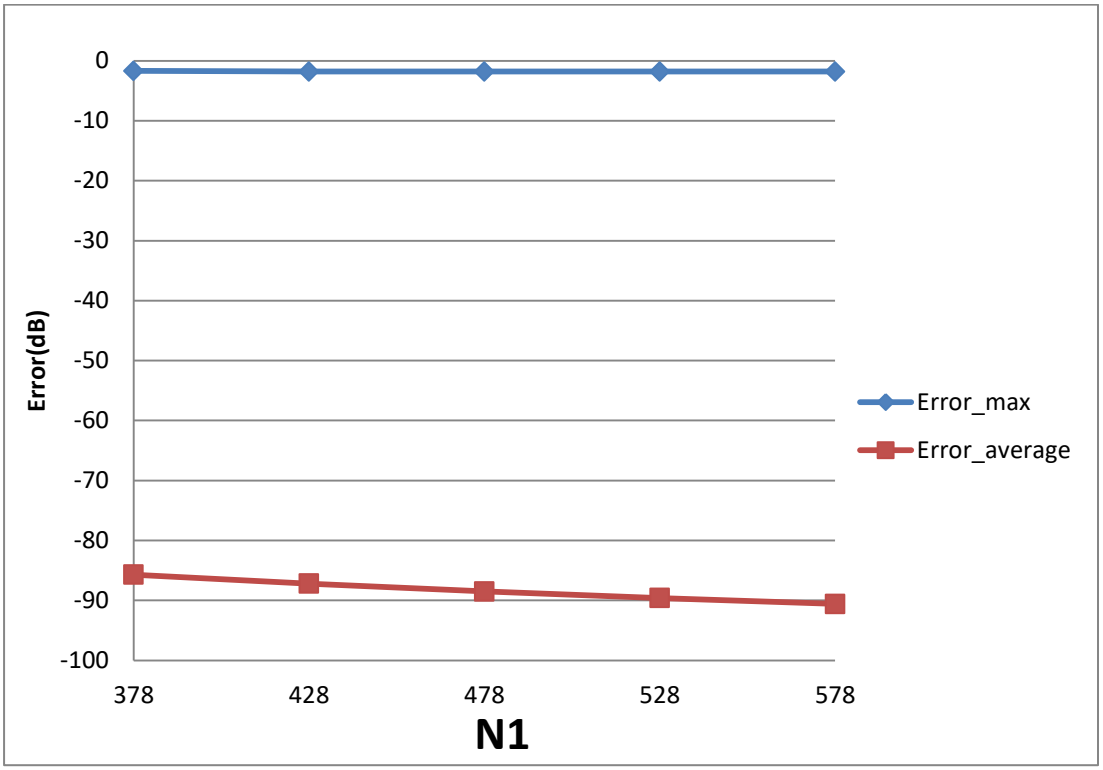

Figure 80 Error of inverse transform for 'Square & Modified Exponential' function with fixed N_2 (61) and varying N_1

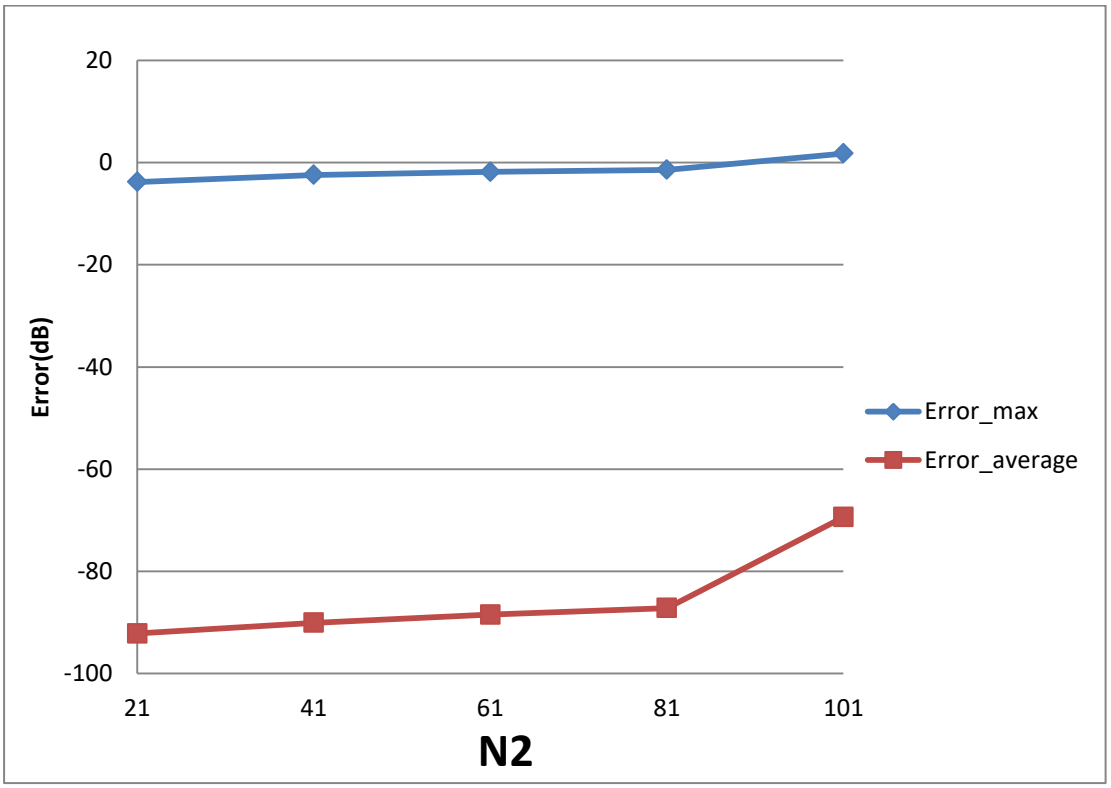

Figure 81 Error of inverse transform for 'Square & Modified Exponential' function with fixed N_1 (478) and varying N_2

A similar trend as seen with the forward transform is obtained. Performing 2D-DFT and 2D-IDFT results in $\varepsilon = 2.8689 \times e^{-14}$ where ε is calculated by equation (6.2) .

7 Improving the computing time of the transform

One of the advantages of the traditional Fourier transform is that the computing speed is fast by using the now well-established *fft* algorithm. Improvement is done to reduce the computing time of the 2D DFT in polar coordinates by

1. Interpreting the transform as three operations instead of a single four-dimensional matrix.
2. Pre-calculating and saving the Bessel zeros.

7.1 Reducing computing time by interpreting the transform as three operations in sequence

As defined in Section 3.4, the matrix f_{pk} is transformed into the matrix F_{ql}. The intuitive way to interpret the transform kernel is to think of it as a four-dimensional matrix or matrices in a matrix. However, as discussed in Section 4.1 and 4.2, interpreting the transform as a 1D-DFT of each column, a 1D-DHT of each row and then a 1D-IDFT of each column makes it possible to use the Matlab built in functions *fft* and *ifft*, which significantly reduced the computational time.

7.2 Reduce computing time by pre-calculating the Bessel Zeros

After defining the transform as three operations in sequence and using the matrix for the discrete Hankel transform defined in [14], it was found that a lot of computational time was used to calculate the Bessel zeros for every different test case, even though the Bessel zeros are the same in every case. Pre-calculating the Bessel zeros for large numbers of N_1 and N_2 saves a lot of time.

Table 15 shows the computing time of a forward transform on the same computer (Processor: Intel(R) Core(TM) i7-4710HQ CPU, RAM:12GB) for three cases:

1. Evaluate the transform as matrices in a matrix without pre-calculating the Bessel zeros.
2. Evaluate the transform as a DFT, DHT and IDFT in sequence without pre-calculating the Bessel zeros.
3. Evaluate the transform as a DFT, DHT and IDFT in sequence with pre-calculating the Bessel zeros.

The Gaussian function was used as the test function therefore N_1=383 and N_2=15.

Table 15 Computing time of three cases: Case1: Run the transform as matrixes in matrix without pre-calculating the Bessel zeros; Case2: Run the transform as DFT,DHT and IDFT in sequence without pre-calculating the Bessel zeros; Case3: Run the transform as DFT,DHT and IDFT in sequence with pre-calculating the Bessel zeros

Test cases	Total computing time(seconds)
Case 1	3346.5
Case 2	321.1
Case 3	14.3

From Table 15, it can be clearly observed that the computing time by running the transform as matrices in a matrix costs 3346.5s, which is not acceptable as an applicable transform. Testing the transform as three operations turns 3346.5 seconds into 321.1 seconds. This is much better and acceptable. Finally, pre-calculating the Bessel Zeros makes the transform much faster and useful.

8 Summary and Conclusions

8.1 Accuracy and Precision of the transform

The discrete 2D-Fourier Transform showed an acceptable accuracy. In [14],[6]and[28], the one dimensional Hankel transform of a sinc function showed similar dynamic error, which could be used as a comparative measure. Since the discrete Hankel transform is one step of the discrete 2D-Fourier Transform defined in this thesis and the definition of the Hankel transform is based on [14], a similar dynamic error should be expected.

The test cases showed that the transform introduced very small errors ($\varepsilon = 1.4004 \times e^{-12}$ for worst case) by performing a forward transform and an inverse transform sequentially, which demonstrates that the algorithm showed good precision.

8.2 Guidelines of choosing sample size

As discussed in Chapter 5 and proved by test cases, the sample size N_1 (sample size in the radial direction) and N_2 (sample size in the angular direction) does not have to be of the same order. When the sampling theorem is satisfied, increasing N_1 tends to decrease the dynamic error while increasing N_2 tends to increase the dynamic error. Therefore for any case, keeping N_2 at the lowest value will ensure the best result. For functions that need large value of N_2 (functions that have sharp features in angular direction and therefore require larger number of Fourier coefficients), a larger N_1 will be needed to compensate.

Moreover, due to the special sample points, the sample grid cannot cover the origin in both space and frequency domains. For space limited functions, if there is much energy at the origin in the space domain, a large number of N_1 will be needed to ensure the sample grid gets as close to the origin as possible in the space domain. If the function has much energy at the origin in the frequency domain, large values of N_1 and R are required simultaneously. For a frequency limited function, if it has much energy at the origin in the frequency domain, large values of N_1 will be needed to ensure the sample grid gets as close to the origin as possible in the frequency

domain. If the function has much energy at the origin in the space domain, large values of both N_1 and W_p are required simultaneously.

References

[1] J. W. Cooley and J. W. Tukey, “An Algorithm for the Machine Calculation of Complex Fourier Series,” *Math. Comput.*, vol. 19, no. 90, pp. 297–301, 1965.

[2] Y. Xu, D. Feng, and L. V. Wang, “Exact frequency-domain reconstruction for thermoacoustic tomography. I. Planar geometry,” *Med. Imaging IEEE Trans. On*, vol. 21, no. 7, pp. 823–828, 2002.

[3] M. C. Scott *et al.*, “Electron tomography at 2.4-ångström resolution,” *Nature*, vol. 483, no. 7390, p. 444, Mar. 2012.

[4] B. P. Fahimian *et al.*, “Radiation dose reduction in medical x-ray CT via Fourier-based iterative reconstruction,” *Med. Phys.*, vol. 40, no. 3, p. n/a-n/a, Mar. 2013.

[5] E. Lee *et al.*, “Radiation dose reduction and image enhancement in biological imaging through equally-sloped tomography,” *J. Struct. Biol.*, vol. 164, no. 2, pp. 221–227, 2008.

[6] M. Guizar-Sicairos and J. C. Gutiérrez-Vega, “Computation of quasi-discrete Hankel transforms of integer order for propagating optical wave fields,” *JOSA A*, vol. 21, no. 1, pp. 53–58, Jan. 2004.

[7] D. W. Zhang, X.-C. Yuan, N. Q. Ngo, and P. Shum, “Fast Hankel transform and its application for studying the propagation of cylindrical electromagnetic fields,” *Opt. Express*, vol. 10, no. 12, pp. 521–525, Jun. 2002.

[8] A. W. Norfolk and E. J. Grace, “Reconstruction of optical fields with the Quasi-discrete Hankel transform,” *Opt. Express*, vol. 18, no. 10, pp. 10551–10556, May 2010.

[9] A. E. Siegman, “Quasi fast Hankel transform,” *Opt. Lett.*, vol. 1, no. 1, pp. 13–15, Jul. 1977.

[10] G. P. Agrawal and M. Lax, “End correction in the quasi-fast Hankel transform for optical-propagation problems,” *Opt. Lett.*, vol. 6, no. 4, pp. 171–173, Apr. 1981.

[11] A. Agnesi, G. C. Reali, G. Patrini, and A. Tomaselli, “Numerical evaluation of the Hankel transform: remarks,” *JOSA A*, vol. 10, no. 9, pp. 1872–1874, Sep. 1993.

[12] H. F. Johnson, “An improved method for computing a discrete Hankel transform,” *Comput. Phys. Commun.*, vol. 43, no. 2, pp. 181–202, 1987.

[13] L. Yu, M. Huang, M. Chen, W. Chen, W. Huang, and Z. Zhu, “Quasi-discrete Hankel transform,” *Opt. Lett.*, vol. 23, no. 6, pp. 409–411, Mar. 1998.

[14] N. Baddour and U. Chouinard, “Theory and operational rules for the discrete Hankel transform,” *JOSA A*, vol. 32, no. 4, pp. 611–622, Apr. 2015.

[15] E. Suli and A. Ware, “A Spectral Method of Characteristics for Hyperbolic Problems,” *SIAM J. Numer. Anal.*, vol. 28, no. 2, pp. 423–445, 1991.

[16] A. Dutt and V. Rokhlin, “Fast Fourier Transforms for Nonequispaced Data,” *SIAM J. Sci. Comput.*, vol. 14, no. 6, pp. 1368–1393, Nov. 1993.

[17] C. Anderson and M. Dahleh, “Rapid Computation of the Discrete Fourier Transform,” *SIAM J. Sci. Comput.*, vol. 17, no. 4, pp. 913–919, Jul. 1996.

[18] A. F. Ware, “Fast Approximate Fourier Transforms for Irregularly Spaced Data,” *SIAM Rev.*, vol. 40, no. 4, p. 838, Dec. 1998.

[19] A. Averbuch, R. R. Coifman, D. L. Donoho, M. Elad, and M. Israeli, “Fast and accurate Polar Fourier transform,” *Appl. Comput. Harmon. Anal.*, vol. 21, no. 2, pp. 145–167, 2006.

[20] N. Baddour, “Two-Dimensional Fourier Transforms in Polar Coordinates,” *Adv. Imaging Electron Phys.*, vol. 165, pp. 1–45, Jan. 2011.

[21] N. Baddour, “Operational and convolution properties of two-dimensional Fourier transforms in polar coordinates,” *JOSA A*, vol. 26, no. 8, pp. 1767–1777, Aug. 2009.

[22] N. Baddour, “Operational and convolution properties of three-dimensional Fourier transforms in spherical polar coordinates,” *JOSA A*, vol. 27, no. 10, pp. 2144–2155, Oct. 2010.

[23] N. Baddour, “Towards a Discrete 2D Fourier Transform in polar coordinates,” 2017.

[24] G. B. Arfken, *Mathematical methods for physicists*, 6th ed.. Boston: Elsevier, 2005.

[25] C. E. Shannon, “Communication in the presence of noise,” *Proc. IEEE*, vol. 72, no. 9, pp. 1192–1201, 1984.

[26] D. W. Lozier, “NIST Digital Library of Mathematical Functions,” *Ann. Math. Artif. Intell.*, vol. 38, no. 1–3, pp. 105–119, 2003.

[27] A. D. Poularikas, *Transforms and Applications Handbook, Third Edition*. CRC Press, 2010.

[28] W. Higgins and J. Munson D., “An algorithm for computing general integer-order Hankel transforms,” *Acoust. Speech Signal Process. IEEE Trans. On*, vol. 35, no. 1, pp. 86–97, 1987.

Appendix A – Matlab Code

A-1. theta matrix for space limited function

```
% N1 sample size in radial direction
% N2 sample size in angular direction
function theta=thetamatrix_SpaceLimited(N2,N1)
theta=zeros(N2,N1-1);
M=(N2-1)/2;
for ii=1:N2;
    p=ii-1-M;
    for k=1:N1-1;
        theta(ii,k)=(p/N2)*2*pi;
    end
end
```

A-2. r matrix for space limited function

```
% N1 sample size in radial direction
% N2 sample size in angular direction
% R effective space limit
% zeromatrix precalculated Bessel zero
function r=rmatrix_SpaceLimited(N2,N1,R,zeromatrix)
M=(N2-1)/2;
for ii=1:N2;
    p=ii-1-M;
    for k=1:N1-1;
        zero2=zeromatrix(5001-abs(p),:);
        jpk=zero2(k);
        jpN1=zero2(N1);
        r(ii,k)=(jpk/jpN1)*R;
    end
end
```

A-3. psi matrix for space limited function

```
% N1 sample size in radial direction
% N2 sample size in angular direction
function psi=psimatrix_SpaceLimited(N2,N1)
psi=zeros(N2,N1-1);
M=(N2-1)/2;
for ii=1:N2;
    q=ii-1-M;
    for l=1:N1-1;
        psi(ii,l)=(q/N2)*2*pi;
    end
end
```

A-4. rho matrix for space limited function

```
% N1 sample size in radial direction
% N2 sample size in angular direction
% R effective space limit
% zeromatrix precalculated Bessel zero
function rho=rhomatrix_SpaceLimited(N2,N1,R,zeromatrix)
M=(N2-1)/2;
for ii=1:N2;
    q=ii-1-M;
    for l=1:N1-1;
        zero2=zeromatrix(5001-abs(q),:);
        jql=zero2(l);
        rho(ii,l)=jql/R;
    end
end
```

A-5. Y matrix Assembly Function

```
% Y is the N-1 x N-1 transformation matrix to be assembled
%
% n is the order of the bessel function
% N is the size of the transformation matrix
%zeros are the bessel zeros passed to the function
%
%



function Y = YmatrixAssembly(n,N,zero)
%tic


for l=1:N-1

    for k=1:N-1

        jnk=zero(k);
        jnl=zero(l);
        jnN=zero(N);
        jnplus1=besselj(n+1, jnk);

        Y(l,k)=(2*besselj(n,(jnk*jnl/jnN)))/(jnN*jnplus1^2);


    end
end

%toc

end
```

A-5. Forward transform of Gaussian function

```
N2=15; %number of sample points in angular direction
N1=383; %number of sample points in radial direction
M=(N2-1)/2; %highest order of bessel function
R=40;% space limit
Wp=30; % band limit
a=0.1;
load('zeromatrix.mat')
theta=thetamatrix_SpaceLimited(N2,N1); %Sample point in angular direction in space
domain.
r=rmatrix_SpaceLimited(N2,N1,R,zeromatrix);%Sample point in radial direction in space
domain.
psi=psimatrix_SpaceLimited(N2,N1);%Sample point in angular direction in frequency
domain.
rho=rhomatrix_SpaceLimited(N2,N1,R,zeromatrix);%Sample point in radial direction in
frequency domain.
[x,y]=pol2cart(theta,r); %sample points in Cartesian coordinates in space domian
[x1,y1]=pol2cart(psi,rho); %sample points in Cartesian coordinates in frequency domian


%Dicretizing the function
for ii=1:N2
    for jj=1:N1-1
        f(ii,jj)=exp(-r(ii,jj)^2);
    end
end
% DFT
fnk=circshift(fft(circshift(f,M+1,1),N2,1),-(M+1),1);
% DHT
for n=-M:M
    ii=n+M+1;
    zero2=zeromatrix(5001-abs(n),:);
    jnN1=zero2(N1);
    if n<0
    Y=((-1)^abs(n))*YmatrixAssembly(abs(n),N1,zero2);
    else
    Y=YmatrixAssembly(abs(n),N1,zero2);
    end
    fnl(ii,:)=(Y*fnk(ii,:)')';
    Fnl(ii,:)=fnl(ii,:)*(2*pi*(i^(-n)))*(R^2/jnN1);
end
% IDFT
TwoDFT=circshift(ifft(circshift(Fnl,M+1,1),N2,1),-(M+1),1);
%creating a discrete 2D Fourier transform
for ii=1:N2
    for jj=1:N1-1
        trueFunc(ii,jj)=pi*exp((-rho(ii,jj)^2)/4);
    end
end

%calculating the dynamic error from transform and true function
error= 20*log10(abs(trueFunc- TwoDFT)/max(max(abs(TwoDFT))));
```

```
figure(1)
subplot(2,1,1)
surf(x1,y1,abs(trueFunc))
title('\fontsize{24}Sampled Continuous Forward Transform')
subplot(2,1,2)
surf(x1,y1,abs(TwoDFT))
title('\fontsize{24}Discrete Forward Transform')

figure(2)

surf(x1,y1,error)
xlabel('x');
ylabel('y');
zlabel('db')
str=sprintf('Error distribution with N2 = %d, N1 = %d,R= %d, a= %d ', N2,N1,R,a);
title(['\fontsize{24}Error distribution with N2=',num2str(N2),', N1=',num2str(N1),',
R=',num2str(R), ', Wp=',num2str(Wp)]);

mean1=mean(mean(error)); % Average dynamic error
max1=max(max(error)); % Maximum dynamic error
```

A-6. Inverse transform of Gaussian function

```
N2=15 ; %number of sample points in angular direction
N1=383; %number of sample points in radial direction
M=(N2-1)/2; %highest order of bessel function
R=40;% space limit
Wp=30; % band limit
a=0.1;
load('zeromatrix.mat')
theta=thetamatrix_SpaceLimited(N2,N1);%Sample point in angular direction in space
domain.
r=rmatrix_SpaceLimited(N2,N1,R,zeromatrix);%Sample point in radial direction in space
domain.
psi=psimatrix_SpaceLimited(N2,N1);%Sample point in angular direction in frequency
domain.
rho=rhomatrix_SpaceLimited(N2,N1,R,zeromatrix);%Sample point in radial direction in
frequency domain.
[x,y]=pol2cart(theta,r); %sample points in Cartesian coordinates in space domian
[x1,y1]=pol2cart(psi,rho); %sample points in Cartesian coordinates in frequency domian

%creating a discrete true function
for ii=1:N2
    for jj=1:N1-1
       trueFunc(ii,jj)=pi*exp((-rho(ii,jj)^2)/4);
    end
end
% DFT
FNL=circshift(fft(circshift(trueFunc,M+1,1),N2,1),-(M+1),1);
% DHT
for n=-M:M
    ii=n+M+1;
    zero2=zeromatrix(5001-abs(n),:);
```

```
    jnN1=zero2(N1);
    if n<0
    Y=((-1)^abs(n))*YmatrixAssembly(abs(n),N1,zero2);
    else
    Y=YmatrixAssembly(abs(n),N1,zero2);
    end
    YO=Y';
    Fnk(ii,:)=FNL(ii,:)*YO;
    fnk(ii,:)=Fnk(ii,:)*((jnN1)*(j^n))/(2*pi*R^2);

end
% IDFT
TwoDIFT=circshift(ifft(circshift(fnk,M+1,1),N2,1),-(M+1),1);

%%dicretizing the function in space domain
for ii=1:N2
    for jj=1:N1-1
        f(ii,jj)=exp(-r(ii,jj)^2);
    end
end
%calculating the dynamic error from transform and origal function
error= 20*log10(abs(f- TwoDIFT)/max(max(abs(TwoDIFT))));

figure(1)
subplot(2,1,1)
surf(x,y,abs(f))
title('\fontsize{24}Continuous Inverse Transform')
subplot(2,1,2)
surf(x,y,abs(TwoDIFT))
title('\fontsize{24}Discrete inverse Transform')

figure(2)
surf(x,y,error)
xlabel('x');
ylabel('y');
zlabel('db')
str=sprintf('Error distribution with N2 = %d, N1 = %d,R= %d, a= %d ', N2,N1,R,a);
title(['\fontsize{24}Error distribution with N2=',num2str(N2),', N1=',num2str(N1),',
R=',num2str(R), ', Wp=',num2str(Wp)]);


mean=mean(mean(error)); % Average dynamic error
max=max(max(error));% Maximum dynamic error
```

Appendix B – Approximation to the Bessel zeros

B-1. Approximation to sampling points evaluated at approximate Bessel zeros

It is pointed out in [24] that the zeros of $J_n(z)$ are *almost* evenly spaced at intervals of π and that the spacing becomes exactly π in the limit as $z \to \infty$. In fact, it is shown in [24] that a simple asymptotic form for the Bessel function is given by

$$J_n(z) \approx \sqrt{\frac{2}{\pi z}} \cos\left[z - \left(n + \frac{1}{2} \right) \frac{\pi}{2} \right] \tag{B.1}$$

Equation (B.1) becomes a better approximation to $J_n(z)$ as $z \to \infty$. The zeros of the cosine function are at odd multiples of $\pi/2$. Therefore, an approximation to the Bessel zero, j_{pk} is given by

$$j_{pk} - \left(p + \frac{1}{2} \right) \frac{\pi}{2} \approx (2k - 1) \frac{\pi}{2} \tag{B.2}$$

or equivalently

$$j_{pk} \approx \left(2k + p - \frac{1}{2} \right) \frac{\pi}{2}. \tag{B.3}$$

The approximation in equation (B.3) gets better as k gets larger and is also better for smaller p. Numerical simulations with equation (B.3) show that this approximation is an overestimate of the true value.

Using equations (3.35) and (3.36), along with the approximation in equation (B.3), we can generate approximate values for the spatial and frequency-spatial grids so that

$$r_{pk} = \frac{j_{pk} R}{j_{pN_1}} \approx \frac{\left(2k + p - \frac{1}{2} \right) R}{\left(2N_1 + p - \frac{1}{2} \right)} \qquad \theta_p = \frac{p 2\pi}{N_2} \tag{B.4}$$

and

$$\rho_{ql} = \frac{j_{ql}}{R} \approx \left(2l + q - \frac{1}{2} \right) \frac{\pi}{2R} \qquad \psi_q = \frac{q 2\pi}{N_2} \tag{B.5}$$

These approximations can be used to plot an approximate value for the polar grid and to calculate the error between the approximate values of *r* given in equation (B.4) and the exact values given in equation (3.35). The same can be done for the exact and approximate values of ρ. For comparison purposes, we use the same values that were employed to generate Figure 1-Figure 4. For $R=1$, $N_1=16$ and $N_2=15$, the *maximum* error in the spatial grid r values is 19.63% and the average error is 1.88%, while the maximum error in the frequency-space grid ρ values is 20.43% and the average error is 2.16%. For $R=1$, $N_1=96$ and $N_2=95$, the maximum error in the spatial grid r values is 40.0% and average error is 2.4% while the maximum error in the frequency-space grid ρ values is 41.12% and average error is 2.7%.

Figure 82 shows the comparison of the exact r grid to the grid that uses the above approximation to the Bessel function zeros. Figure 83 shows the comparison of the exact ρ grid to one generated using an equis-paced radial/angular grid. Both are for the case $R=1$, $N_1=16$ and $N_2=15$.

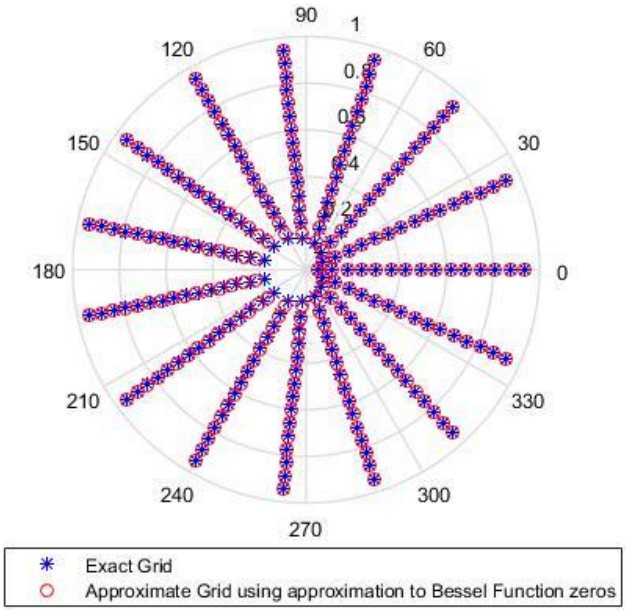

Figure 82 Comparison of exact r domain grid to equispaced grid using approximation to Bessel function zeros. R=1, N_1=16 and N_2 = 15

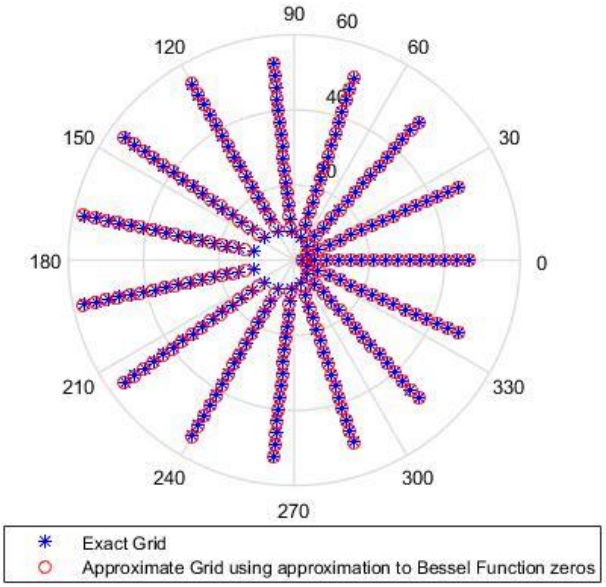

Figure 83 Comparison of exact ρ domain grid to equispaced grid using approximation to Bessel function zeros. R=1, N_1=16 and N_2 = 15

It can be clearly seen from Figure 82 and Figure 83 that the equispaced grid covers most of the area of the true grid but shows poor coverage near the origin.

B-2. Approximation to discrete kernel evaluated at approximate Bessel zeros

Here, a comparison is made between the true value of the kernel to an approximation of the kernel evaluated at approximations to the Bessel function zeros. The approximate kernel is defined as

$$E_A^-(ql;pk)=\frac{2}{N_2}\sum_{n=-M}^{M}\frac{J_n\left(\frac{\hat{j}_{nk}\hat{j}_{nl}}{\hat{j}_{nN_1}}\right)}{\hat{j}_{nN_1}J_{n+1}^2\left(\hat{j}_{nk}\right)}i^{-n}e^{-in\frac{2\pi p}{N_2}}e^{+in\frac{2\pi q}{N_2}}$$

$$E_A^+(ql;pk)=\frac{2}{N_2}\sum_{n=-M}^{M}\frac{J_n\left(\frac{\hat{j}_{nk}\hat{j}_{nl}}{\hat{j}_{nN_1}}\right)}{\hat{j}_{nN_1}J_{n+1}^2\left(\hat{j}_{nk}\right)}i^{n}e^{+i\frac{2\pi np}{N_2}}e^{-i\frac{2\pi nq}{N_2}} \tag{B.6}$$

where $\hat{j}_{nl}$ is the approximation to the true Bessel function zero j_{nl}.

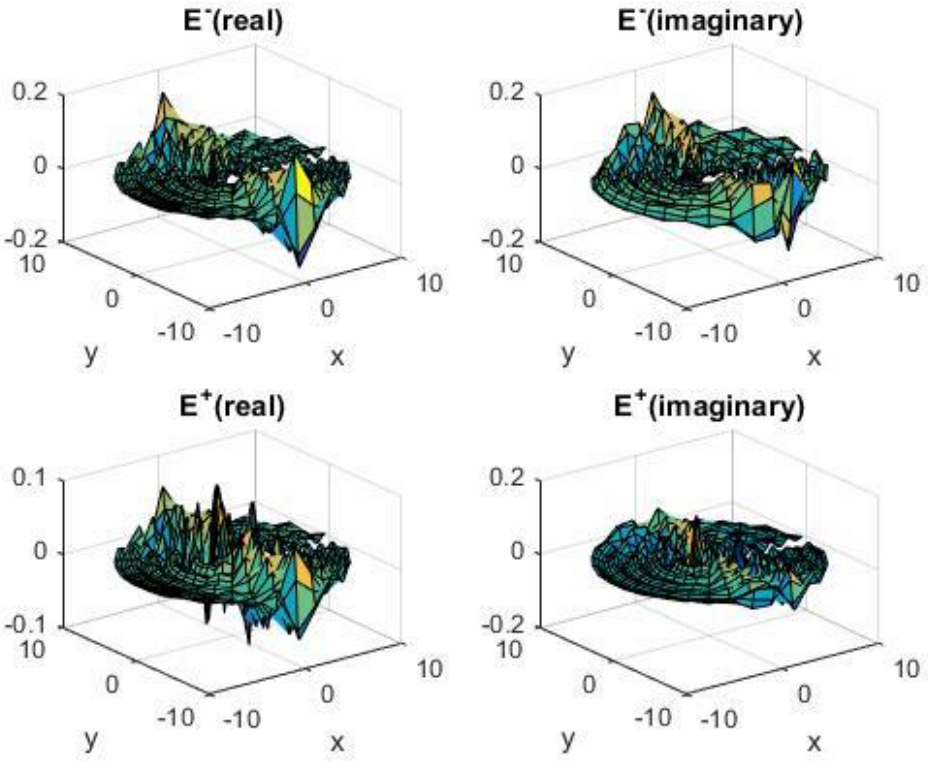

Figure 84 True value of discrete kernel for R=1, q=0, l=10, N_1=32, N_2=31

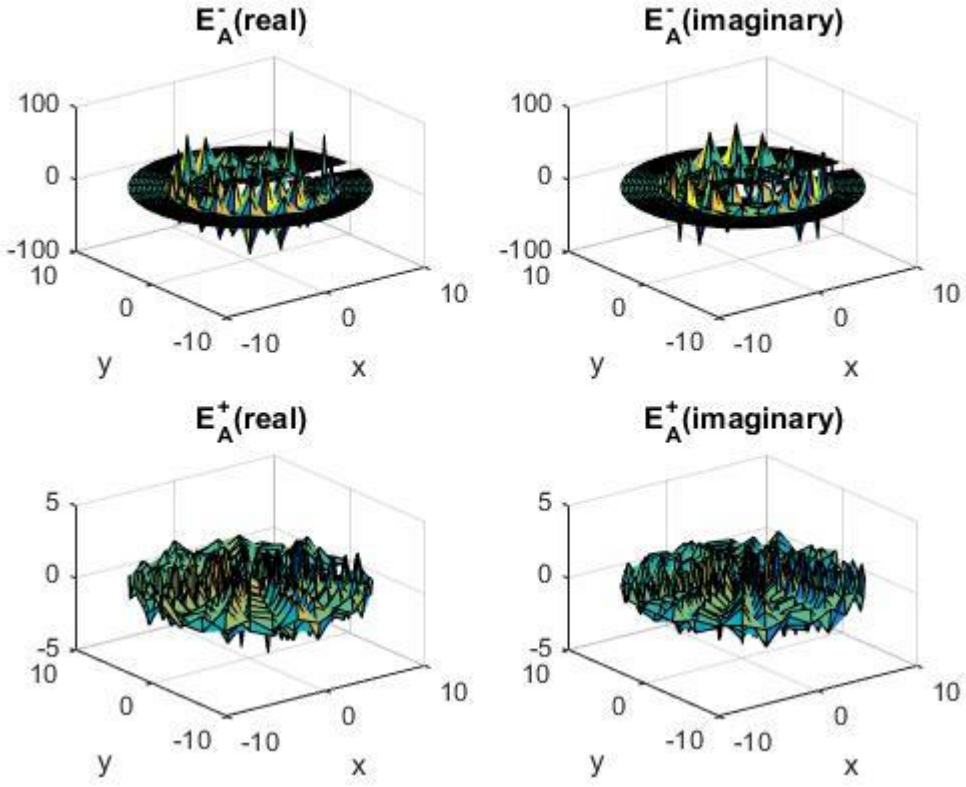

Figure 85 Approximation of the kernel evaluated at approximations to the Bessel function zeros for R=1, q=0, l=10, N_1=32, N_2=31

Figure 84 shows the true continuous kernel defined in equation (3.11). Figure 85 shows the approximation of the kernel evaluated at approximations to the Bessel function zeros, as defined in equation (B.6). From these figures, it is clear that these two are different. Checking the orthogonality of the approximate kernel (as defined in equation (B.6)) shows that

$$\sum_{l=1}^{N_1-1}\sum_{q=0}^{N_2-1} E_A^-(ql,pk)E_A^+(ql,p'k') \neq \delta_{pp'}\delta_{kk'} \tag{B.7}$$

Equation (B.7) implies that the approximate kernel is not orthogonal. Therefore, the approximate kernel cannot be used in the problem.